Development of Optimal Electromagnetic Resonance Rewarming Technology for Cryopreservation

Jiaji Pan

A dissertation

submitted in partial fulfillment of the

requirements for the degree of

Doctor of Philosophy

University of Washington

2018

Reading Committee:

Dayong Gao, Chair

John Kramlich

Ming Chen

Program Authorized to Offer Degree:

Mechanical Engineering

University of Washington

Abstract

Development of Optimal Electromagnetic Resonance Rewarming Technology for Cryopreservation

Jiaji Pan

Chair of the Supervisory Committee:
Professor Dayong Gao
Department of Mechanical Engineering

The development of successful cryopreservation technology has been restricted to small biological materials due to the limited effective rewarming techniques. Either for conventional cryopreservation techniques which remain a certain fraction of ice crystals or vitrification which aims to exclude ice crystal in the subzero temperature range completely, the rewarming rapidity plays a significant role in the recovery of the biological materials after cryopreservation. Additionally, for larger materials such as tissues and organs, the uniformity of the temperature profile is indispensable to maintain the integrity of the cryopreserved biological matrix. The major challenges for traditional convective rewarming method, i.e., water bath, lie in that the high specific heat of cryopreserved materials likely result in a slow warming by the unsatisfactory heat source; and a large temperature gradient is induced by conductive heat

transfer within the sample. The cryopreserved cells are exposed to cryoinjuries for a longer time if rewarming is insufficiently rapid in the case of conventional cryopreservation. For tissue or organ preservation, even if a vitrified state has been achieved by the addition of high concentration cryoprotective agent (CPA) solutions and/or designed cooling process, the slow rewarming can lead to devitrification and recrystallization, introducing considerable ice crystals that should be avoided. On the other hand, the non-uniform temperature profile brought by the convective heating method leads to the thermal stress induced fractures, which can tear apart the vitrified tissues. Hence, an effective rewarming should be both rapid and uniform, to guarantee the successful cryopreservation or vitrification of biological materials. Potentially it may be the most promising to achieve the goal by utilizing the electromagnetic waves, but several issues remain to inhibit the further practical applications.

This dissertation reports on research in which an electromagnetic resonance rewarming technique is developed and optimized aiming for the organ and tissue preservation. An optimization procedure is established as the following steps: (1) determination of the essential physical properties of the CPA/vitrification solutions; (2) analysis and estimation of the combined electromagnetic and heat transfer phenomenon; (3) theoretical simulation and investigation of the rewarming process based on the measured properties; and (4) practical setup of an electromagnetic resonance system and enhancement by adding superparamagnetic nanoparticles.

First, the effectiveness of vitrification of bulk biological material is mainly dominated by the composition and concentration of the vitrification solutions. To avoid devitrification or fractures which relies upon the absorption of electromagnetic energy and heat diffusion, the fundamental electric properties, thermal properties of vitrification solutions are indispensable for

the following estimation of the electromagnetic rewarming efficacy. The dielectric properties were determined by a designed measurement system adopting the cavity perturbation method. The thermal conductivities were measured, and differential scanning calorimeter was used to determine the specific heat. The analysis of these preliminary measurement results was conducted for a selection of CPA/vitrification solutions.

Due to the nonlinearity of the coupled electromagnetic and heat transfer equations, an accurate analytic prediction is hardly achieved to the electromagnetic rewarming outcomes. Hence, a numerical simulation model was established to estimate the warming procedure and select CPA solutions, optimal geometry of the cryopreserved materials and several other parameters before conducting experiments. In particular, a hybrid electromagnetic-conduction rewarming concept was raised and tested to maintain the higher warming rate and reduce the temperature non-uniformity of the cylindrical cryopreserved materials.

The numerical model can simulate the field and optimize the parameters of the electromagnetic rewarming system, to achieve a higher power utilization efficiency. With the assistance of a numerical model, the electromagnetic resonance rewarming system was designed, assembled, and optimized, particularly the coupling between the system source and resonance chamber. In addition, a frequency tracking component was added to ensure the resonant state during the rewarming process, when the cryopreserved materials shift the resonance as temperature increases.

Finally, to fully utilize the electromagnetic field energy provided by the dynamic controlled electromagnetic resonance rewarming system, we took advantage of magnetic nanoparticles (MNPs) to absorb magnetic field energy to further enhance the energy conversion efficiency, which overcame the low electromagnetic energy absorption ability problem that

previous attempts suffer from. An ultra-high power utilization efficiency was obtained and we achieved over 200 °C min^{-1} rewarming rate for tens of mL cryopreserved samples. In addition, we also investigated the effect of nanoparticle size and concentration on the rewarming results and thermal properties. The closed system preventing electromagnetic radiation outwards reduced the possible concomitant side effects when increasing nanoparticles or raising the electromagnetic power. With the remarkably low dosage of nanoparticles (0.1 mg mL^{-1} Fe) compared to other MNPs based rewarming applications (over 1 mg mL^{-1} Fe), this study opens a door for new approaches to explore novel rewarming techniques for the tissue and organ preservation.

TABLE OF CONTENTS

LIST OF FIGURES

LIST OF TABLES

ACKNOWLEDGEMENTS

The author would like to express his gratitude to all the people who provided kind help to him during this long journey towards his finale of the PhD study.

I would like to thank my supervisor Dr. Dayong Gao. When I was an undergraduate student in University of Science and Technology of China, he put faith in me and supported my application for the direct PhD program in University of Washington. During the time in University of Washington, he cared about and helped in every aspect of my personal development various from course study, teaching, presentation skills, and the research. I received tremendous invaluable advices from him when I faced new challenges each time. I appreciate Dr. Ming Chen (the Boeing Company) for his great support in my exploration in this study. When I got stuck in the design or encountered any technical problems testing the experimental results, he always provided me with valuable ideas and professional instructions. The inspirations from Dr. Gao and Dr. Chen helped me to develop the capabilities to conduct independent researches. I am grateful to have them as my respected advisors for this PhD study as well as in my future life and career. With their support and guidance, I developed a lot from this research project which is both scientifically interesting and engineering intellectually challenging.

I am delightful to have Dr. John Kramlich (Mechanical Engineering) and Dr. Yong Tan (Business School) in my committee. Thanks for their input in this research work. Their suggestions and insightful comments are helpful in improving the quality of the study. I also

appreciate the support from ME department staffs, especially Wanwisa Kisalang, Nancy Moses and Helen Llamado for their assistances in grant applications, financial related administrative issues.

Moreover, without the care and love from my family, I may not be able to stay abroad for such a long period of time. I appreciate for everything I gained from my parents and grandparents. Thanks to my uncle Dr. Xianwu Luo and my aunt Dr. Ronghua Ni. They encouraged me in pursuing my goal and broaden my horizons. Also, I feel lucky to meet a large number of smart and warm-hearted friends including but not limited to: Dr. Yu Jin, Dr. Mengfei Cao, Dr. Xiao Su, Dr. Zhiquan Shu, Dr. Gang Zhao, Dr. Weiping Ding, Dr. Yuyin Sun, Dr. Cifeng Fang, Dr. Sijie Sun, Dr. Qi Zeng, Dr. Luhong Diao, Dr. Junsheng Chu, Ms. Ni Luo, Mr. Shen Ren, Mr. Ji Peng, Mr. Jinyuan Zhang, Mr. Lei Yao, Mr. Ning Zhang and etc. Thanks for all the good time we spend together.

Chapter 1. Introduction

1.1 Fundamental Principles of Cryopreservation

Cryobiology is the study of the effects of low temperature on biological materials or systems. This study has broad applications across food industries, agriculture, reproductive sciences and biomedicine. The systematic study of cryobiology begins in 1949. Since the accident finding that sperm with glycerol could go through the freezing and thawing alive [1], the exploration in cryobiology has attracted scientists, surgeons and engineers with various background including bioengineering, mechanical engineering and electrical engineering.

Cryopreservation is one of the essential practical applications of cryobiology capitalizing specific designed protocols and low-temperature techniques to preserve biomaterials including cells, tissues, and even organs. The structure integrity and functions of the biological matrixes are maintained through the specific cryopreservation procedures down to cryogenic temperature for storage. The low storage temperature in cryopreservation ranges from −80 °C down to −196 °C. In addition, the viability and function of biomaterials could be sustained for a certain amount of time ranging from weeks to decades, depending on the storage temperature and the type of materials. Upon the request of those bio-samples in various applications, cryopreserved materials will be brought back to the physiologically appropriate temperature to satisfy the specific needs. Nowadays cryopreservation is the most widely accepted methods for long term preservation of biomaterials. A lot of fields from fundamental biomedical research to clinical treatment benefit from this emerging subject.

The reason that biomaterials such as cells, tissues and larger biological systems can be preserved at low temperature lies in that the biological activities would be inhibited by low

temperature. Metabolism, although involving with different kinds of cells, chemical materials, and specific enzymes, are subject to specific governing laws of physical chemistry reactions. The Arrhenius equation show that the rates of reaction fall off quickly as temperature decreases. These bio-reactions could be retarded significantly in low temperature. Hence, the biomaterials could be preserved theoretically with small consumption of energy and low reaction rates.

Through effective protocols, red blood cells [2], sperm [3, 4], oocytes [5, 6], stem cells [7], liver cells [8], skin [9], cornea [10] and immune cells [11] can be successfully preserved. Those successful cryopreservation protocols lay the foundation of establishing biobanks of biomaterials including but not limited to blood, sperm, skin, and some synthetic tissues and thus cryopreservation can bring tremendous following advantages:

1. The biobank of those materials provides a solution for the time conflict between donors and recipient. Patients in urgent circumstances could receive necessary biomaterials for surgical operations.
2. It allows for sufficient time for the screening of transmissible disease, donor-recipient matching including size, blood type and human leukocyte antigen (HLA) typing.
3. It assists in some vaccine and drug development. The tested materials for study could be collected at different time and medical sites, while to be analyzed simultaneously at one medical center.
4. The biobank of sperms and oocytes could help infertile couples to receive childbearing.
5. Some donors can preserve their own stem cells or tissues, and make use of their private cells or tissues for the later treatment without transplant rejection at all.
6. Biological data could be extracted conveniently within these established biobanks and used for precision medicine and disease diagnosis based on big data analysis.

7. The gamete of endangered species could be stored and may be used to save those creatures.

However, it may not be that effortless to maintain the viability and functions of biomaterials by simply putting them into a cryogenic temperature environment. The cooling could be dangerous to biomaterials. During the procedure of cryopreservation, the biomaterials are exposed to lethal threats so called “cryo-injury”. Lovelock raised that the increase of solution concentration resulted in the damage to the cell membrane and injury to the cells [12]. Meryman suggested the increase of extracellular osmolality lead to the cell damage when intracellular volume reach beyond critical volume [13]. Later it was proposed that the rate of kinetic cooling and warming process were important in the cryopreservation. In 1972, Mazur initially proposed “Two factor hypothesis” of freezing injury based on the study of Chinese hamster tissue [14]. During the cooling process, two distinct types of cryoinjuries determine the life or death of the cells, which are affected by the cooling rate. Neither too high nor too low cooling rate is favored for the cryopreservation.

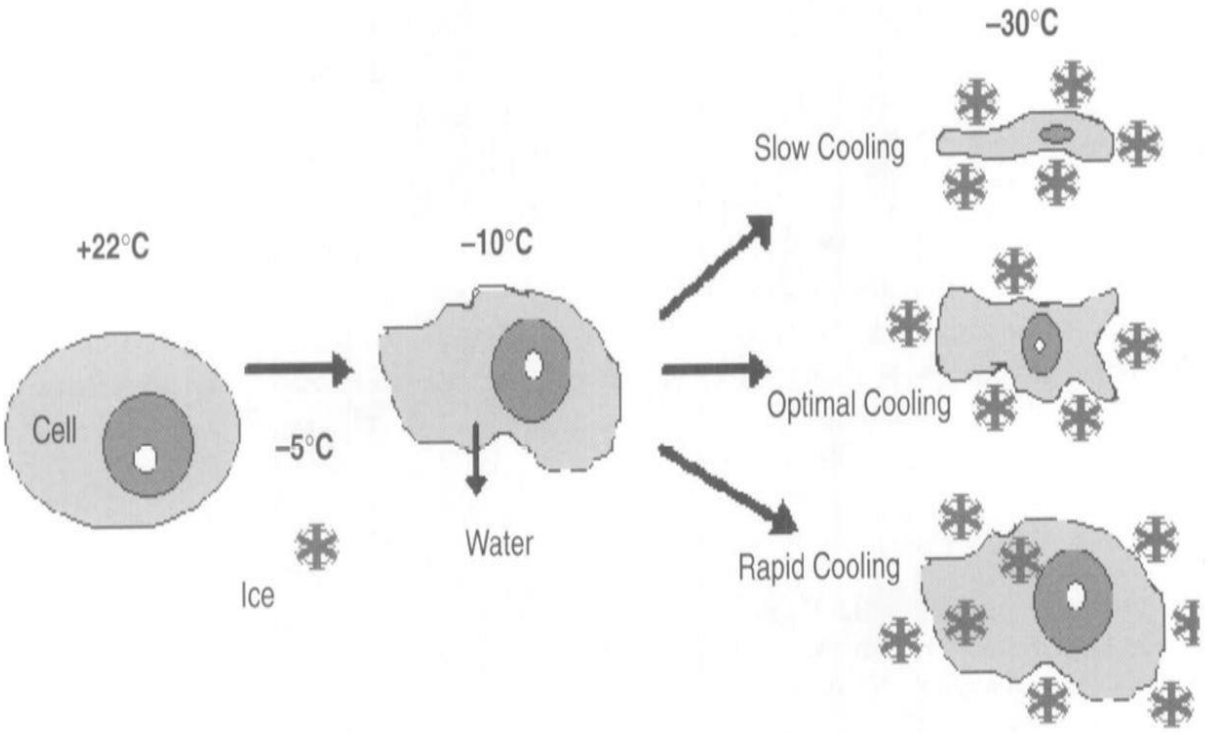

Figure 1-1. Schematic drawing of physical events in cells during freezing [15].

As shown in Figure 1-1 [15], when the cells are cooled down to subzero temperatures under a normal pressure, ice crystals emerge and grow in the suspensions outside the cell membrane in the beginning. The external ice growth into cells are blocked by the plasma membrane. The cytoplasmic region remains unfrozen and supercool state due to some huge molecules inside the membrane [16, 17]. However, the increase of osmolality, chemical potential due to the external ice formation will serve as a driving force between the intracellular components and extracellular environment, pulling water out of cell membranes. If the cooling is too rapid, there is insufficient time for the water to flow out the membrane. As the temperature goes down rapidly, the unfrozen and supercooled state is disturbed and the intracellular ice formation (IIF) emerges [18]. The lethal IIF can rupture the cell membranes and leads to the cell death. On the other hand, if the cooling rate is too slow, intracellular ice may be reduced. The

plenty of time permits water transport out of the membrane under the influence of the osmolality difference driving force. Cells then suffer from high concentration of intracellular solute/electrolytes which is called “solution effects” and severe dehydration. The slower cooling process may expose the cells to “solution effects” for a longer time, which is unacceptable for the cells. Therefore, the cooling rate may not be too high or too low based on the “two factor hypotheses”.

As can be seen in Figure 1-2, the relationship between percentage of cell survival and cooling rate displays an inverted “U” shape [19]. Each specific type of cells has an optimal cooling rate. For each specific type of cells, the optimal cooling rate is different which relies on the ability of water to transport across the cell membrane, i.e. the water permeability of the cell membrane [15].

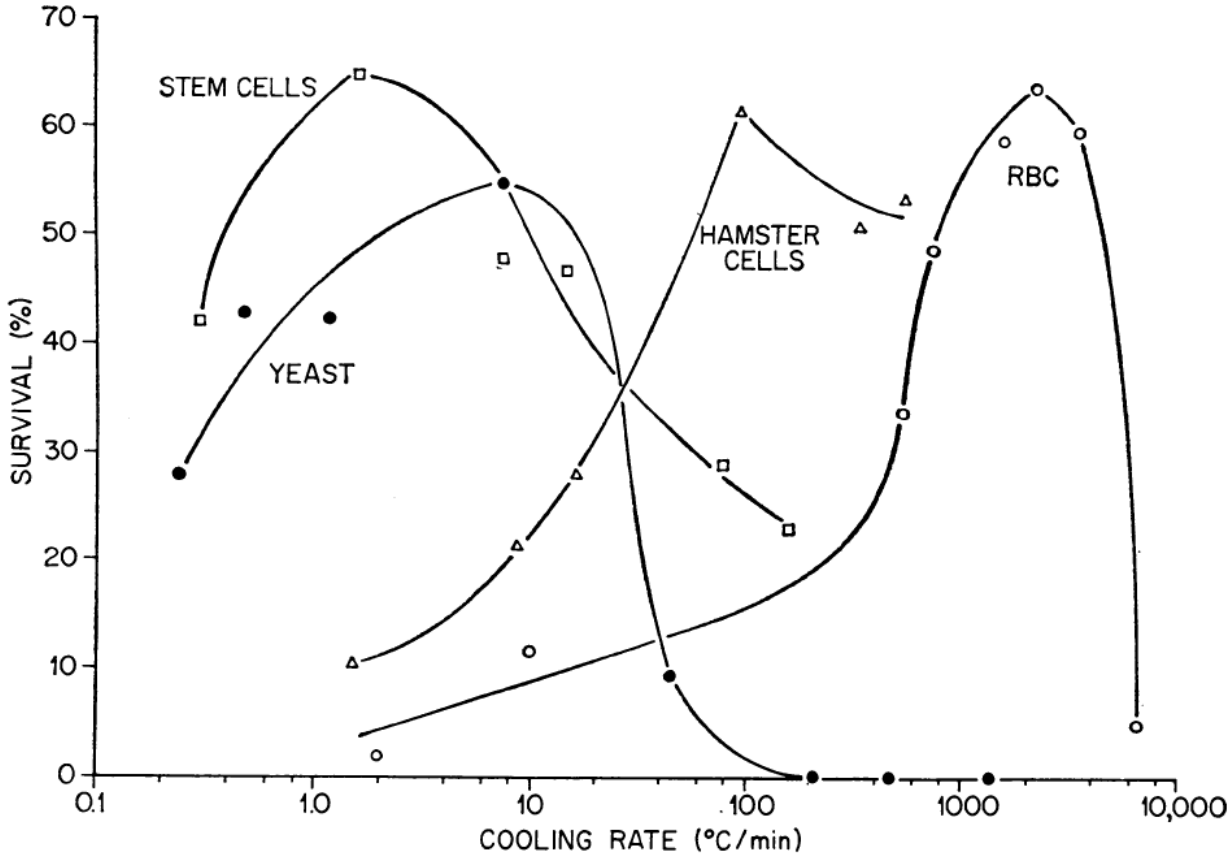

Figure 1-2. Comparative effects of cooling velocity on the survival of various cells cooled and thawed rapidly [15].

Since the cryoinjuries remain a barrier in the cryopreservation of cells, a lot of cryoprotective agents (CPA) have been discovered and added to the cell suspensions to reduce the cryoinjury, they have the same function as glycerol in the unintentional successful freezing-thawing preservation of sperm in 1949 [1]. There are two different kinds of CPAs in general: penetrating CPAs and non-penetrating CPAs. Penetrating CPAs, such as Dimethyl Sulfoxide (DMSO), glycerol and formamide, can move across cell membranes and avoid severe cell volume shrinkage. The penetrating CPAs also reduce the intracellular freezing by lowing the cell water contents at the subzero temperature. Thus IIF is inhibited [20]. Non-penetrating CPAs, such as Hydroxy-ethyl-starch (HES), Polyvinyl Pyrrolidone (PVP) and trehalose, cannot get into

the cell membrane. These compounds can affect the extracellular matrix, drag water outside of the membrane and prevent intracellular freezing in the early stage of freezing [20].

A typical successful cryopreservation procedure is composed of five steps:

a) Addition of appropriate CPA;
b) Optimized cooling process;
c) Storage at the low temperature (−80 °C fridge or −196 °C liquid nitrogen tank);
d) Rewarming process to physically normal temperate;
e) Removal of CPA.

1.2 VITRIFICATION

Due to the cryoinjuries, effective cryopreservation protocols are still in need for many specific types of cells. In addition, the difficulty of cryopreserving biomaterials increases with samples' sizes and levels of their structure complexity. Compared to simple biological systems, tissues and organs, are composed of different types of cells. The cryopreservation protocol for each type of cells may not be the same coincidentally. The optimal cooling rate, choice of type and concentration of CPA could be drastically different. The relationship between single or different types of cells in the complex biological system may also influence the optimal cooling rate. During the cooling process, water from dehydrated cells fluxed into blood vessels could lead to vascular damage and structural destruction. The extracellular ice formation usually regarded as tolerable in cell preservation could be devastating in the tissue preservation[20].

Vitrification, as an alternative approach, may be effective to deal with the problems encountered in the traditional methods and cryopreserve more complex biological systems successfully. As the name implies, vitrification, also known as glassification, refers to the process in which liquids are solidified into an amorphous state instead of in crystalline solid

pattern [21]. The idea of vitrifying liquid solutions emerged over one century ago, but the rapid development of its application in cryopreservation started in the 1980s [22]. As shown in Figure 1-3 [23], the transparent rabbit kidney at −140 ℃ implies there are no ice crystals in the vitrified rabbit kidney (right). Whereas the rabbit kidney frozen by traditional cryopreservation method demonstrates a substantial amount of ice formation which can cause membrane ruptures and solution effects due to severe dehydration. The associated side effects in the conventional cryopreservation can be avoided if the glass state is achieved and maintained without apparent physically shape change during the cooling process. Hence, there is no need to compromise between the two distinct mechanisms of cryoinjuries and discover the optimal cooling rate for the various types of cells. Those remaining obstacles to conventional cryopreservation methods could be avoided by the method of vitrification. Nowadays vitrification is regarded as the most promising technique for preserving complex multicellular tissues and organs.

To achieve vitrification, biological systems with a high concentration of CPA should be cooled down to the glass transition temperature (T_G) at an ultra-fast rate so that there is insufficient time for ice crystals to form during the freezing process and accomplish the transition from liquid to non-crystalline amorphous solid. The minimal cooling rate above which vitrification may happen is called the “critical cooling rate” [24]. And the critical cooling rate depends on the type and concentration of adopted CPA. Normally in the vitrification protocols, a very high concentration of CPA solutions would be added to increase the viscosity and inhibits molecular realignment into crystalline patterns. Thus, the critical cooling rate for the biological matrix is lowered by added CPA solutions. For pure water, the critical cooling rate can be as high as ~ 10^7 °C min^{-1} [25]. After adding sufficient CPA solutions, the critical cooling rates could be minimized to thousands or even hundreds of °C min^{-1}.

Figure 1-3. Comparison between frozen and vitrified rat kidney: ice crystals formed in the traditional preserved method while no ice formation in the vitrified kidney [23].

As the vitrification leads to merely no ice crystallization in both intra- and extra-cellular fluids, cryoinjuries were avoided, and an ideal state was created for the biomaterials. By adopting vitrification method, monocytes, ova, early embryos, pancreatic islets, blood vessels and articular cartilage [26-38] have been successfully cryopreserved.

1.3 REWARMING CONCERN

Vitrification, as introduced above, would be favored for complex biomaterial preservation since it can avoid large ice crystal formation and avoid the need to find an optimal cooling rate between several different types of cells. After cooling below the glass transition temperature, the vitreous state can be maintained, and biological systems can be stored for a long time. However, the warming procedure for vitrification, is critical in that it may lead to the failure of the desired outcome. When the vitrified biomaterials are rewarmed from the storage temperature below T_g back to the physically normal conditions (e.g., 20 °C or 37 °C), the vitreous state is easily shattered since the vitrified materials in that temperature range are extremely brittle. The fragile vitrified materials need care during the rewarming process for two reasons. First, a minimal rate is mandatory, which is also called critical warming rate, corresponding to the critical cooling rate in the cooling process. The warming rate should be rapid enough to reach the liquid state and surpass the kinetic large ice crystal growth. A warming rate lower than that critical rate would lead to "devitrification". Devitrification is not a neutral reverse sequence of vitrification. It is associated with a fatal process that a lot of large ice crystals grow which is called "ice recrystallization". Second, the temperature distribution should be uniform to avoid thermal stresses. The thermal stress induced from large temperature gradient would cause mechanical injuries and tissue fractures.

In the 51st annual meeting of Society for Cryobiology, Mazur who invoked the "Two Factor Hypothesis" raised a new idea that the ultrahigh warming rate is even more vital than high concentrations of cryoprotective solutes or extremely rapid cooling rate which is partly against the previous theoretic foundation. This point of view has not been widely accepted by cryobiologists because the number of similar cases is limited for now. Whereas numerous studies

could be explained and guided based on the “Two Factor Hypothesis”. But it is of no doubt that the warming rate should be increased to avoid fracturing and stresses because ice crystals will grow in the sample [21]. In addition, the recent finding that the sample under suboptimal cooling protocol could be might be recovered by sufficiently rapid rewarming [39] is of practical importance in the development of productive cryopreservation techniques.

However, current rewarming technique, typically thawing by a 37 °C water bath, leaves organs and large tissues vulnerable to cryoinjuries. The water bath is a convective rewarming approach in which heat is conducted from the outer boundaries that is by the side of hot water to the inner portion of the cryopreserved biological samples. Because of the high specific heat of cryopreserved materials, it requires a great amount of heat to rewarm the biomaterials. Another obstacle for the rewarming process is the low thermal conductivity of biomaterials. External heat from the boundary water bath cannot be quickly transmitted into the core area of large biological systems. For single type of cell suspensions, the small thermal conductivity may possibly be avoided by the design of sample holder (e.g. extending the surface area and reducing the thickness of cell suspensions) [40]. However, for most tissues and organs which have much smaller radio between the surface area and the volume, they cannot be sliced or pressed into a thin film to increase the heat transfer area by convective water bath warming. In this case, a large temperature difference will occur and lead to thermal stresses that can result in the fracture of vitrified samples. Therefore, traditional boundary convective rewarming method is not appropriate for cryopreservation of large biomaterials by vitrification which will lead to devitrification and tissue fracture. Now that a uniform and ultrafast rewarming method is hardly achieved by boundary thawing, volumetric rewarming technique should be considered.

1.4 BASICS OF ELECTROMAGNETICS

The electromagnetic field is a combination of the electric field and the magnetic field generated by charged objects. The electric field and magnetic field are coupled with each other. A time varying electric field (contrary to static field) induces magnetic field changing over time and vice versa. The distribution and propagation of electromagnetic fields are governed by Maxwell's equations. An electromagnetic wave is the propagation of the electromagnetic field through media such as air, water, etc. This propagation also refers to radiation transmitting the electromagnetic energy, momentum and angular momentum through space. As one of the basic forces of nature, the propagating electromagnetic fields interact with other materials and generate different effects depending on the frequency and power. Based on the mechanisms behind these interactions electromagnetic waves and other materials, electromagnetic waves have been applied in broad aspects including: telecommunications such as mobile phone calling, the short wave broadcast, TV signals transmission and connections between the spaceship and base on earth; remote sensing for the weather forecasting, land mapping and infrared radiation detecting; X-rays and CT for the disease diagnoses and radiotherapy which employs higher energy radiation to kill cancer cells. These various applications are closely related to the spectrum of electromagnetic waves. The most commonly used frequency band is at radio frequency (RF) electromagnetic wave and microwave which are illustrated in Figure 1-4.

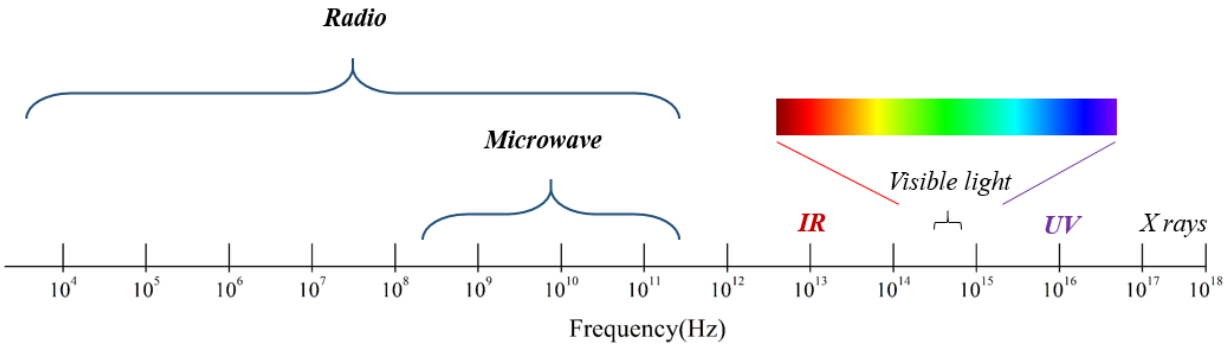

Figure 1-4. Frequency band of electromagnetic waves.

1.5 ELECTROMAGNETIC REWARMING

The thermal effects of electromagnetic waves benefit the organism on earth even long before the prehistory. The thermal energy transmitted by the electromagnetic waves emitted from the sun allows the survival of plants, animals. This electromagnetic wave emitted from the sun, or sunlight, is distributed across almost the entire spectrum but with major intensity on infrared, visible and ultraviolet frequency ranges. These major component visible light has a frequency range in several hundreds of THz. Higher frequency electromagnetic waves such as X-rays carry much higher energy and are used for radiation therapy killing the tumor cells by ionizing the molecules. In the lower frequency range, electromagnetic waves (radio frequency electromagnetic waves, microwave) can hardly excite ionization with less energy but can result in thermal effects with materials.

The investigation of the heating phenomenon by microwave occurred in the 1940s. A candy bar under an active microwave generating devices melted and the engineer used this observation to develop equipment for preparing and heating food utilizing the thermal effects of microwave radiation [41-44]. Since then, not only has the commercialization of the microwave oven become widespread, scientists also began to study the potential benefits for industry and

medicine. Most of food is a dielectric material that can interact with the electromagnetic fields in the microwave oven due to a large portion of water in the contents. The water molecules are dipole molecules comprising an electrical positive charged end and an electrical negative charged end. Under the influence of electric fields, these dipole molecules will align themselves with the applied electric fields. When the directions of external electric fields are changing as in the oscillating electromagnetic waves, the dipole molecules will rotate to follow up with the changing fields. The interactions between the rapid changing electromagnetic fields and water dipole molecules will cause mechanical friction forces among the water molecules. The frictions between these micro molecules generate heat volumetrically. Similarly to the food in the microwave oven for heating, the biological materials in cryopreservation are organisms that are primarily composed of water. Therefore, microwave can also be used for the heating of biological systems. Here it is used to solve the rewarming problems in the cryopreservation.

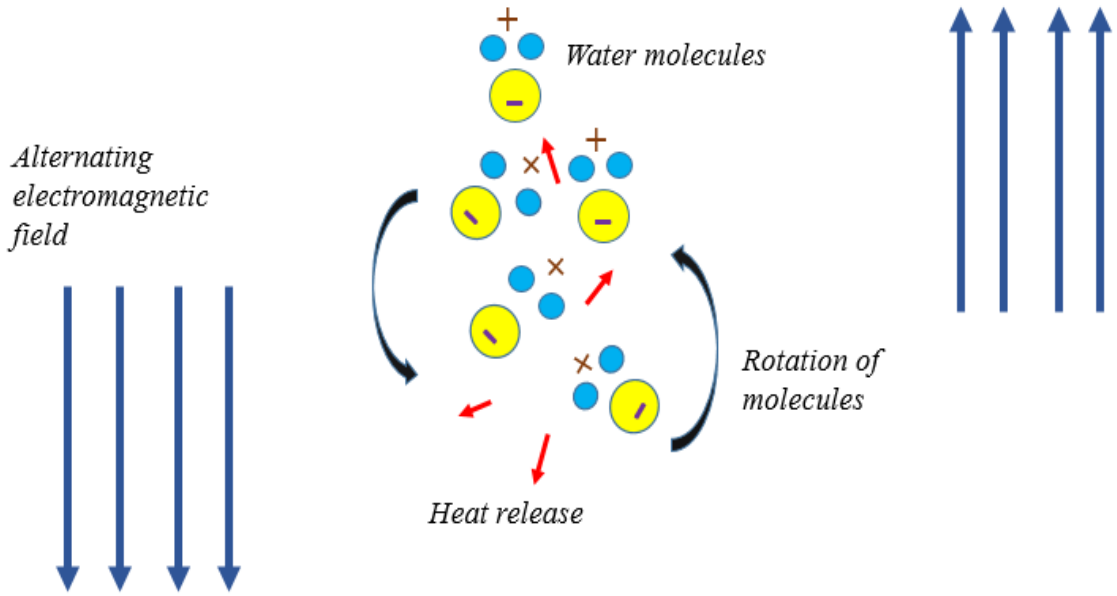

Figure 1-5. Illustration of heat generation under the influence of electromagnetic waves.

When using microwave as the rewarming approach in the cryopreservation, the biomaterials interact with applied electromagnetic field. Since most biomaterials are nonmagnetic, the forced movement of molecules are mainly due to the electric field component of the electromagnetic field. As shown in Figure 1-5, a distinct advantage microwave rewarming has when comparing with traditional water bath rewarming is that the heat is generated over the entire region of the material which overcomes the low thermal conductivity problem. The electrical parameter that characterizes the interaction between the material and electric field component is relative complex permittivity, or dielectric property:

$$\varepsilon_r = \varepsilon' - i\varepsilon'' \tag{1.1}$$

The real part of complex permittivity ε' , also known as dielectric constant, represents the ability of storing electric field energy. The imaginary part of complex permittivity ε'', known as dielectric loss, represents the ability to absorb electric field energy. The heat generation density q due to the electromagnetic rewarming in the material is given by:

$$q = \pi f \varepsilon_0 \varepsilon'' |\mathbf{E}|^2 \tag{1.2}$$

where f is the frequency of electromagnetic wave, ε_0 is the electric permittivity of free space. $|\mathbf{E}|$ is the root mean square magnitude of electric field. In order to deal with the slow warming obstacle due to the high heat capacity, two straightforward solutions can be figured out based on the heat generation principle. One is to select material with higher dielectric loss, the other approach is to increase the magnitude of the electric field exposed to the cryopreserved biomaterial. Provided a strong electric field intensity, the rewarming of cryopreserved biomaterials by electromagnetic wave could be ultrafast which seems to be a promising approach to avoid devitrification.

1.6 Previous Electromagnetic Rewarming Attempts by Cryobiologists

The development of electromagnetic rewarming systems is limited by the cost and inadequate theoretical guidance. The establishment of an electromagnetic resonance rewarming system involves the selection of frequency source and power, manufacturing of the resonance chamber, optimization of the electromagnetic energy feeding approach to the cryopreserved materials. Setting up a specific resonance rewarming system can take a few months to years and requires substantial funding support. When the system is going to be scaled up to materials of a larger dimension, various parameters of the system should be replaced which will extend the

time required for the optimization. The first experimental investigation of using electromagnetic energy in cryopreservation began in the 1970s. In Kettrer's experiment [45], 20 kidneys rewarmed by a microwave generation device with power control were considered partial success. By using a commercial 1.35 kW Toshiba microwave oven which generated by 2.45 GHz magnetron, Guttman [46] reported the electromagnetic rewarming of 16 cryopreserved canine kidneys. Half of the dogs receiving transplantation of these kidneys survived months.

However, in Pegg's attempt [47] to repeat the rewarming of dog kidneys with commercial microwave oven, none of the post-thawing dog kidneys function properly.

Another device designed by Burdette [48] generated an electromagnetic field with an open electromagnetic illumination system. The frequency can be adjusted to several distinct values. The rewarming results of rabbit and canine kidneys were published without the following viability analysis.

These preceding explorations opened a new area for cryobiologists, most specialized in biomechanical and biochemical physics, to implement new technologies from electrical engineering in the application of cryopreservation. A major problem for these early investigations of electromagnetic rewarming is that the frequency of the commercial microwave oven is too high to penetrate the inner part of the cryopreserved biomaterials. A good uniformity should be achieved with lower frequency electromagnetic waves. In addition, electromagnetic rewarming can result in a "thermal runaway" problem, which leads to an increasing temperature difference across the sample volume.

Thermal runaway phenomenon is depicted in Figure 1-6. Due to the complex interactions between the material and the applied electromagnetic wave. The temperature distribution may not be that uniform initially. If the slightly warmer area of the biological samples has a higher

ability to absorb energy from electromagnetic waves and convert into heat than colder area. The temperature difference between these components will be magnified. When the difference in governing properties is significant and favors the ultrafast thawing of the hot area, the non-uniform temperature gradient is even intensified.

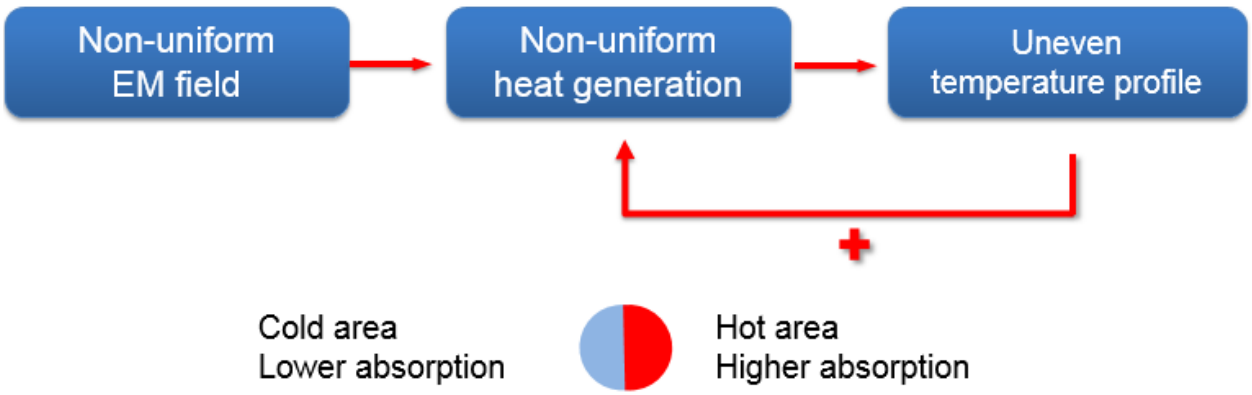

Figure 1-6. Introduction of "thermal runaway" phenomena: the appearing of large temperature gradient by electromagnetic rewarming.

In order to avoid the localized warming associated with "thermal runaway" and limited penetration depth for the 2.45 GHz high frequency electromagnetic waves, more delicate controlled electromagnetic rewarming systems operating in lower frequencies are required for cryopreservation.

Thereafter, a rewarming system using helical coil to generate tens of MHz electromagnetic waves was used to rewarm CPA solutions as a preliminary trial [49]. But the rewarming rate was moderate achieved by this open system.

Later on, a few scientists reconsidered the electromagnetic rewarming in closed systems to confine electromagnetic energies [50, 51]. Unlike the commercial microwave oven in which the generated signal shifted around ±50 MHz, the electromagnetic wave was synthesized by voltage controlled oscillators. The stability of frequency was improved so that the design of chamber could fit with the electromagnetic source and establish resonant state to concentrate the electromagnetic energy.

A major problem for these resonant systems may come from an intention to reduce the non-uniformity by adopting multimode resonant cavities. In Rachman's electromagnetic resonance cavity rewarming system [50], two resonant states of the cavity were excited (TE111 and TM010). Another multimode cavity rewarming system, designed by Robinson [51] excited three different modes. The results of the warming test for CPA solutions were improved while the spatial temperature difference was not greatly reduced, which means thermal runaway could not be entirely eliminated.

The theorem behind this is due to the interaction between the cryopreserved CPAs and the properties of the resonant cavity. Multimode cavities resonating at different frequencies bring more difficulties in the control of signal frequency at each port to feed electromagnetic energy into the cavity. Hence, a single mode resonant cavity which excites only at a specific frequency may be superior in the control of field distribution in the rewarming process. The details in terms of the design will be introduced in Chapter 3 and Chapter 4.

1.7 RESEARCH OBJECTIVE

Our ultimate goal is to achieve effective cryopreservation protocol for organs and large tissues. In this work, the target is to optimize electromagnetic rewarming systems for the rapid and uniform rewarming, laying down the foundation for large tissue and organ preservation. This development process necessitates solid understanding of the coupled electromagnetic and heat transfer physical model, thermal runaway phenomenon analysis and solution, assembly of electromagnetic devices and parameters optimization. Thus, theoretical and experimental approaches should be utilized and combined to deliver considerable progress. The specific aims for this research are:

a) Set up measurement systems to determine mechanical and electrical properties of CPAs in the subzero temperature range, select appropriate traditional CPA solution to protect from cryoinjuries as well as facilitate electromagnetic rewarming;

b) Establish validated numerical simulation model, optimize the components of experimental system based on the computation results of the electromagnetic rewarming process;

c) Develop an electromagnetic rewarming system to achieve rapid and uniform warming with preliminary insights from CPA properties and numerical simulation results; Conduct freeze-thawing experiments and compare with traditional warming method;

d) Adopt additional materials and designs to enhance the ultimate results combining the numerical simulation and experimental results;

e) Propose innovative electromagnetic rewarming systems based on the current rewarming results for future development.

1.8 THESIS OUTLINE

This dissertation introduces our development process of a single mode electromagnetic resonance system aiming for cryopreservation of large tissues and organs. Through continuous efforts in developing the electromagnetic rewarming system, the advantages of electromagnetic rewarming over traditional water bath could be revealed and the challenging "thermal runaway" problem could likely be suppressed. The structure of this dissertation is organized as follows:

In Chapter 2, the system setup for the measurement of fundamental physical properties of cryopreserved materials is presented and these properties of cryopreserved materials have been determined. The potential impact of these properties on the electromagnetic rewarming is discussed and selection criteria of CPA solutions is proposed.

Secondly, Chapter 3 comes up with the modelling of electromagnetic rewarming process. The electromagnetic field and heat transfer are coupled and calculated to determine the temperature profile. Numerical simulation of the electromagnetic rewarming of several CPA solutions have been conducted. The predicted relationship between the properties and thermal runaway was tested in the model. In addition, a combined electromagnetic-conductive heat transfer method was proposed to minimize the temperature gradient.

In Chapter 4, the detailed development of our single mode electromagnetic rewarming system is presented. The essential function of each equipment in the rewarming system is introduced and the design process of crucial microwave components is demonstrated. In Chapter 5, a preliminary exploration of the effects of magnetic nanoparticles addition in the electromagnetic resonance rewarming were conducted and tested data suggested further promising application of nanoparticles in the electromagnetic rewarming.

Chapter 6 describes the limitation of the current electromagnetic resonance system and the cryopreservation by vitrification. Future improvement of the rewarming system is proposed. Other alternative approaches rather than this resonance rewarming are discussed.

Chapter 2. Characterization of essential physical properties of vitrification solutions

2.1 Determination of the Electrical Properties

The dielectric properties of the biomaterials characterize the interaction between applied electromagnetic field and the biomaterials, and thereby determine the absorption of electromagnetic energy by the biomaterials [52, 53]. The dielectric properties are temperature dependent. If the warmer part of the biomaterial absorbs more heat, the temperature at that warmer part would be further increased, increasing temperature gradients and therefore inducing thermal stresses. A large thermal stress can destroy the viability of cryopreserved materials, and can be even more threatening to tissues and organs [54, 55]. Since the dielectric properties play a key role in the absorption of electromagnetic energy, it is a priority to discover the dielectric properties of the biomaterials. In cryopreservation, particularly in vitrification using a high concentration cryoprotective agent, the CPA/vitrification solutions dominate the properties of the cell suspensions or tissues. Hence, the dielectric properties of the CPA/vitrification solutions should be determined so that electromagnetic rewarming can be optimized.

The measurement of the dielectric properties of biomaterials requires sensing and monitoring tools. In many biomedical applications, various measurement methods including transmission and reflection techniques have been used to determine dielectric properties [56-60]. The samples measured by transmission and reflection methods usually are fixed without morphologically change. But in the application of electromagnetic rewarming, the measurement of dielectric properties must be carried out in the subzero temperature range which may involves phase change and rules out the possibility using transmission and reflection techniques. The

cavity perturbation method has been used for measuring the electric properties of different kinds of materials [61-65] due to its ability to measure the dielectric properties of low loss dielectric materials [66]. In the subzero temperature range, the dielectric properties of biomaterials and CPA/vitrification solutions can be very small. Therefore, in this work, we adopted a cavity perturbation method to determine the dielectric properties of three different vitrification solutions at low temperatures. Briefly, a resonant cavity was designed and manufactured to measure the dielectric properties of cryopreserved biomaterials at 434 MHz. By inserting samples with different permittivity into the resonant cavity, the resonant frequency and quality factor could be changed. From the variation of the resonant frequency and the quality factor, the dielectric properties can be derived.

2.1.1 *Perturbation theory*

Through the change of resonant frequency Δf and inverse of quality factor ΔQ, the dielectric property (or complex permittivity) of these CPA/vitrification solutions was obtained. The mathematical derivation is shown as the following[67, 68]:

$$\frac{\Delta\tilde{\omega}}{\tilde{\omega}} = \frac{\Delta f}{f_0} + \frac{i}{2}\left(\frac{1}{Q} - \frac{1}{Q_0}\right) \tag{2.1}$$

$$\frac{\Delta\tilde{\omega}}{\tilde{\omega}} = -\frac{\int_{V_s}(\Delta\varepsilon\mathbf{E}\mathbf{E}_0^* + \Delta\mu\mathbf{H}\mathbf{H}_0^*)d\nu}{\int_{Vc}(\varepsilon\mathbf{E}\mathbf{E}_0^* + \mu\mathbf{H}\mathbf{H}_0^*)d\nu} \tag{2.2}$$

where f_0 and Q_0 are resonant frequency and quality factor of unperturbed cavity, $\mathbf{E}_0$ and $\mathbf{H}_0$ represent electric field and magnetic field inside the unperturbed cavity, $\mathbf{E}$ and $\mathbf{H}$ represent those fields for the cavity with sample to be measured inside, ε and μ are complex permittivity and permeability of the sample, i is an imaginary number of which the square equals −1.

For nonmagnetic material, μ can be regarded as the permeability of free space μ_0. Eq.(2.2) is simplified to:

$$\frac{\Delta\tilde{\omega}}{\tilde{\omega}} = -(\varepsilon_r - 1)\frac{\int_{V_s} \mathbf{E}_{\text{int}}\mathbf{E}_0^* d\nu}{2\int_{Vc}|\mathbf{E}_0|^2 d\nu} \tag{2.3}$$

$$\varepsilon_r = \varepsilon' - i\varepsilon'' \tag{2.4}$$

where $\mathbf{E}_{\text{int}}$ represents the incident electric field inside the sample. ε_r is the relative permittivity of a material, which is the permittivity ε divided by the permittivity of the free space ε_0. ε' is the real part of the relative permittivity, also referred to as dielectric constant. The real part of permittivity characterizes the electromagnetic energy stored in the material when exposed to electromagnetic waves. ε'' is the imaginary part of relative permittivity, or referred to as dielectric loss, which characterize the electromagnetic energy dissipation.

Substituting eq.(2.4) into eq.(2.3), we have

$$\frac{\Delta\tilde{\omega}}{\tilde{\omega}} = -(\varepsilon_r - 1)\frac{\int_{V_s} \mathbf{E}_{\text{int}}\mathbf{E}_0^* d\nu}{2\int_{Vc}|\mathbf{E}_0|^2 d\nu} = -(\varepsilon' - 1)\frac{\int_{V_s} \mathbf{E}_{\text{int}}\mathbf{E}_0^* d\nu}{2\int_{Vc}|\mathbf{E}_0|^2 d\nu} + i\varepsilon''\frac{\int_{V_s} \mathbf{E}_{\text{int}}\mathbf{E}_0^* d\nu}{2\int_{Vc}|\mathbf{E}_0|^2 d\nu} \tag{2.5}$$

Comparing the shift of the resonant angular frequency described by eq.(2.1) and eq.(2.5), it can be obtained:

$$-\frac{\Delta f}{f_0} + \frac{i}{2}\left(\frac{1}{Q} - \frac{1}{Q_0}\right) = -\left(\frac{1}{C}\right)K(\varepsilon' - 1) + i\left(\frac{1}{C}\right)K\varepsilon'' \tag{2.6}$$

The parameter C is proportional to $\frac{1}{V_s}\int_{V_c}\frac{|\mathbf{E}_0|^2}{|E_{0\max}|^2}d\nu$ (E_{0max} is the highest electric field intensity value which locates in the center of the rectangular cavity)[69]. K is a shape factor which is dominant by the geometry of the inserted sample due to the different polarization in the sample

with different shapes. Equating the real and imaginary parts on both sides of eq(2.6), the equation can be separated and following relationships could be obtained [70]:

$$\Delta f = C_1 K(\varepsilon' - 1) \tag{2.7}$$

$$\Delta(\frac{1}{Q}) = C_2 K^2 \varepsilon'' \tag{2.8}$$

C_1 and C_2 are constants. For a spherical inserted sample, K is $\frac{3}{\varepsilon' + 2}$ [70]. The following expressions can be derived:

$$\Delta f = k_1 \frac{\varepsilon' - 1}{\varepsilon' + 2} \tag{2.9}$$

$$\Delta(\frac{1}{Q}) = k_2 \frac{\varepsilon''}{(\varepsilon' + 2)^2} \tag{2.10}$$

k_1 and k_2 are constants to be determined.

2.1.2 *Dielectric Property Measurement System and Procedure*

The experimental system is shown in Figure 2-1. A rectangular single-mode resonant cavity resonating at around 434 MHz was manufactured. The dimension of the cavity is 680 × 400 × 350 mm. Copper plates were used to manufacture the cavity due to its low cost and excellent conductivity (to prevent electromagnetic leakage).

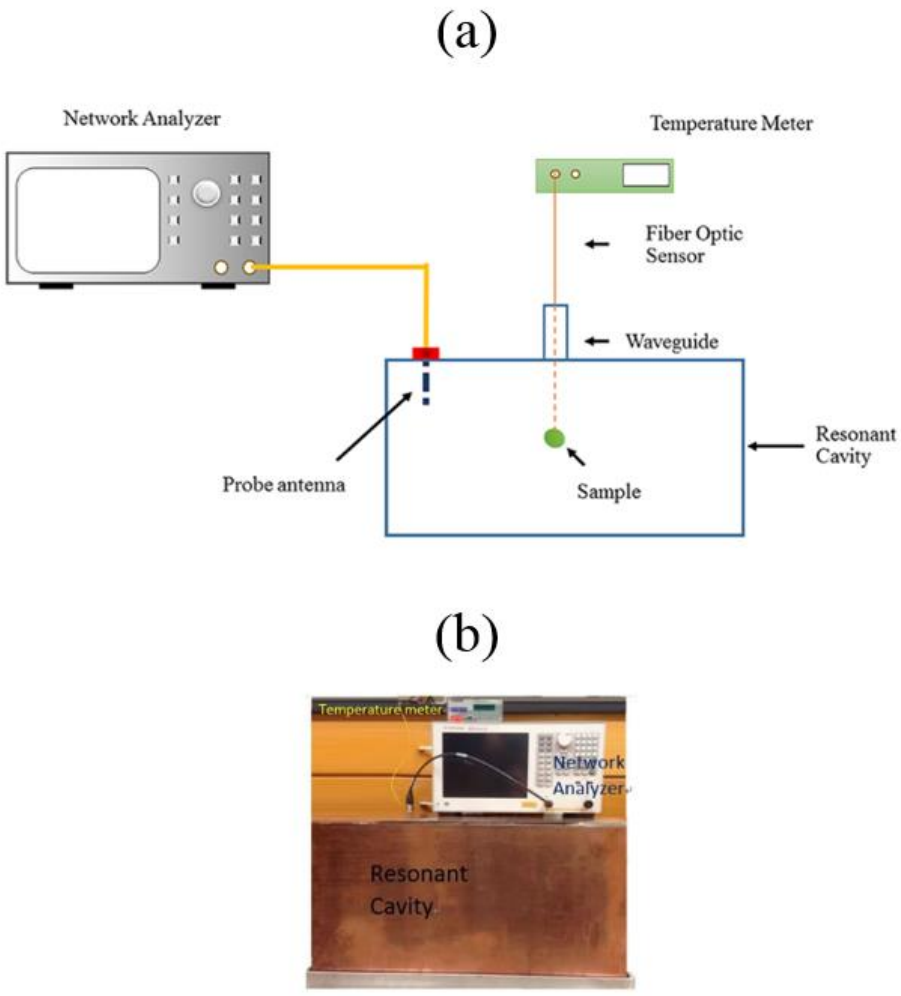

Figure 2-1. Dielectric measurement system. (a) Schematic of the system for measurement of dielectric properties. (b) A front view of the measurement system.

The vitrification solutions, held in a thin plastic spherical shell manufactured in machine shop (18mm radius) was transferred from a −80 ºC freezer to the center of the cavity. The temperature of the sample was gradually increased by the (very slow) warming of natural convection. This method was chosen in preference to using a precise temperature control apparatus because the presence of such a device in the cavity would influence the measurement.

The final temperature difference after the measurement with slow warming in the material was less than 5 °C. To avoid interfering with the electromagnetic field formed in the cavity (and therefore obtaining incorrect measurements), a fiber optic sensor connected to a temperature meter (Reflex, Neoptix, Quebec City, QC, Canada) instead of a thermocouple was inserted into the sample. The temperature was recorded with the fiber optic temperature meter. During the slow warming process, a network analyzer (E5061B, Keysight Technologies, Inc., Santa Rosa, CA, USA) was used to track the resonant frequency and reflection signal S_{11} at various low temperatures of the sample every 5. A simple and accurate analytic method [71] was adopted to calculate the quality factor from the power reflection coefficient.

2.1.3 *Calibration of the Measurement System*

Water, methanol, ethanol, 1-propanol, 2-propanol, ethylene glycol and cyclohexane samples with known properties were used for calibration of the cavity to determine k_1 and k_2. The properties of these calibration solutions are listed in Table 2-1 [72].

Table 2-1 Values of the dielectric properties of available materials in literature for calibration [72]

Substance	Dielectric constant	Dielectric loss
Water	80	1.9
Methanol	33	3.52
Ethanol	22	7.04
1-Propanol	13	8.57
2-Propanol	12	8.08
Ethylene glycol	36	12.09
Cyclohexane	2.02	0

Figure 2-2 shows the resonant frequency shift of the cavity with different calibration solutions. Figure 2-3 shows the quality factor change. The correlation factor R-Square is 0.9943 for the fitting of frequency change and 0.989 for the fitting of quality factor, which demonstrate a good linearity, and consistent with the theoretical derivation. From the linear regression, k_1 = 0.964 MHz and k_2 = 0.2826.

Once k_1 and k_2 had been obtained, unknown cryopreserved materials were inserted into the cavity. Similarly, the resonant frequency and quality factor were changed. According to the shift frequency and quality factor of the cavity, complex permittivity of samples can be derived [51]:

$$\varepsilon' = \frac{k_1 + 2\Delta f}{k_1 - \Delta f} \tag{2.11}$$

$$\varepsilon'' = \frac{1}{k_2}(\varepsilon' + 2)^2 \Delta(\frac{1}{Q}) \tag{2.12}$$

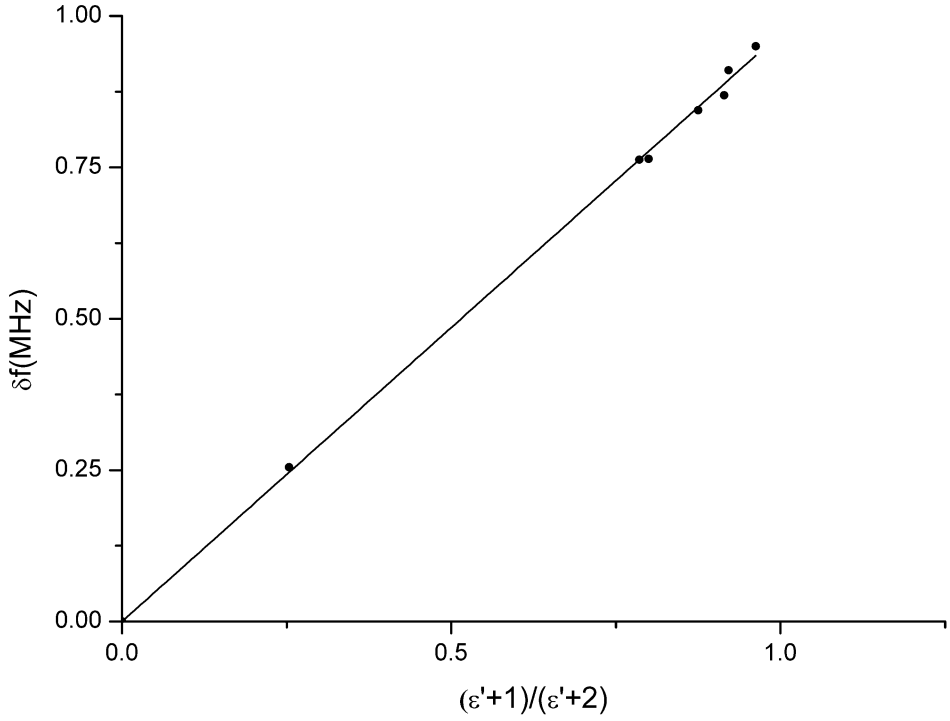

Figure 2-2. Resonant frequency shift of the resonant cavity after loading different calibration solutions: water, methanol, ethanol, 1-propanol, 2-propanol, ethylene glycol and cyclohexane.

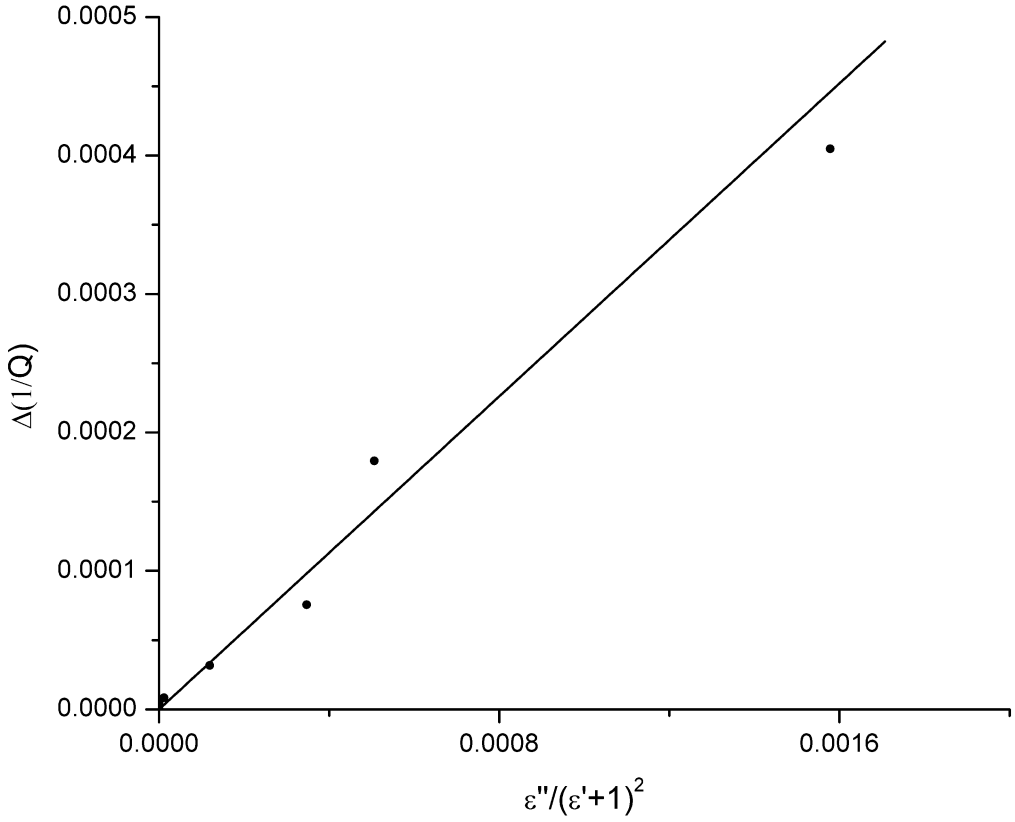

Figure 2-3. Inverse of quality factor change of the resonant cavity after loading different calibration solutions: water, methanol, ethanol, 1-propanol, 2-propanol, ethylene glycol and cyclohexane.

2.2 DETERMINATION OF THE THERMAL PROPERTIES

2.2.1 *Measurement of Specific Heat*

To determine the temperature-dependent specific heat capacity, Differential Scanning Calorimetry (Perkin Elmer DSC 8000) is used to take accurate measurement of various vitrification solutions. DSC precisely measure the heat flow through the vitrification solution samples. Isothermal step scan method is adopted to minimize the experimental error.

$$\Delta Q_{DSC} = C_p m \Delta T \tag{2.13}$$

ΔQ_{DSC} is the heat flow through the vitrification solution sample. m is the mass of vitrification solution sample. T is the temperature. The heat flow at each temperature was obtained at cooling and rewarming process. Each set of vitrification solution sample was measured for three times. The latent heat was incorporated into the effective specific heat capacity when the phase transition occurs.

Figure 2-4. Differential scanning calorimetry.

2.2.2 *Measurement of Thermal Conductivity*

Thermal conductivity of CPA solutions is measured using a micro thermal sensor developed by Liang, *et al*. [73] and manufactured in our lab. The sensor works on the principle of Transient Hot Wire (THW). This miniaturized device utilizes a SiO2/Au/SiO2 sandwiched structure to protect the microfabricated serpentine gold coil, which functions as both the heater and a passive thermometer. The sensor has already been tested and shown to measure thermal conductivity of biomaterials and solutions with high accuracy, repeatability and reliability. All experiments were performed more than 3 times at 20 °C.

2.3 VITRIFICATION SOLUTIONS

Electromagnetic rewarming is the only possible solution to rewarm large tissues and organs. The vitrification is the most promising approach to achieve successful tissue and organ preservation. To optimize the electromagnetic rewarming process, the fundamental requirement is to select optimal vitrification solutions. Most cryobiologists focus on the study of toxicity, the tendency to achieve vitrification of vitrification solutions. This study to preselect vitirfication solution by measured properties is based on the previous study which focus on the design and toxicity of vitrification solutions by Fahy [74]. Then from the perspective of electromagnetic rewarming, these representative vitrification solutions were analyzed based on the measurement results of material properties and the following rewarming results obtained in the numerical simulation. The composition of the vitrification solutions is shown in Table 2-2 [74].

Table 2-2 Composition of tested vitrification solutions [74]

Solution	Composition	Concentration (g/dl)			
		D	E	P	PVP
DPVP	D+PVP	41			6
EPVP	E+PVP		44		6
PPVP	P+PVP			36	6
DPPVP	DP+PVP	20		20	6
EPPVP	EP+PVP		20	20	6

D: dimethyl sulfoxide; E: ethylene glycol; P: propylene glycol; PVP: polyvinylpyrrolidone K30(M_r~40,000Da)

2.4 MEASUREMENT RESULTS OF TESTED VITRIFICATION SOLUTIONS

2.4.1 *Dielectric Properties of Tested Vitrification Solutions*

Figure 2-5 shows the variation in the dielectric constant ε' of the vitrification solutions over temperature. For all the vitrification solutions, the dielectric constant increased as temperature increased throughout the subzero temperature range. Figure 2-6 shows the dielectric loss ε'' of the vitrification solutions in this low-temperature range. The electromagnetic power decreases exponentially from the boundary to the center. Penetration depth δ is used to define the distance that the electromagnetic power has decreased to 1/e (e is natural constant ~ 2.7183) of its initial magnitude at the surface. Once the dielectric properties ε' and ε'' of a material are known, δ can be determined by [75]

$$\delta = \frac{c}{2\pi f \sqrt{2\varepsilon \left[\sqrt{1+\left(\frac{\varepsilon''}{\varepsilon'}\right)^2} - 1 \right]}} \tag{2.14}$$

The penetration depth of electromagnetic waves into the vitrification solutions at different low-temperature ranges was calculated based on the results of dielectric properties ε' and ε''. The penetration depth in the subzero temperature range for these vitrification solutions is shown in Figure 2-7.

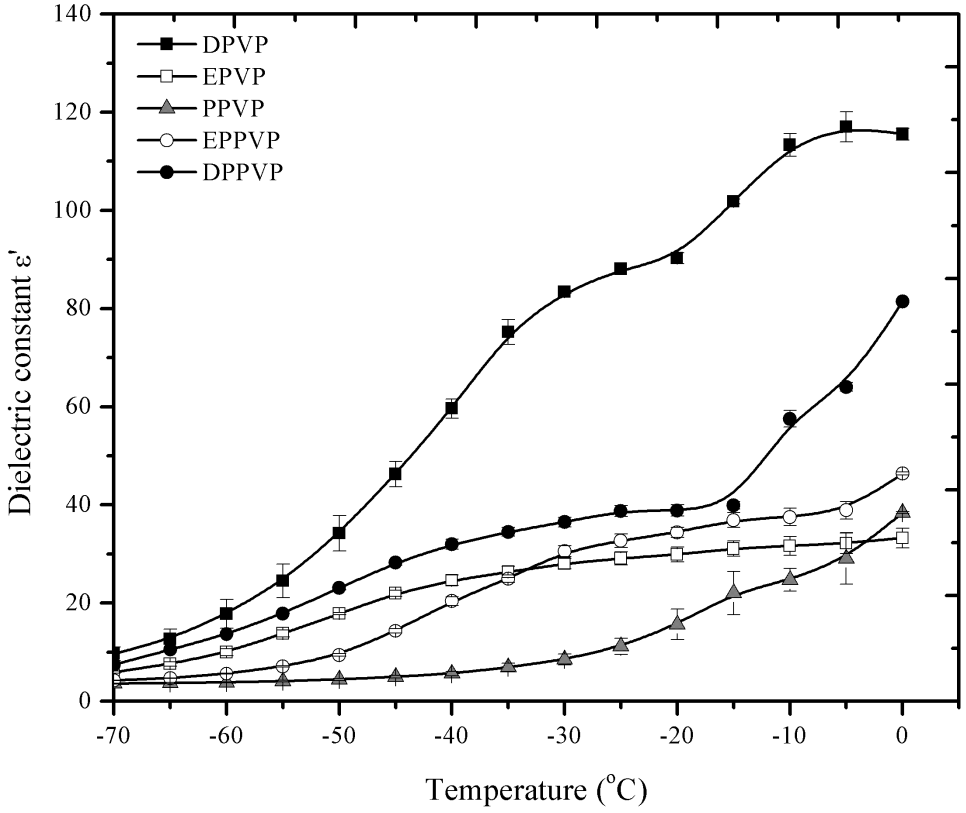

Figure 2-5. Dielectric constant of different kinds of vitrification solutions in the low temperature range.

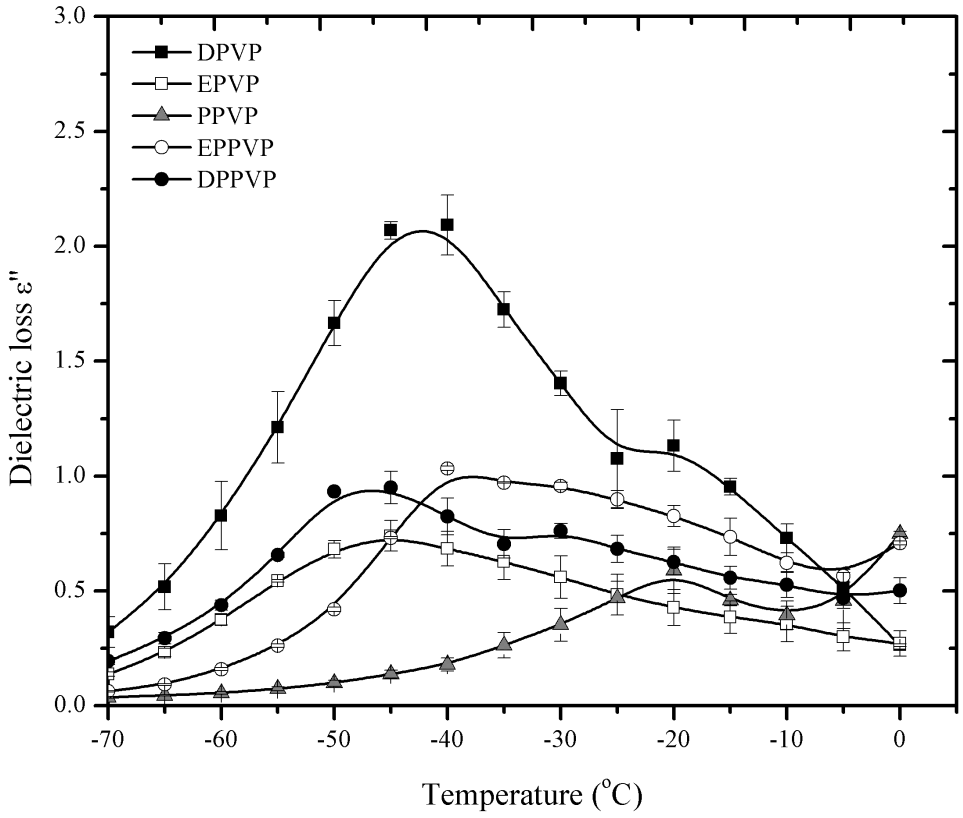

Figure 2-6. Dielectric loss of different kinds of vitrification solutions in the low temperature range.

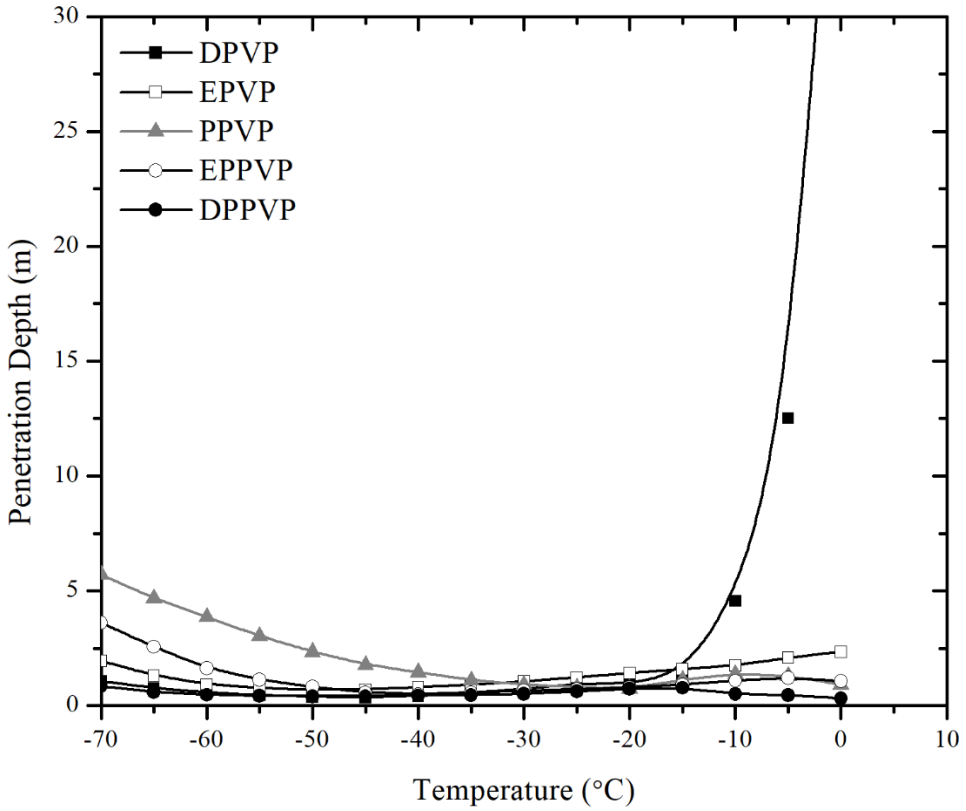

Figure 2-7. Penetration depth of different kinds of vitrification solutions in the low temperature range.

2.4.2 *Thermal Properties of Tested Vitrification Solutions*

After measuring by DSC, the specific heat of tested vitrification solutions during the low temperature range is shown in Figure 2-8.

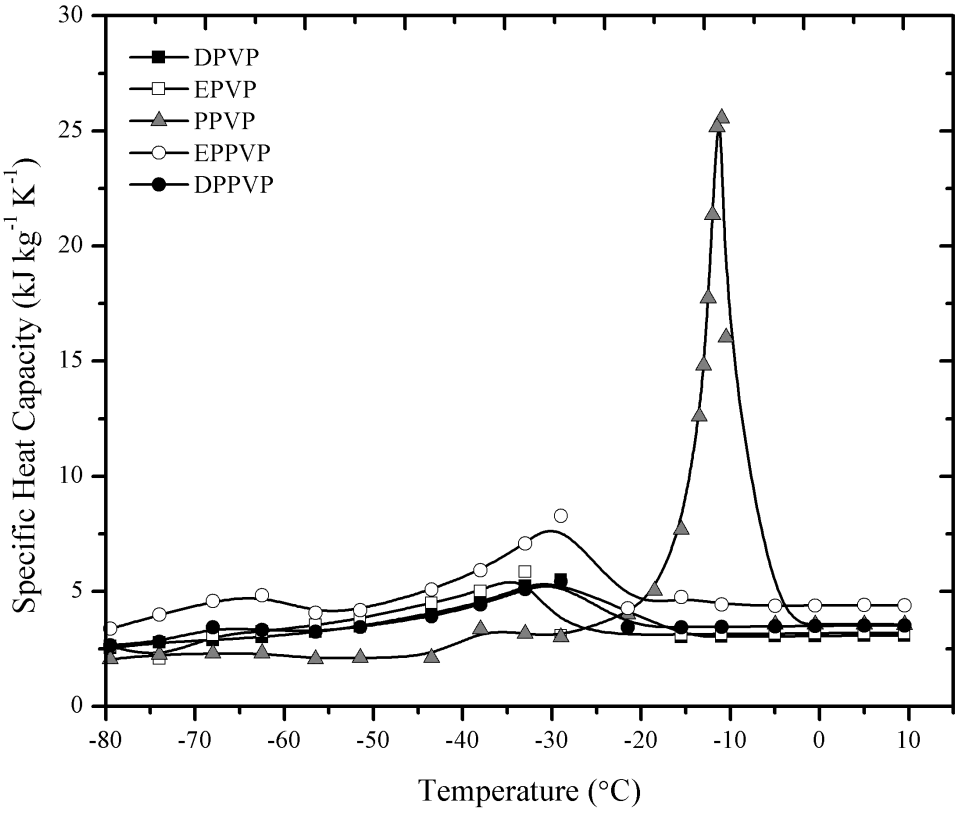

Figure 2-8. Specific heat of different kinds of tested vitrification solutions.

The thermal conductivity and density of tested vitrification solutions were measured and the results are shown in Table 2-3.

Table 2-3 Thermal properties of tested vitrification solutions

Solution	Density (g/ml)	Thermal conductivity (W/m·K)
DPVP	0.92	0.408
EPVP	0.894	0.407
PPVP	0.796	0.454
DPPVP	0.932	0.423
EPPVP	1.018	0.542

2.5 Discussion of the Physical Properties for Electromagnetic Resonance Rewarming

The shortest penetration depth of the tested CPA solutions at subzero temperature was 0.36 m (−45 °C DPVP solution). The characteristic size (diameter of a sphere) of cryopreserved samples heated by electromagnetic systems was limited to within 6 cm. At this scale of sample size, traditional water-bath warming could lead to a large temperature gradient. Since the penetration depths are much larger, electromagnetic waves could penetrate into the core of these tested CPA solutions. The vitrification solutions we tested can be applied in the electromagnetic heating application.

The combined heat transfer equation with electromagnetic energy as a heat source is shown in eq.(2.15). If the electromagnetic field intensity is sufficiently high, the heat source due to the temperature gradient (first term on the right-hand side of eq.(2.15)) can be ignored. In the second term, the electromagnetic energy source is the major contributor to the heating of a material.

$$\rho C \frac{\partial T}{\partial t} = \nabla \cdot (k \nabla T) + \pi f \varepsilon_0 \varepsilon'' \left| \mathbf{E} \right|^2 \tag{2.15}$$

Dielectric loss ε'' characterizes the ability to absorb electromagnetic power. For different CPA solutions, dielectric loss ε'' is key in determining how fast the solution could pass through the frozen zone: the larger the dielectric loss, the absorption of electromagnetic energy by the material is more efficient, which leads to an increased heating rate. The dielectric loss of all the CPA solutions we tested was small when the temperature was lower than −70 °C. This indicates that the heating of the frozen CPA/vitrification solutions by electromagnetic waves should be relatively slow initially. Based on our measurement, the dielectric property values change very little when the temperature is lower than −70 °C. In cryopreservation, the dangerous temperature range is between −70 °C and 0 °C (more specifically −60 °C to −5 °C) [15]. Therefore, we did not measure the dielectric property values starting from −196 °C . As the temperature increases, the dielectric loss of all the solutions increases until a peak is reached. For the five CPA/vitrification solutions, the temperature corresponding to this peak varies from −45 °C to −20 °C; then the dielectric loss decreases as the temperature increases further. The dielectric loss of PPVP increased after reaching its lowest point as the temperature increased further. For DPVP and EPVP, whilst in the subzero temperature range, the dielectric loss continued to decrease with increasing temperature, until the temperature reached 0 °C.

The inverted ‘U’ shape of DPVP and EPVP solutions reveals that after their peak values, their dielectric loss decreases as temperature increases. Therefore, the warming rate of the area at higher temperature would slow down, and the colder area could be heated relatively more quickly to reduce the intra-sample temperature difference. Among these CPA/vitrification solutions, DPVP has a higher dielectric loss. The higher dielectric loss may lead to a higher

ability to absorb electromagnetic energy, provided with same magnitude of electric field intensity.

In the measurement of thermal properties, no significant difference in the density of different vitrification solutions was observed. For traditional boundary warming method (water bath), thermal conductivity plays a vital role in the heat transfer within the sample by conduction. Using the MEMS sensor, the thermal conductivity of tested CPA solutions was determined (Table 2-3). Consider the heat transfer equation(2.15), when the electromagnetic energy serves as the major heating energy source, the heating due to heat conduction within the sample (first term in the right hand side of equation (3)) has less contribution to the temperature change.

The experimentally determined heat capacity is of higher significance in the numerical simulation. The amount of latent heat may greatly affect the warming rate in the context of phase transition. Here enthalpy method was used to simulate the phase-change cases. Among the five different CPA solutions, the effective specific heat of PPVP and EPVP are much higher (Figure 2-9), which demonstrates more energy required for the rapid rewarming. Based on the analysis of determined electric and thermal properties, DPVP has a higher absorption ability of the electromagnetic field energy while relative lower specific heat, which should have a superior warming rate than the other CPA solutions.

It is found that the error in the dielectric loss measurement is larger than that of dielectric constant. In the calibration processes, the linearity of the quality factor change related to ε'' and ε' is not as good as the linearity of frequency change related to ε'. The calibration process should incorporate more solutions to reduce the error. During the slow warming of sample solutions by natural convection, the temperature profile is not uniform: a maximum temperature

difference of 5 ºC between the surface and the core was observed. This inconsistent temperature brings some uncertainty to the dielectric properties of CPA solutions at a specific temperature. This system error could be minimized if using an advanced temperature control device which could achieve desired low temperatures.

2.6 CONCLUSION

The aim of this investigation was to find optimal vitrification solutions for electromagnetic rewarming. A dielectric property measurement system for vitrification solutions and biomaterials was designed and set up in this work. The cavity perturbation technique was utilized in the measurement system. The linearity of frequency shift and quality factor change in calibration results show that the resonant cavity returns results that are concordant with theoretically estimated values. We measured several vitrification solutions in the subzero temperature range and calculated penetration depths in vitrification solutions based on the experimental results. The penetration depths are deep enough for electromagnetic waves to propagate into and heat the tested vitrification solutions. Among these vitrification solutions, DPVP (41% DMSO and 6% PVP) solution is preferred in electromagnetic warming, due to its relatively smaller specific heat, higher dielectric loss ε'' and the inverted U shape of its dielectric loss graph in the subzero temperature range. The warming rate would be higher and thermal runaway problem could be minimized if this vitrification solution were adopted in electromagnetic rewarming. This study focuses only the selection of vitrification solutions for an efficient and uniform rewarming by electromagnetic heating system. The dielectric measurement system can be used to determine optimal CPA/vitrification solutions or biomaterials for electromagnetic rewarming in cryopreservation. It may also be beneficial other biomedical

applications involving electromagnetic waves such as microwave heating hyperthermia therapy or microwave tomographic imaging.

Chapter 3. Optimization of Electromagnetic Resonance Assisted With Numerical Simulation

3.1 INTRODUCTION

Previous cryobiologist have developed electromagnetic cavity rewarming for cryopreserved tissues and organs. Evans[76], Robinson [51] and Luo [77] built electromagnetic heating systems that could resonate at around 434MHz, but working at different modes. The sample was placed at the center with a large magnitude of the electric field, which is critical to rapid rewarming. The size of the sample was controlled to reduce temperature gradients resulted from the electromagnetic field attenuated away from the center. For multimode resonant cavity rewarming system, it could be difficult to control the resonant state or field distribution with several electromagnetic power inputs. While single mode cavity system [77] is easier to concentrate a strong electromagnetic field and control in the rewarming process. Therefore, multimode resonant rewarming systems are excluded for optimization here. In previous electromagnetic rewarming tests, the number of vitrification solutions is limited partly due to the inability to establish electromagnetic rewarming systems or a lack of understanding of vitrification in the early time. According to the warming results, electromagnetic rewarming has already demonstrated more effective than traditional water bath method. But it still needs to be improved, particularly in combination with the vitrification. Ideal vitrification solutions for different cells, tissues are different. Therefore, further optimization of the electromagnetic rewarming system is carried out.

Several theoretical studies have been performed [78-80] to provide guidance for the design of electromagnetic rewarming systems aiming to avoid those unsatisfactory effects

associated with electromagnetic rewarming. Method of moments (MoM) was used to predict the electric field distribution [79] and the finite-difference time-domain (FDTD) method was used to determine the electromagnetic rewarming temperature distribution [81]. But these two models consume much computing resource for curve-shaped samples. A resonance rewarming model with addition of nanoparticles for enhanced warming rate was tested [82]. However, in the simulation the application of 8000 W power input for electromagnetic cavity rewarming [83] is not realistic currently. Another model [84] adopted a combination of water bath and a radiofrequency antenna heating, but even with nanoparticles, this models is not feasible yet in cryopreservation due to a high thermal gradient (28.7 °C mm^{-1}). Recently, the utilization of radiofrequency (RF, a frequency band in the electromagnetic wave spectrum) coil heating achieved rapid rewarming for large samples [85, 86]. The rapidity and uniformity of the magnetic heating rely on the high concentration of nanoparticles incorporated in the cryopreserved materials. Optimization of rewarming systems and CPA solutions may reduce the amount of added nanoparticles to avoid possible side effects associated with the high dosage of nanoparticles.

In this chapter, a more efficient and effective model based on finite element method combining electromagnetic wave propagation and heat transfer process was presented and validated. The optimization of the shape of cryopreserved sample was performed numerically. Since CPA solutions play a critical role in preventing cryoinjuries and dominate the properties of the cryopreserved biomaterials [52], the essential physical properties of several CPA solutions including complex permittivity, specific heat, and thermal conductivity characterized experimentally in Chapter 2 were used in this simulation test. The optimum CPA solution was determined using the numerical model. Finally, based on the numerical optimization of the

sample shape and CPA type, a conceptual hybrid electromagnetic-conduction heating method was proposed, experimentally tested, and compared with the conventional electromagnetic heating, which turned out to be a promising method to reduce the non-uniformity of electromagnetic heating. This work provides insights on the selection of vitrification solutions and development of the electromagnetic rewarming system in pursuit of ultimate organ preservation.

3.2 THEORETICAL FORMULATION

In this chapter, the fundamental configuration of the electromagnetic rewarming system illustrated in Figure 3-1 is based on our previous design, which includes an electromagnetic signal source and a resonant chamber to concentrate electromagnetic energy in the center where cryopreserved materials were heated. The electromagnetic wave is fed into this rectangular cavity through a coaxial transmission line. A probe antenna is used to excite the electric field and establish a standing wave pattern of electromagnetic field in the rectangular resonant cavity. The highest electric field intensity is achieved in the center where the cryopreserved sample is located.

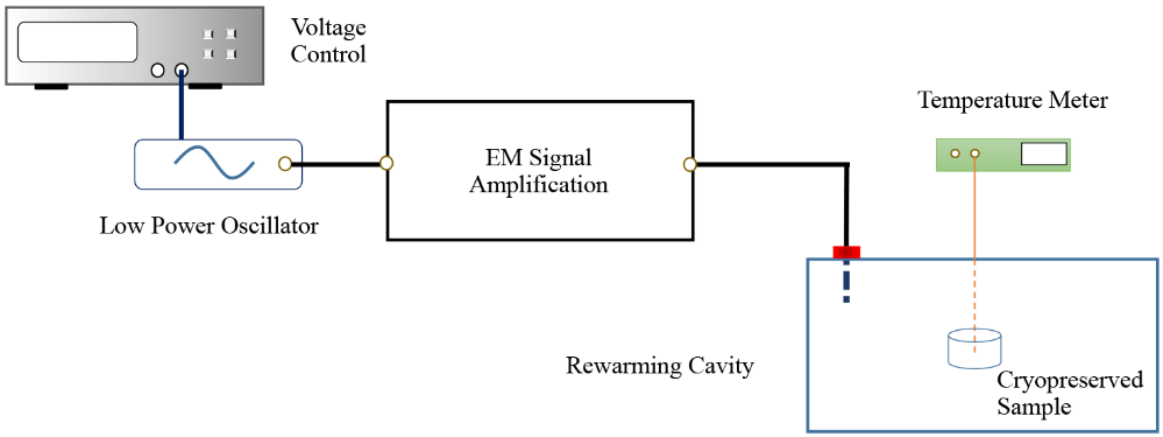

Figure 3-1. Schematic description of the experimental setup of the electromagnetic rewarming system.

3.2.1 *Electromagnetic and heat transfer analysis*

For a nonmagnetic material, e.g. the cryopreserved tissue, with electric parameters of ε (complex electric permittivity, F m^{-1}), σ (electrical conductivity, S m^{-1}), and $\mu = \mu_0$ (magnetic permeability of the free space, H m^{-1}), the electric field distribution in the material can be determined by solving the following frequency domain Maxwell equations:

$$\nabla \times \mathbf{E} = -j\omega\mu\mathbf{H} - \mathbf{M} \tag{3.1}$$

$$\nabla \times \mathbf{H} = -j\omega\varepsilon\mathbf{E} + \sigma\mathbf{E} + \mathbf{J} \tag{3.2}$$

where $\mathbf{E}$ (V m^{-1}) and $\mathbf{H}$ (A m^{-1}) are the electric field and magnetic field components. $\mathbf{M}$ (A m^{-1}) and $\mathbf{J}$ (A m^{-2}) are the equivalent primary sources which can be omitted because no magnetic or electrical current source exists in the domain. ω (rad s^{-1}) is the angular frequency of the EM field. The complex electric permittivity $\varepsilon = \varepsilon' - i\varepsilon''$. The real part ε', also known as dielectric constant represents the ability of storing electric field energy. The imaginary part ε'', known as dielectric loss, represents the ability to absorb electric field energy. This energy

absorption or dielectric heating is due to the vibration of molecular dipoles under the influence of electromagnetic field. The absorbed power density q in the material is given by:

$$q = \pi f \varepsilon_0 \varepsilon'' |\mathbf{E}|^2 \tag{3.3}$$

where f (Hz) denotes the freuqency of the electromagnetic field. q (W m^{-3}), the total absorbed power from the electromagnetic field, can be combined into the heat transfer equation as the heat source term [87]:

$$\rho C \frac{\partial T}{\partial t} = \nabla \cdot (k \nabla T) + \pi f \varepsilon_0 \varepsilon'' |\mathbf{E}|^2 \tag{3.4}$$

where ρ (kg m^{-3}) denotes the density of the cryopreserved material, C (J kg^{-1} K^{-1}) stands for the specific heat, k (W m^{-1} K^{-1}) is the thermal conductivity, T (K) is the temperature of the material and t (s) is the time.

In this numerical study, the cryopreserved material properties were set to be dependent on temperature based on experimental measurements. After determining the temperature distribution from (4), the thermal and electrical properties were updated accordingly. Electromagnetic field distribution was altered with material parameters updated with the temperature. Thereafter the heating source was updated by the applied electromagnetic field and the sample's dielectric loss ε''. Hence, the temperature and electromagnetic fields are coupled. The boundary conditions of the sample was set to be adiabatic ($q_{conv} = 0$) which excludes natural convection. The inner wall of the resonance chamber was set to be perfect conductor ($\vec{n} \times \mathbf{E} = 0$, $\vec{n}$ represents the unit vector of the electromagnetic cavity inner surface).

3.2.2 *Hybrid electromagnetic-conduction rewarming*

In the following experiment test after numerical study, we propose that a combination of conduction and electromagnetic heating may facilitate the uniformity of the post-thawing profile.

An embedded rod which has a higher efficiency in absorbing electromagnetic energy was inserted in the center of cryopreserved material. As shown in Figure 3-2, a central auxiliary rod was designed to be heated up by the electromagnetic field in the same mechanism described above but at a higher warming rate than the cryopreserved sample material, serving as a conduction heat source to the surrounding cryopreserved material to reduce the temperature difference within the sample and minimize thermal runaway effect.

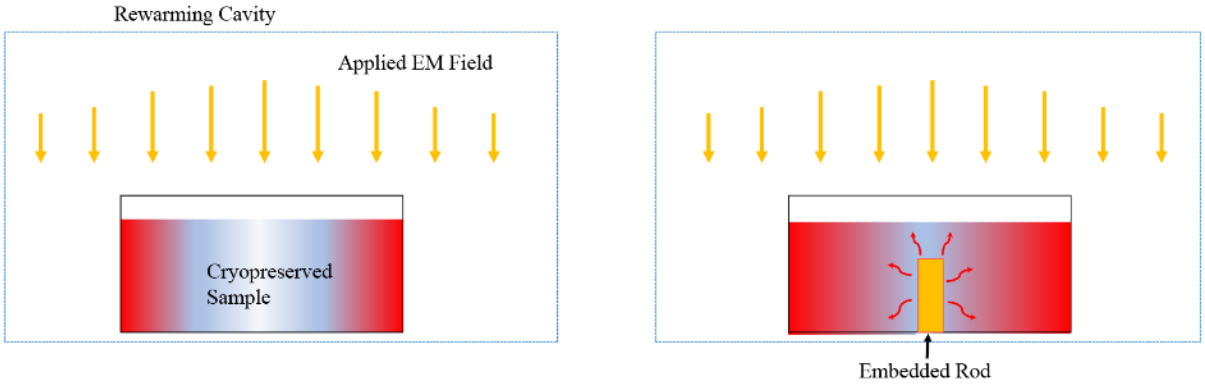

Figure 3-2. Illustration of the electromagnetic heating and proposed hybrid EM-conduction heating mechanism.

3.3 NUMERICAL SIMULATION

Adopting finite element method, the numerical simulation was performed using COMSOL Multiphysics software 5.1(COMSOL, Burlington, MA, USA). The combined electromagnetic and heat transfer process within the rewarming chamber as shown in Figure 3-3 was performed following the procedure (Figure 3-4) discussed in the previous theoretical formulation part. In this simulation, the parameters of the numerical model were set as shown in Table 3-1 and the physical properties were determined by the methods as described in Chapter 2.

Table 3-1 Geometry and material properties of the cavity system.

Parameters	Value	Unit
Length of the cavity	680	mm
Width of the cavity	400	mm
Height of the cavity	350	mm
Probe antenna length	40	mm
Probe antenna radius	1.5	mm
Coaxial transmission line impedance	50	Ω
Power input	400	W
Electrical conductivity of Copper	5.59×10^{7}	S m^{-1}
Relative permittivity of Air	1	
Electrical conductivity of Air	0	S m^{-1}

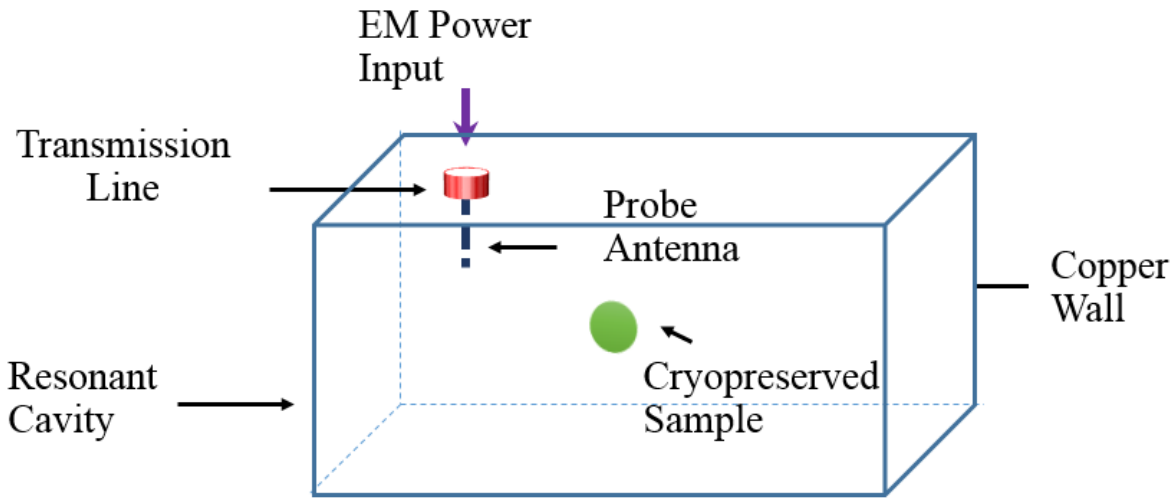

Figure 3-3. Schematic description of the simulated resonant electromagnetic rewarming cavity.

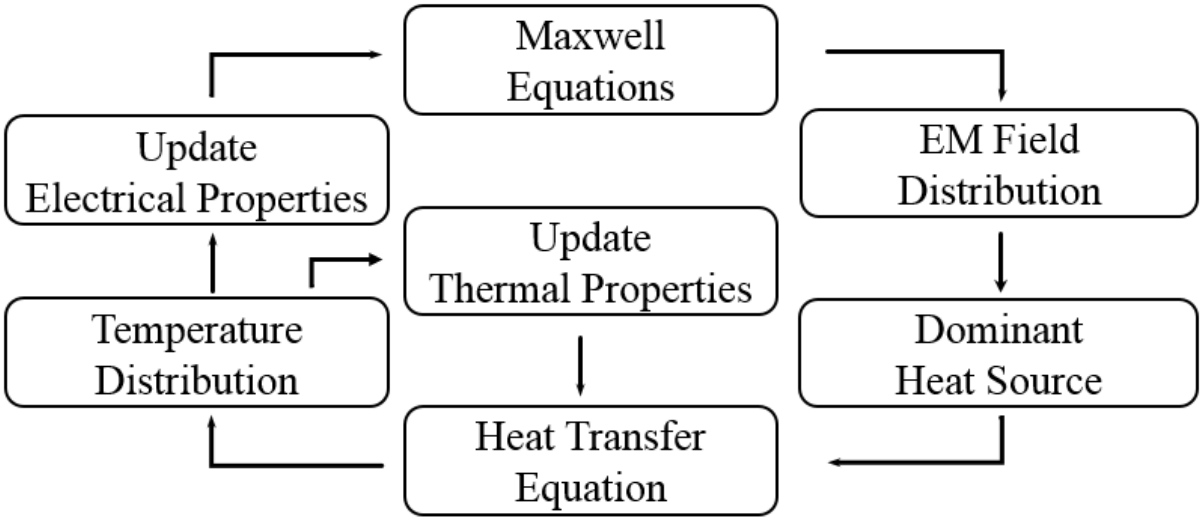

Figure 3-4. Computational flow chart description of the electromagnetic resonant rewarming.

As for the meshing grid of this numerical model, based on Nyquist criterion [88], the maximum element grid size should be less than half the wavelength of the electromagnetic wave. It was also suggested to use six grids per wavelength in finite element analysis solving Maxwell's equation [89]. The discretization of the rewarming system grid size was set to be smaller than those criteria using tetrahedral grids. The tetrahedron grid size of the cavity was less than one tenth of the wavelength of the input electromagnetic signal. In the mesh generation (shown as Figure 3-5), we used adaptive tetrahedral meshing and refined meshes near all boundaries (~988,000 elements were generated). A mesh-refinement was performed in the probe antenna area and the cryopreserved sample domain. If smaller grid size (~163,000 elements) was utilized, the temperature profile result difference was less than 0.5% over the entire domain.

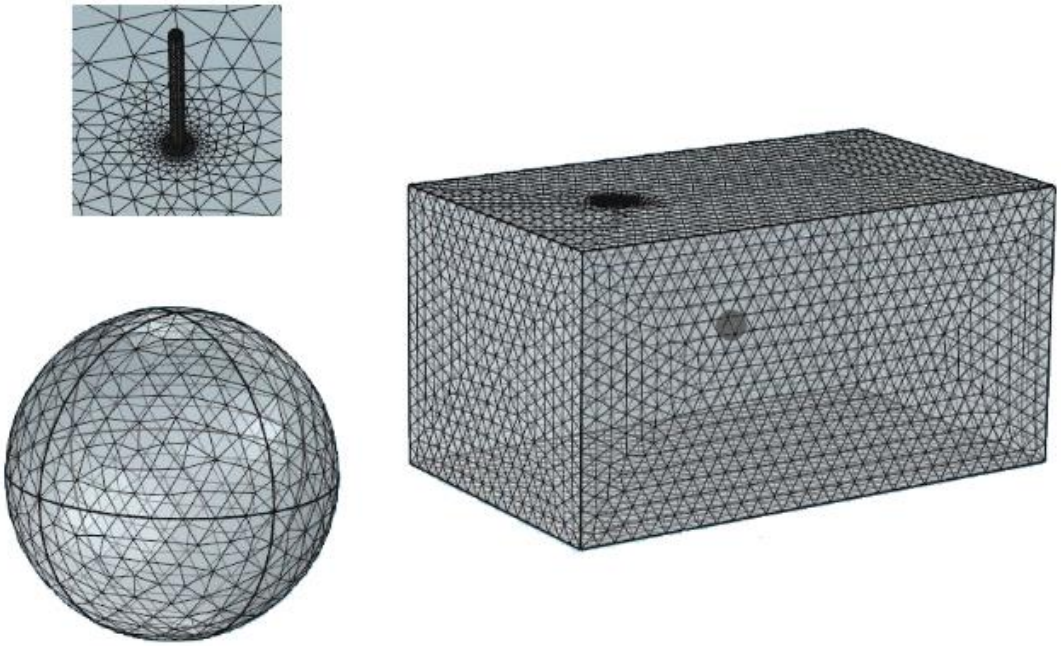

Figure 3-5. Geometric gridded model of the resonant cavity for simulation.

3.4 HEATING EXPERIMENT SETUP

A small electromagnetic signal was generated by a voltage controlled frequency synthesizer (Mini-Circuits, Brooklyn, NY, USA) and magnified by a power amplifier (OPHIR RF, Los Angeles, CA, USA). The amplified electromagnetic wave was transmitted into a resonant chamber manufactured with copper in university machine facility with dimensions 68 cm × 40 cm × 35 cm. Two types of sample holders were used in the rewarming experiment to test the hybrid warming enhancement. One was cylindrical and the other one was cylindrical holder with a central rod made of Micarta (Figure 3-6). This rod was chosen from a variety of materials because of a higher conversion rate of EM energy by testing in the heating system. The temperature was monitored by a fiber optic temperature meter (Micronor, Newbury Park, CA, USA).

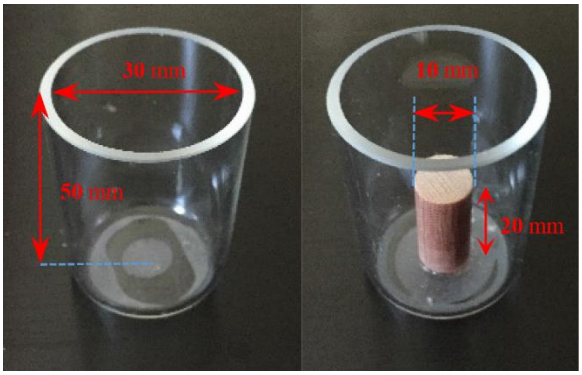

Figure 3-6. Photo of cylindrical sample holder and holder with an auxiliary heating rod.

3.4.1 *Single mode electromagnetic resonant cavity*

The resonant cavity is made of copper due to the good conductivity and relatively low cost. The cavity is designed to resonant at around 434 MHz in TE101 mode. To derive the dimensions of the resonant cavity, it should be started from Maxwell's equations which includes a group of partial differential equations on the basis of Gauss' Law, Faraday's Law and Ampere's Law. In the region with no electrical source (charges) and no magnetic source (currents) as in the space within the resonant cavity, the governing equations can be represented by:

$$\nabla \cdot \mathbf{E} = 0 \tag{3.5}$$

$$\nabla \cdot \mathbf{B} = 0 \tag{3.6}$$

$$\nabla \times \mathbf{E} = -\frac{\partial \mathbf{B}}{\partial t} \tag{3.7}$$

$$\nabla \times \mathbf{B} = \frac{1}{c^2}\frac{\partial \mathbf{E}}{\partial t} \tag{3.8}$$

where $c^2 = \dfrac{1}{\mu_0 \varepsilon_0}$, μ_0 and ε_0 are the permeability and permittivity of free space. Wave equations can be obtained by taking the curl of these equations:

$$\frac{1}{c^2}\frac{\partial^2 \mathbf{E}}{\partial t^2} - \nabla^2 \mathbf{E} = 0 \tag{3.9}$$

$$\frac{1}{c^2}\frac{\partial^2 \mathbf{B}}{\partial t^2} - \nabla^2 \mathbf{B} = 0 \tag{3.10}$$

with $\mathbf{B} = \mu \mathbf{H}$, $\frac{\partial^2 \mathbf{E}}{\partial t^2} = -\omega^2 \mathbf{E}$, also the boundary conditions for the cavity should apply:

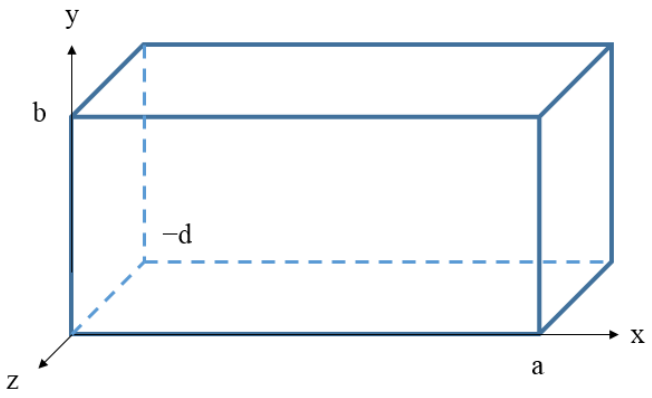

Figure 3-7. Rectangular waveguide geometric schematic.

$$E_x = E_z = 0 @ y = 0, b \tag{3.11}$$

$$E_y = E_z = 0 @ x = 0, a \tag{3.12}$$

$$E_x = E_y = 0 @ z = 0, d \tag{3.13}$$

By applying the boundary conditions with the wave equations, the electric field in x, y and z components can be solved:

$$E_x = \left(\frac{j\omega\mu}{h^2}\right)\left(\frac{n\pi}{b}\right)\cos\left(\frac{m\pi}{a}x\right)\sin\left(\frac{n\pi}{b}y\right)\sin\left(\frac{p\pi}{d}z\right) \tag{3.14}$$

$$E_y = -\left(\frac{j\omega\mu}{h^2}\right)\left(\frac{m\pi}{a}\right)\sin\left(\frac{m\pi}{a}x\right)\cos\left(\frac{n\pi}{b}y\right)\sin\left(\frac{p\pi}{d}z\right) \tag{3.15}$$

$$E_z = 0 \tag{3.16}$$

$$H_x = -H_0\left(\frac{1}{h^2}\right)\left(\frac{m\pi}{a}\right)\left(\frac{p\pi}{d}\right)\sin\left(\frac{m\pi}{a}x\right)\cos\left(\frac{n\pi}{b}y\right)\cos\left(\frac{p\pi}{d}z\right) \tag{3.17}$$

$$H_y = -H_0\left(\frac{1}{h^2}\right)\left(\frac{n\pi}{b}\right)\left(\frac{p\pi}{d}\right)\cos\left(\frac{m\pi}{a}x\right)\sin\left(\frac{n\pi}{b}y\right)\cos\left(\frac{p\pi}{d}z\right) \tag{3.18}$$

$$H_z = H_0\cos\left(\frac{m\pi}{a}x\right)\cos\left(\frac{n\pi}{b}y\right)\sin\left(\frac{p\pi}{d}z\right) \tag{3.19}$$

Where m, n = 0, 1, 2…, p = 1, 2, 3… m and n can't be 0 at the same time. $h^2 = \left(\frac{m\pi}{a}\right)^2 + \left(\frac{n\pi}{b}\right)^2$.

The resonant frequency for TE_{mnp} modes is given by:

$$\left(f_r\right)_{mnp}^{TE} = \frac{1}{2\pi\sqrt{\mu\varepsilon}}\sqrt{\left(\frac{m\pi}{a}\right)^2 + \left(\frac{n\pi}{b}\right)^2 + \left(\frac{p\pi}{d}\right)^2} \tag{3.20}$$

In this work, TE_{101} mode was selected. The geometry of the cavity is length: 0.4m, width: 0.35m and depth: 0.68m. It was designed to resonant at around 434 MHz.

3.5 RESULTS

3.5.1 *Field distributions in the resonant chamber*

The validation process was carried out first to validate the numerical model. The resonant frequency computed by the model was 434.767 MHz, which was the same as the analytic solution. At the resonant state, the numerical result of normalized electric field distribution in the resonant cavity was plot in comparison with the analytic solution (Figure 3-8), which indicated a good agreement between these results. The intensity of the electric field inside the chamber increases drastically with the position approaching the center where cryopreserved samples are placed. Thus the electromagnetic energy can be intensified at the center and utilized at a significantly high efficiency under a resonance state.

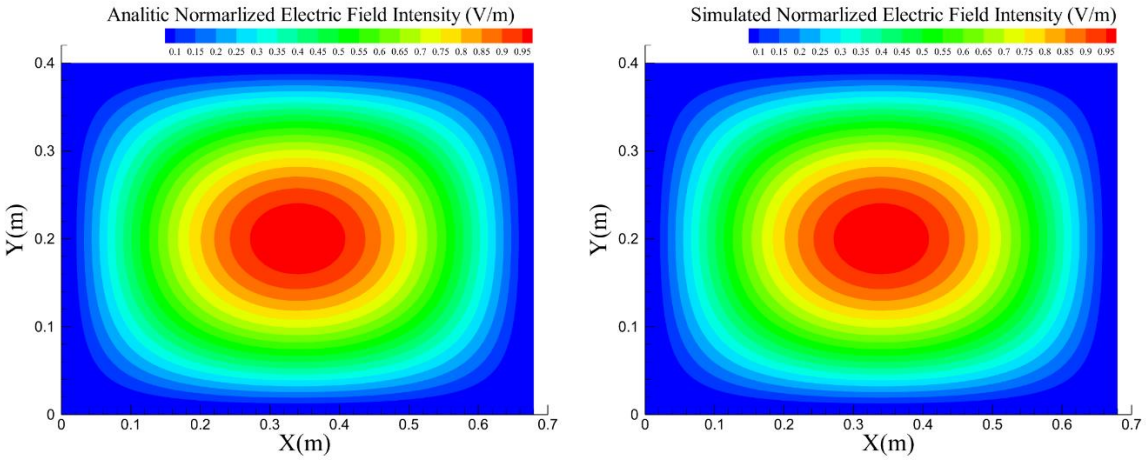

Figure 3-8. Distribution of the electrical field magnitude at the central cross-sectional plane in the electromagnetic rewarming chamber. Analytical and simulated results show that electric field energy is focused in the center of the cavity.

3.5.2 *Rewarming result of 50% DMSO solution*

In addition to comparing the electric field intensity, the simulation of rewarming 24 mL 50% DMSO solution (a considerable volume in cryopreservation) from –80 °C to 0 °C was performed to validate the coupled electromagnetic-Heat transfer process. The configurations of the simulation including the onset rewarming temperature, applied electromagnetic frequency (around 430 MHz), and 400 W source power input were consistent with the previous experimental study [77]. Before performing the numerical simulation, physical properties were determined. The thermal conductivity k was 0.468 W m^{-1} K^{-1} and the density was 1.056 g mL^{-1} at room temperature. Both were set as constants in the simulation. Figure 3-9 and Figure 3-10 show the complex permittivity and specific heat of 50% DMSO solution in the subzero temperature range. The simulated warming process demonstrated the same trend with experimental result as shown in Figure 3-11. The consistency between the numerical simulation and experimental heating results confirmed the reliability of this numerical model. In the numerical simulation, the resonant cavity which converts electromagnetic energy into heat was assumed to be an ideal resonator. Thus, the slightly lower warming rate (2.5 % difference) in the experiment may be due to the imperfect manufactured resonant chamber with undermined electromagnetic energy conversion ability. Caution should be exercised in the manufacturing of the electromagnetic resonant chamber. Electromagnetic energy leakage should be restricted to avoid decelerating the warming rate. Most electromagnetic rewarming experimental platforms used temperature sensors [72, 76, 90, 91] penetrating the cavity to monitor the real-time inside temperature of the cryopreserved material, which could lower the efficiency of the heating cavity. With an extensive temperature profile obtained by the numerical models, the number of sensors used in the experimental platforms may be reduced.

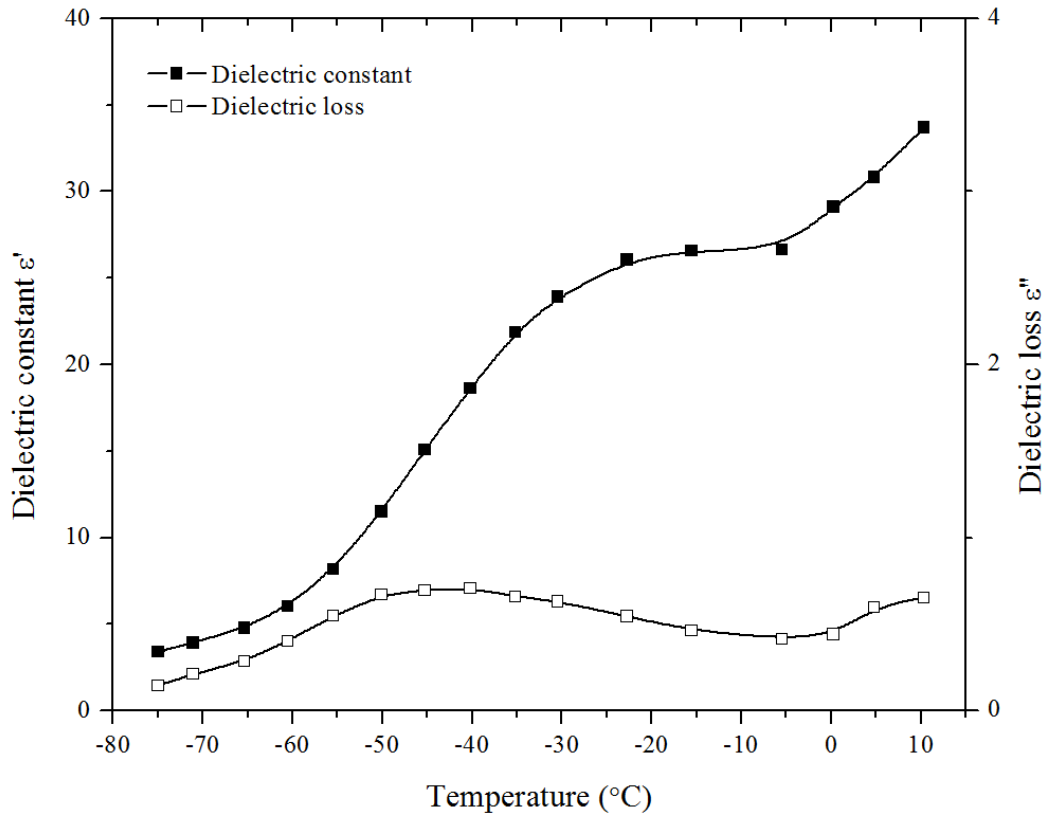

Figure 3-9. Complex electric permittivity of 50% DMSO solution [39].

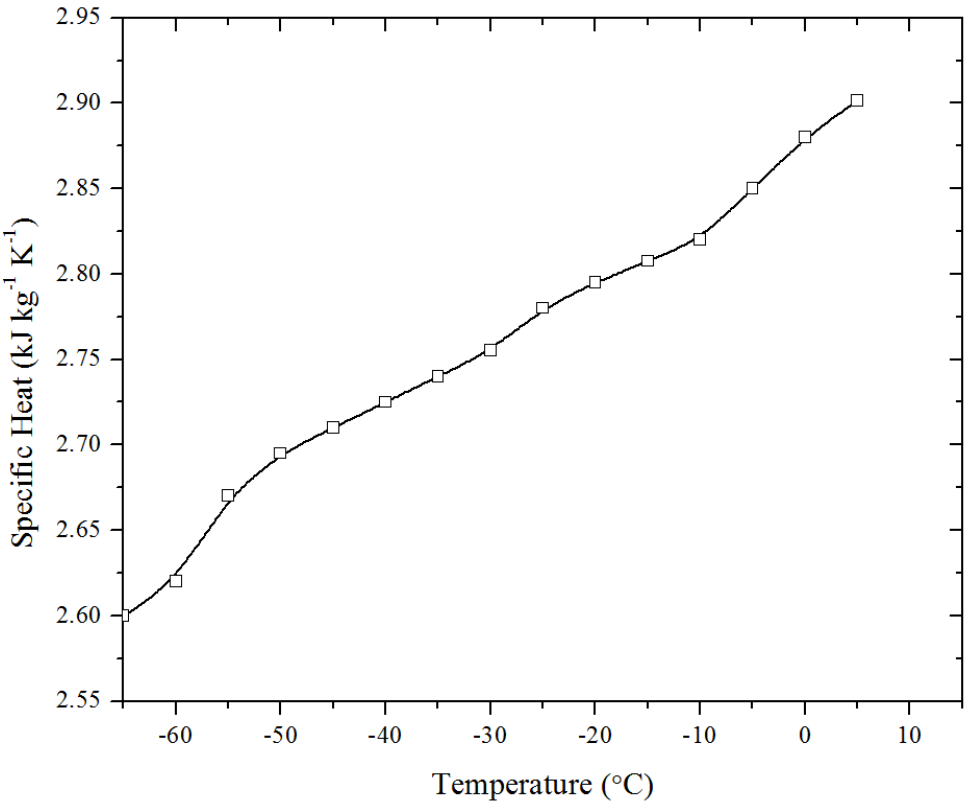

Figure 3-10. Specific heat of 50% DMSO solution.

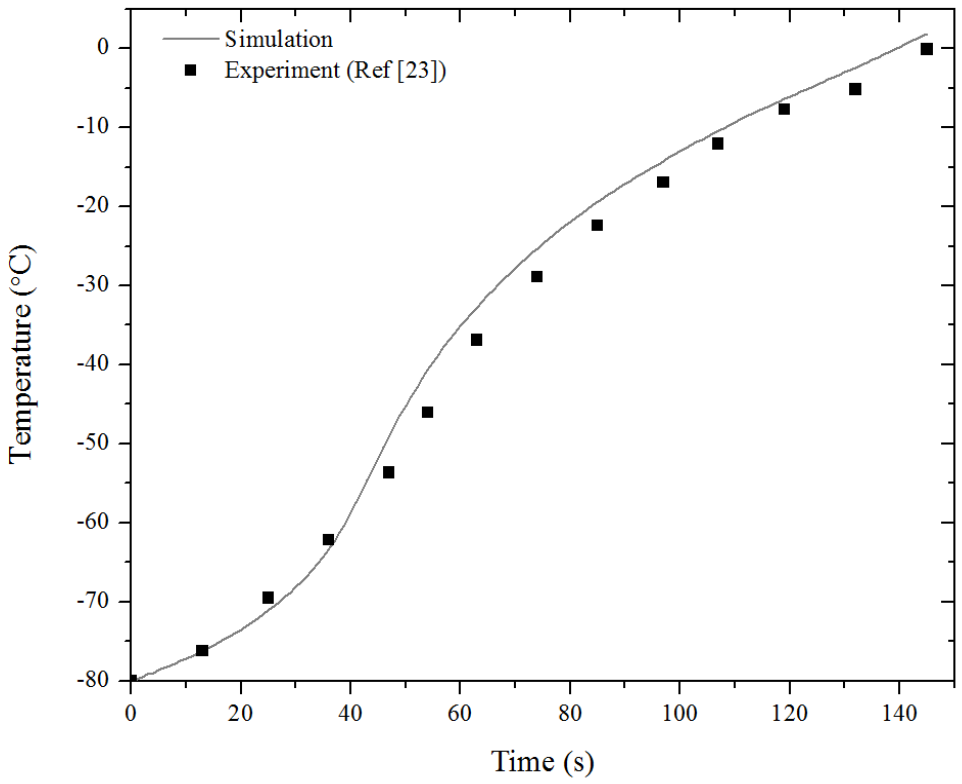

Figure 3-11. Validation of the model by comparing the experimental result (black squares) [23] and simulated result (gray line) of electromagnetic heating of 50% DMSO solution.

3.5.3 *The effect of sample shape on the rewarming*

Investigating optimized sample shape for the electromagnetic rewarming is significant to avoid thermal stresses induced by non-uniform heating as well as subsequent design of specific electromagnetic field patterns corresponding to specific cryopreserved material shapes. Due to the difficulty in studying the complex interactions analytically and accurate temperature monitoring experimentally, in this numerical study, four different sample shapes (dimensions shown in Table 3-1) with the same volume (24.4 mL) were compared to investigate the sample shape effect on the rewarming. As the temperature changed from –80 °C to 0 °C shown in Figure 3-12, the average warming rates of cylindrical, ellipsoidal, spherical, and cubic samples with the

same volume were determined to be 70.5, 61.2, 43.6, and 24.1 °C min^{-1}, respectively. Higher warming rates could be achieved by cylindrical and ellipsoidal sample shapes.

Table 3-2 Dimensions of sample holder shapes

Parameter	Value (mm)
Radius of sphere	18
Radius of cylinder	18
Height of cylinder	20
a-semi axis of ellipsoid	23
b-semi axis of ellipsoid	14
c-semi axis of ellipsoid	18
Side length of cube	29

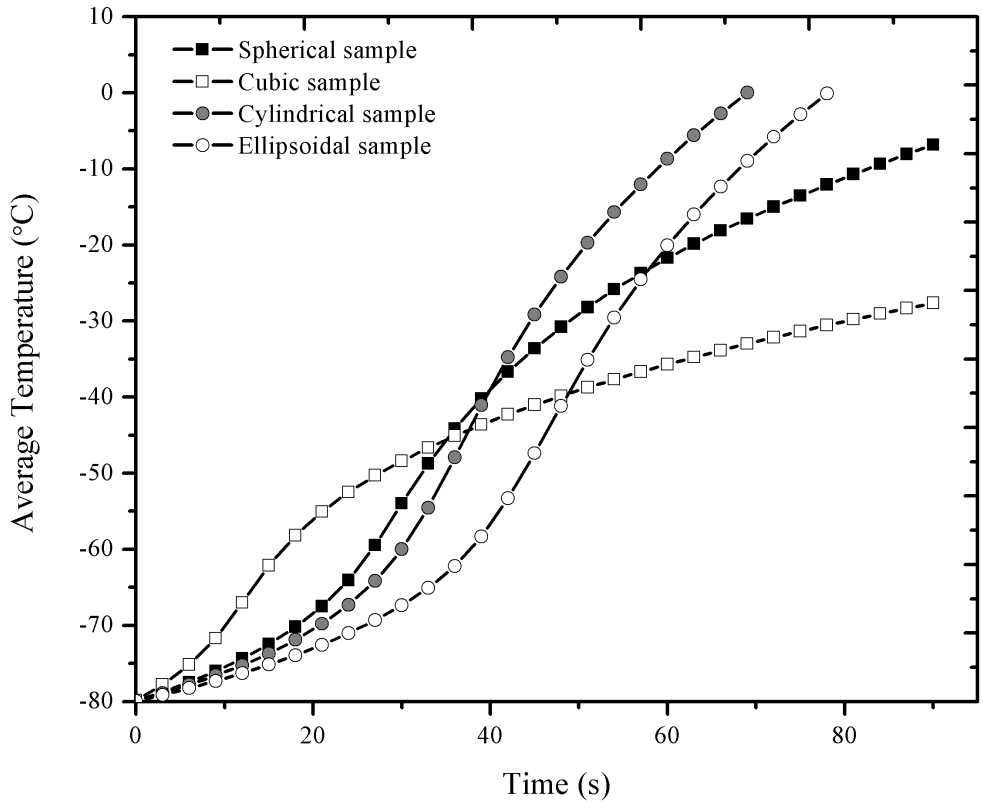

Figure 3-12. Simulated electromagnetic rewarming of cryopreserved DMSO solution in different sample holder shapes. The cubic sample was rewarmed at a slowest rate while the cylindrical was the fastest.

Then the post-thawing temperature profile was evaluated (Figure 3-13). The temperature gradients, defined as the difference between the maximum and minimum temperatures in the sample divided by the distance between them, for cylindrical, ellipsoidal, spherical, and cubic samples were 1.67, 0.78, 0.33 and 1.5 °C mm^{-1}, respectively. Cubic sample not only could hardly be rewarmed rapidly, the final temperature distribution was also excessively non-uniform, which confirmed that samples with sharp edges were not appropriate to be rewarmed by the electromagnetic rewarming technique [52, 79].

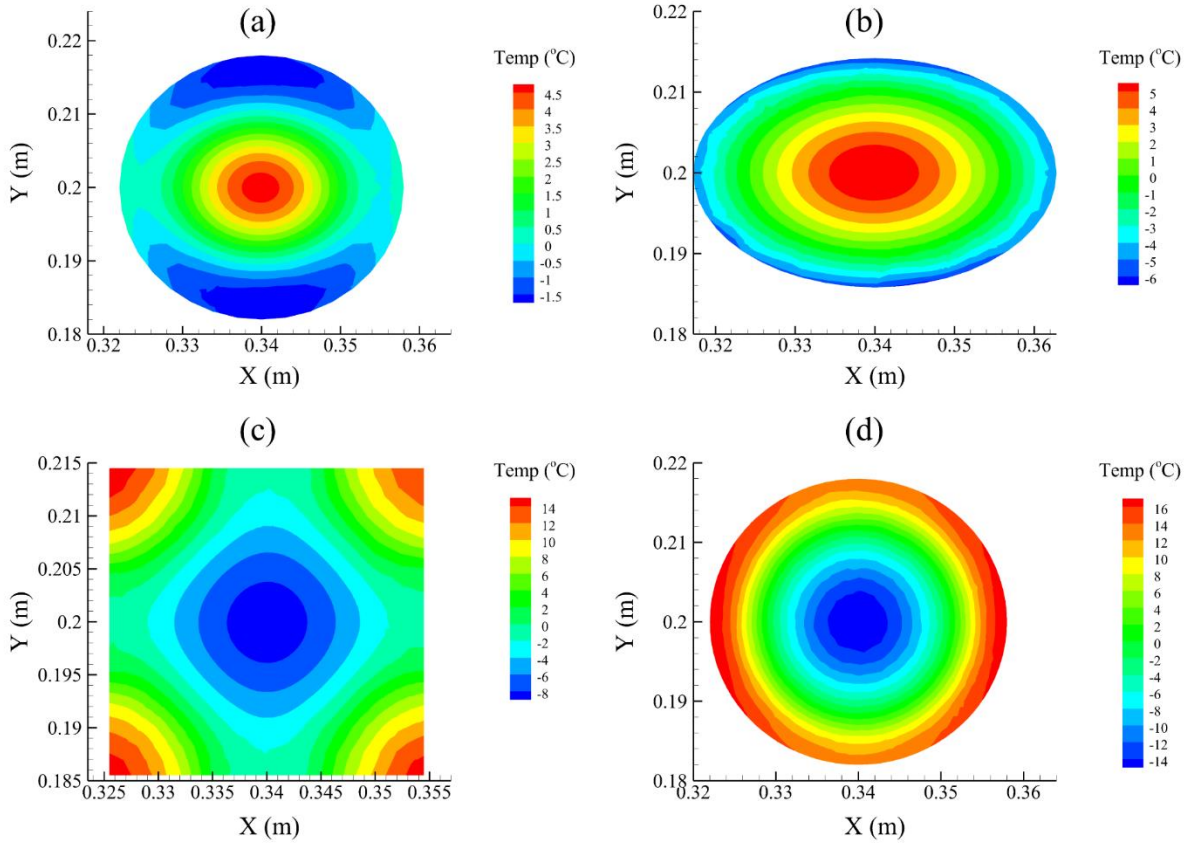

Figure 3-13. Simulated post thawing temperature distribution of cryopreserved DMSO solution in different sample holder shapes. (a) Spherical shape; (b) Ellipsoidal shape; (c) Cubic shape; (d) Cylindrical shape. The spherical and ellipsoidal samples manifested more uniform temperature distribution than cubic and cylindrical samples.

Ellipsoidal sample could be rewarmed at a relative high warming rate. Robinson et al. presumed that ellipsoidal sample shape is more appropriate for electromagnetic rewarming. The investigation used cone-shape sample holder to imitate ellipsoid [52]. The current simulation results affirmed the relative rapidity and uniformity of ellipsoidal sample shape for electromagnetic rewarming. But practical manufacturing problems likely inhibit the adoption of the ellipsoidal or spherical sample shapes. Cryopreserved materials must be placed in the optimal sample holders. The sample holder should be made of thin-layer material with minimal electromagnetic absorption. It is challenging to make such holder with desired dimensions for spherical or ellipsoidal shape. In addition, extra support is needed to fix the ellipsoidal sample at the position to be rewarmed rapidly, which can in turn result in the change of electromagnetic field distribution. Using cylindrical sample holder can avoid these problems. The rapidity of cylindrical shape by electromagnetic rewarming could be taken advantage for the preservation of tissues such as skins or arteries, provided that the non-uniformity was improved. Therefore, the selection of various CPA solutions was performed. Further, the hybrid warming technique was evaluated experimentally for the purpose to improve the non-uniformity based on cylindrical sample holder.

3.5.4 *Uniformity improvement by hybrid rewarming*

As discussed above, the rewarming rate of cylindrical-shape sample is high, but the temperature distribution is non-uniform. To improve the uniformity, a hypothetical hybrid rewarming concept was tested experimentally by inserting an auxiliary rod in the cylindrical sample holder as a passive heating source to reduce the temperature difference between the inner part and boundary of the cryopreserved sample during the electromagnetic rewarming process.

Based on previous simulated rewarming results of tested CPA solutions, DPVP was used as the CPA solution to be rewarmed in the experimental hybrid rewarming investigation.

For the electromagnetic rewarming experiments with or without the embedded central rod, temperature changes at two positions were monitored. One sensor was at the center of the sample and the other position was 10 mm to the center (Figure 3-14(a)). As illustrated by Figure 3-14(b), using the cylindrical sample holder generated a temperature difference over 20 °C between the two monitoring positions. The hybrid rewarming method yielded a rewarming rate of 43.6 °C min^{-1}. The final temperature difference at the two positions was reduced to less than 10 °C. The corresponding temperature gradient (temperature difference divided by the distance) was greatly improved from over 2 °C mm^{-1} to less than 1°C mm^{-1}. Besides, the temperature difference during the hybrid rewarming got minimized as the temperature approached to the end of the rewarming, which indicated the thermal runaway phenomenon was inhibited using this method and CPA, otherwise the temperature difference would keep increasing.

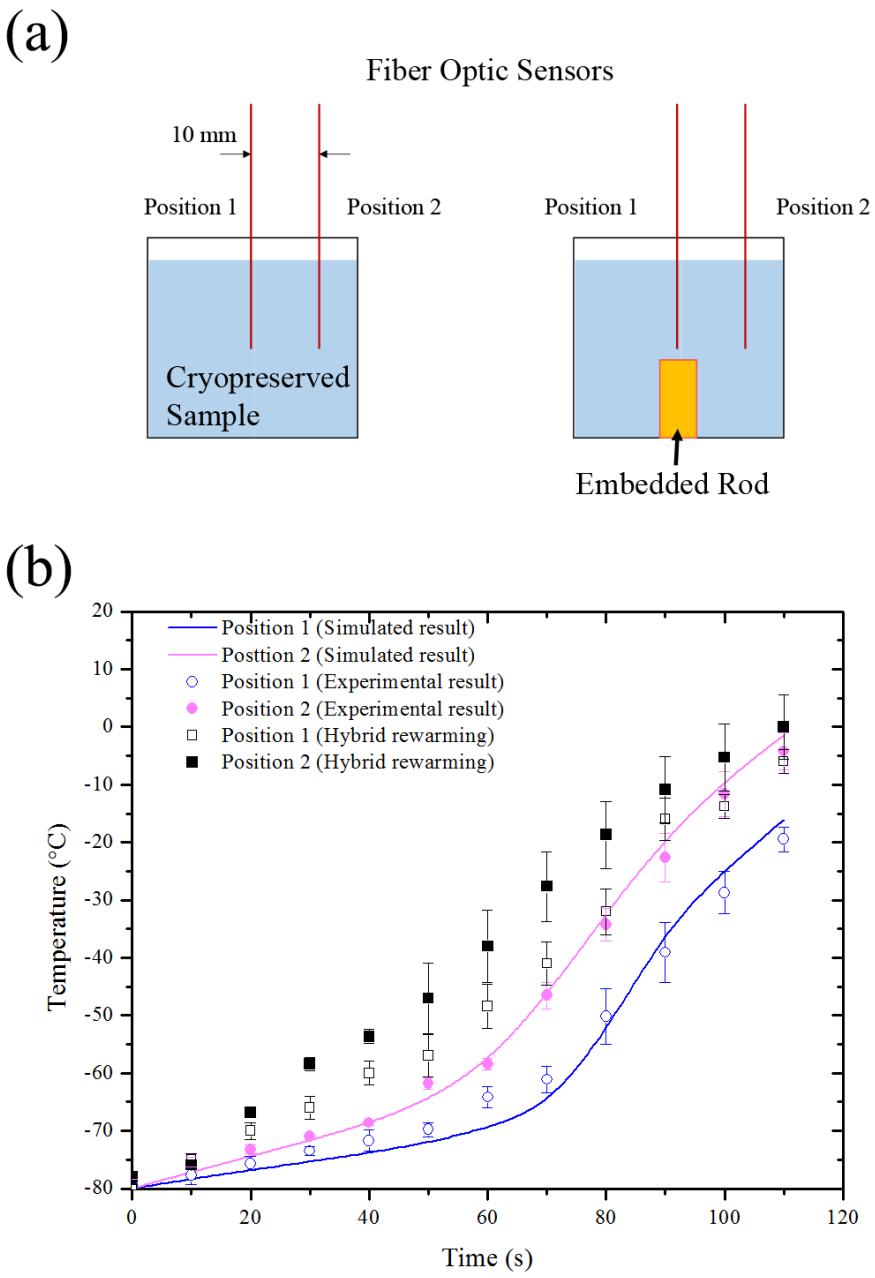

Figure 3-14. (a) Illustration of temperature sampling positions. (b)Rewarming results of DPVP. Blue and magenta lines represent the temperature at two positions from numerical simulation. The experimental temperature change at the two positions during the rewarming are denoted by blue hollow circles and magenta solid circles. Solid and hollow black squares represent the temperature change by electromagnetic -conduction hybrid rewarming method.

3.6 DISCUSSION

The temperature profile in the rewarming process is essential for evaluating the performance of the electromagnetic rewarming system as well as developing efficient rewarming systems. However, the experimentally determination of temperature distribution should compromise between the insufficient temperature sampling points and rewarming efficiency weakened by the increasing penetrating temperature sensors. The imperfect manufacturing of the rewarming cavity and partial temperature monitoring often impede the improvement of the electromagnetic rewarming. Thus, the effective numerical model can be utilized in the optimization of the electromagnetic rewarming from the parameters of the system to the selection of the CPA solutions towards to a higher utilization of electromagnetic energy as well as more uniform temperature distribution, where some parameters can be ameliorated conveniently.

Here in this chapter, combined numerical and experimental investigation of electromagnetic rewarming for cryopreservation was carried out. We established a numerical model to obtain extensive temperature profile of the electromagnetic rewarming results. The shape of sample was optimized numerically, and cylindrical sample holder was selected due to its high rewarming rate. A variety of CPA solutions physical properties were experimentally determined and used for the simulation of electromagnetic rewarming from the perspective of rapidity. The temperature dependence of complex permittivity and specific heat were determined over the rewarming range. But the thermal conductivity is regarded as a constant due to the current limitation of our measurement technique. It would bring large errors in determining the temperature distribution in traditional conductive rewarming simulations (e.g. water bath). But

when the electromagnetic energy serves as the major heating energy source, the heating due to heat conduction within the sample could have less contribution to the temperature change. In the future modelling, thermal conductivity values of the CPA solutions over the entire temperature range should be determined to achieve more accurate results.

Using high power electromagnetic energy in the rewarming system requires delicate control. The source power, if not well controlled, can cause damage to the system itself. We observed that in the heating of some CPA solutions with less absorption of the electromagnetic power, the circuits were burned internally by the reflected electromagnetic power which was supposed to be used for the rewarming of cryopreserved sample. Using numerical simulation can avoid those potential undesired failures and costs. Under the assistance of numerical simulation, higher power can be employed under an optimized condition in the later development of electromagnetic heating systems.

We tested a novel hybrid rewarming concept and found the uniformity of the temperature profile was improved from over 2 °C mm^{-1} to 1 °C mm^{-1}. In a study by Wang *et al.*, nanoparticles were added in CPA solutions to enhance the electromagnetic rewarming [82]. The rewarming rate was increased to 47 °C min^{-1} with a maximum temperature gradient 1.64 °C mm^{-1}. The rewarming rate is of at the same order of magnitude of the current study optimized by the selection of CPA solutions and hybrid rewarming. The final temperature gradient 1.64 °C mm^{-1} corresponds to a large temperature difference for a sample in a size of more than 10 mm. Another study tested the rewarming under the combination of the electromagnetic heating and water bath [84]. However, the temperature gradient turned out to be 28.7 °C mm^{-1}, corresponding to over 200 °C temperature difference in the cryopreserved material of a dimension over tens of millimeters. Thus, these methods could hardly be adopted in the

tissue/organ preservation currently. The hybrid rewarming design in this study may serve as a more appropriate approach from the perspective of uniformity. But the current central rod is inflexible and thick to be employed in the organ preservation. The key material properties of the rod were not determined. We are looking for soft material with high electromagnetic absorption ability as auxiliary conduction heat source in the sample holder to facilitate the rewarming process. Therefore, tissues or small organs can be placed in the holder without being impaired by the rod. The numerical model will be modified based on the new design. In the following efforts to improve the electromagnetic rewarming, since the addition of magnetic nanoparticles presented a higher ability to convert electromagnetic energy into heat [85, 92, 93], the enhancement of nanoparticle will also be evaluated. We will focus on the reduction of the concentration by manipulating electromagnetic field distribution and higher power utilization efficiency. The numerical simulation will be modified as well, with the physical properties of nanoparticle solution determined experimentally in subzero temperature ranges which may involve phase changes.

3.7 CONCLUSION

To summarize, this chapter presented a validated numerical model to facilitate the optimization of the electromagnetic rewarming technique. Essential properties of the CPA solutions determined experimentally were used for the selection of appropriate CPA from the perspective of rapidity of the rewarming with the numerical model. DPVP turned out to be superior among the tested CPA solutions with a higher warming rate 43 °C min^{-1}. The effect of sample shape was investigated by the model and the temperature non-uniformity in cylindrical sample was improved by adopting an auxiliary rod at the center. After using the hybrid rewarming method, the rewarming rate was slightly enhanced to 43.6 °C min^{-1}. More

importantly, the temperature gradient between the sampling positions was reduced to less than 1 °C mm^{-1}, which showed a feasible way to achieve uniform rewarming. This study is of significance to further optimize the electromagnetic rewarming technique for cryopreservation. In Chapter 4, we will introduce an improved electromagnetic resonance rewarming system which is based on the current brief design. In Chapter 5, we will continue to use cylindrical sample holder while optimize the rewarming results in an alternative approach.

Chapter 4. Dynamic Electromagnetic Resonance Tracking Rewarming System Development

As discussed in previous chapters, a rapid and uniform rewarming is indispensable for the cryopreservation of complex large biological systems such as tissues and organs. However, the thermal property measurement results in Chapter 2 demonstrate that the convective warming methods would be hindered by the poor abilities to conduct heat inside the materials. Volumetric heating method is the only possible solution. Whereas previous multimode or commercial microwave systems could not be adopted since they lack a good control to maintain the resonant state, leading to either recrystallization/devitrification due to slow heating with most of electromagnetic energy reflected back or thermal runaway problems creating undesired hot spots. In addition, appropriate CPA/vitrification solutions should be selected for specific electromagnetic resonance rewarming systems. Based on preliminary investigation regarding the electrical properties and established combined electromagnetic-heat transfer model, DPVP (41% DMSO and 6% PVP) was selected to be appropriate CPA solution for electromagnetic rewarming.

But the rewarming rate is still limited. There are two major issues should be considered to achieve the goal of rapid and uniform rewarming. First, the system itself should provide sufficient electromagnetic energy for the biomaterials to be heated. Second, the temperature dependent dielectric properties of the biomaterials progressively shift the resonant frequency of the resonant chamber during the rewarming process. Therefore, when using resonant electromagnetic field as the heating source, if the electromagnetic signal parameters remain stagnant according to the frequency change resulted from the temperature change of

biomaterials, the electromagnetic energy generated may not be converted into the strong electromagnetic field in the resonant chamber to excite resonance.

Moreover, if the electromagnetic system source remains static during the rewarming procedure, severe problems regarding the system safety and efficiency may emerge. A higher portion of reflected electromagnetic power can lead to the damage to the system components as well as potential electromagnetic radiation hazards to the surrounding operators. On the other hand, with smaller electromagnetic energy remaining inside the rewarming chamber, sufficiently strong electromagnetic field inside the resonant cavity could hardly be excited resulting a slow warming. Therefore, it requires delicate control on the set up of the electromagnetic resonant system. We have developed a dynamically controlled single mode electromagnetic resonance rewarming system to achieve a more rapid rewarming and uniform temperature profile.

4.1 Overview of the Improved Electromagnetic rewarming system

As illustrated by the schematic and the overview photograph (Figure 4-1 and Figure 4-2), the electromagnetic rewarming system with dynamic control of the resonance state is upgraded from the previous simply assembled circuits described in Chapter 3 to a more advanced system which is composed of essential components to be introduced in the following contents.

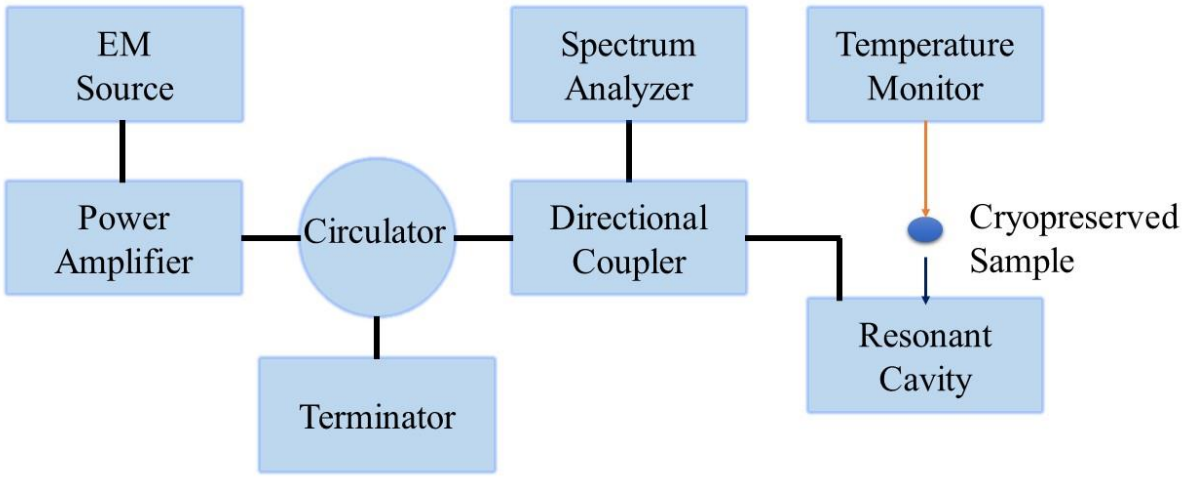

Figure 4-1. Schematic of the single mode dynamic modulated electromagnetic resonance rewarming system.

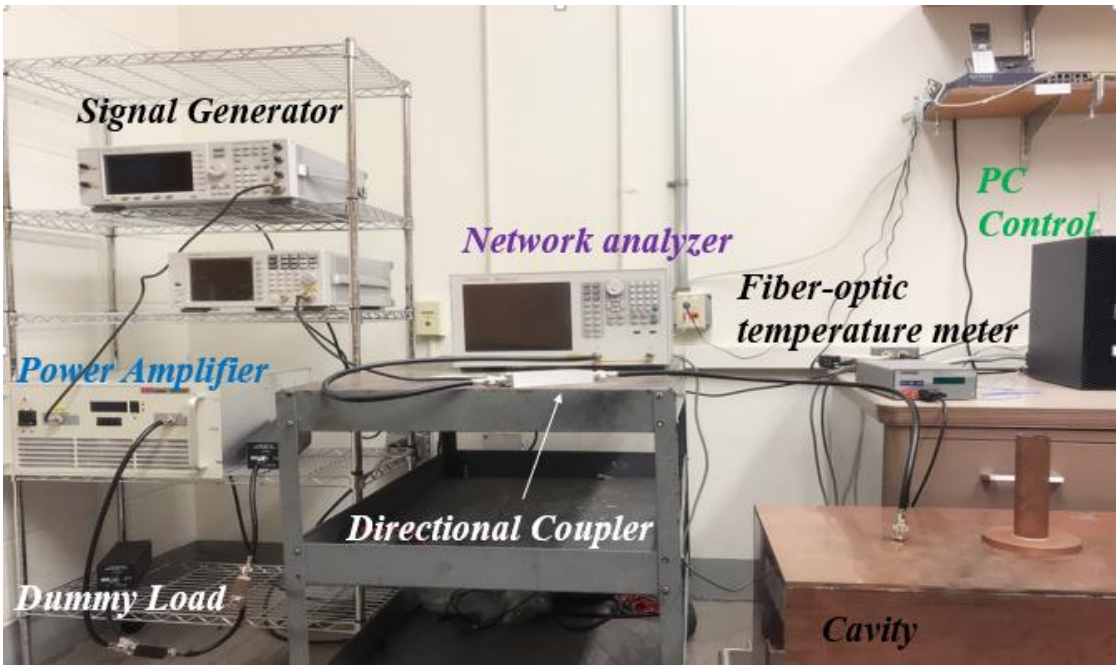

Figure 4-2. Overview photograph of the electromagnetic rewarming system.

4.2 ELECTROMAGNETIC SOURCE

The electromagnetic signal is synthesized by a signal generator (4432B, Agilent, Santa Clara, CA, USA). The signal generator can generate continuous electromagnetic waves between 250 kHz to 3 GHz which covers lower frequency band of radiofrequency and microwave. And the power output range is +7 to −120 dBm (i.e. 0.005 to 10^{-15} W). At this low power output, the electromagnetic field established in the resonant chamber is too weak to rewarm the cryopreserved biomaterials rapid enough avoiding devitrification. In order to intensify the electromagnetic field to achieve higher rewarming rates, a power amplifier (Model 5006, OPHIR RF, Los Angeles, CA, USA) was adopted to increase the electromagnetic power to over 57 dBm (501 W).

The power amplifier has a frequency range between 300 to 500 MHz, which fully covers the working frequency range for this experimental investigation. The reflected power received by

this power amplifier would also be detected by the control circuits. The power amplifier will automatically cut off excessive output generation to protect itself. Due to the relatively high electromagnetic power used in the system, two side panel cooling fans were incorporated to avoid internal circuits overheating and system shutdown. The connections between the signal generator and power amplifier, as well as other microwave components are through 50 Ω coaxial cables. These cables would have some attenuation effects. Thus, in order to maintain the high power signal from the amplifier to the rest part of the system, the length should be as short as possible. The measurement was done by the signal generator and a power meter as shown in Figure 4-3. According to the measurements of six coaxial cables of different lengths, the attenuation for coaxial cables is around 0.1 dB m^{-1}.

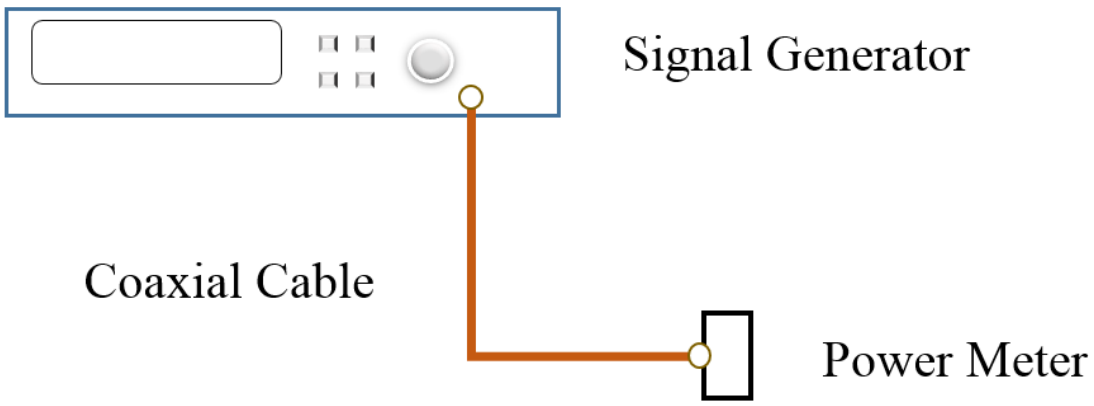

Figure 4-3. Schematic of the coaxial cable loss determination.

The most significant difference between the current resonance system and the previous assembled circuits (introduced in Chapter 3) is attributed to the frequency tracking component. During the rewarming process, the resonant frequency of the resonant cavity with biomaterials would change on account of the temperature dependent dielectric properties of the inside biological samples. To prevent the mismatch between the synthesized electromagnetic source

frequency and the resonant frequency of the rewarming chamber, the generated frequency source should be dynamically adjusted during the rewarming process.

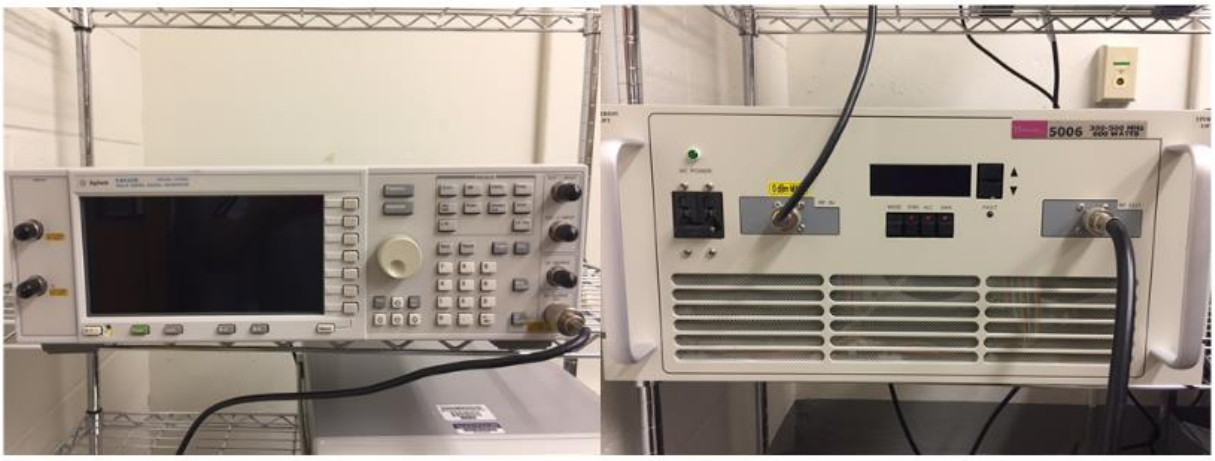

Figure 4-4 Left: signal generator. Right: power amplifier

4.3 FEEDBACK CONTROL

In order to prevent the frequency mismatch between the signal generation and the resonant frequency which is swiftly altered by the massive cryopreserved materials inside, a dynamic feedback control component was added between the electromagnetic source and the resonant cavity (Figure 4-5). A directional coupler was introduced to sample the transmitted and reflected power. And a spectrum analyzer was connected to the port corresponding to the reduced reflected power. The entire spectrum of the reflected power was evaluated and by looking for the highest power peak, the frequency corresponding to the most significant reflected power was determined. During the rewarming process, the frequency generated from the electromagnetic signal source is dynamically changed corresponding to this spectrum and minimize the reflected power. Otherwise, the large portion of reflected power could lead to a slow warming rate with less power into the cavity. In addition, the reflected power can cause a

serious damage to the rest part of the electromagnetic resonance system itself, such as the amplifier, signal synthesizer.

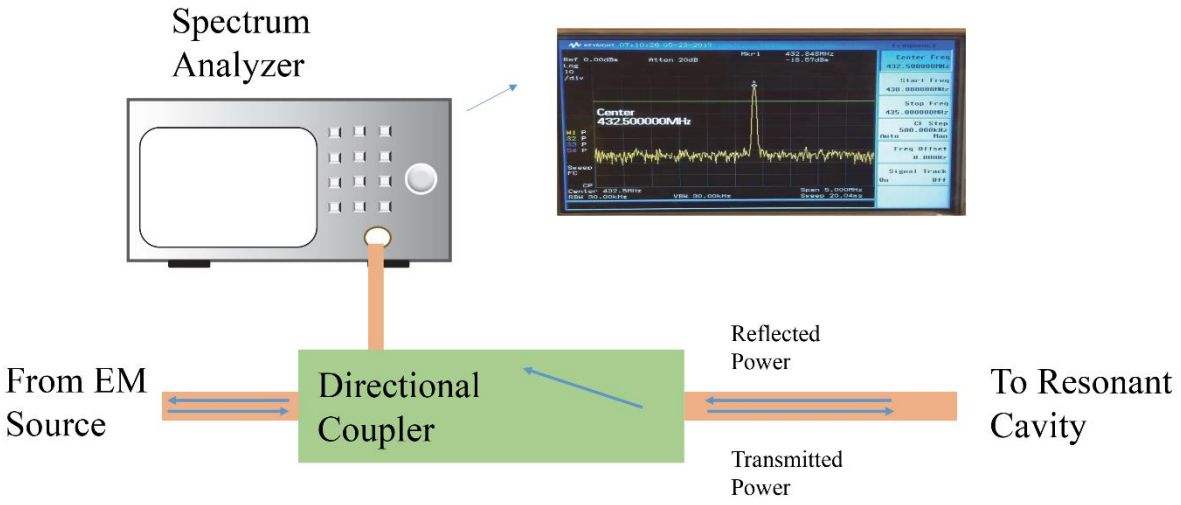

Figure 4-5. Schematic of the dynamic feedback control component.

4.4 TEMPERATURE MEASUREMENT

The temperature measurements were conducted by a fiber optic temperature meter (Reflex Signal Conditioner, Neoptix Inc, Ville de Quebec, QC, Canada) during the rewarming process. The major challenge for the temperature measurement lies in the penetration of cavity wall. The cryopreserved sample remains in the center of the resonant chamber where the highest electromagnetic field was formed. However, the penetration of the cavity wall would undermine the quality factor of the resonant cavity, which means lower portion of electromagnetic energy remained for the rewarming. Additional waveguide was designed to allow for the fiber optic temperature sensor to get through and maintain the quality factor at the same time. This waveguide was designed to have the cutoff frequency higher than the operating frequency during

the rewarming process. Although the side effects associated with the electromagnetic waves are still in debate. It is nevertheless safer to keep away from the possible side effects brought by electromagnetic energy leakage.

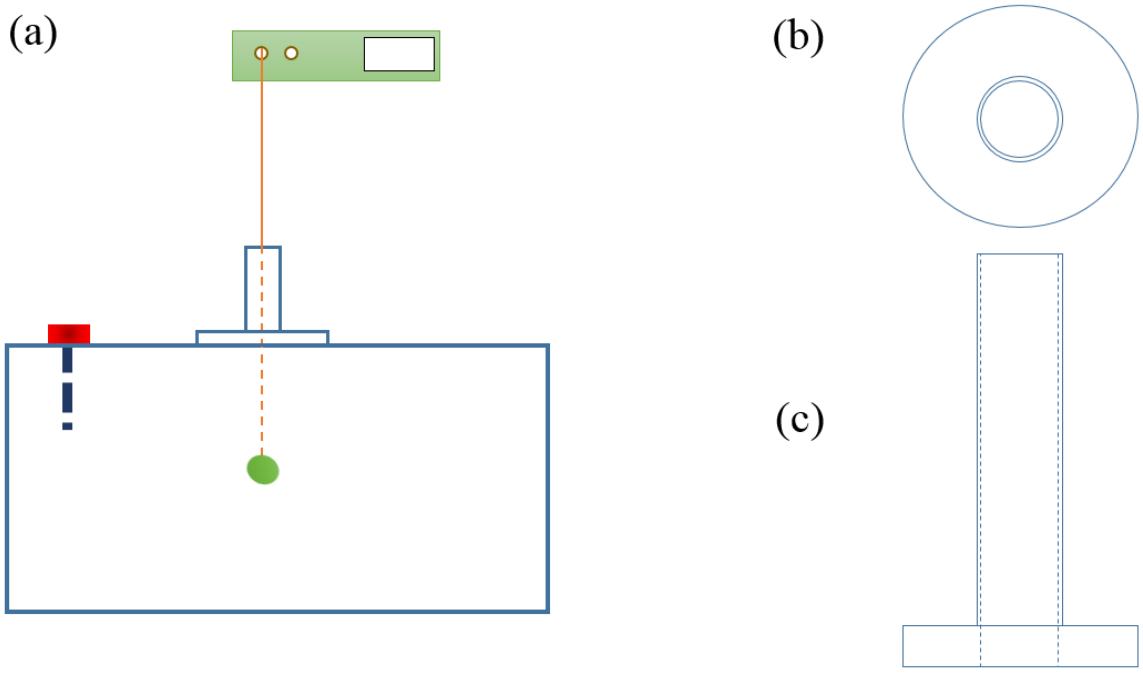

Figure 4-6 Waveguide designed for temperature measurement. (a) Schematic of the waveguide on the resonant cavity. (b) Top view of the waveguide. (c) Side view of the waveguide.

The cutoff frequency of a circular waveguide is given by:

$$f_c = \frac{1.8412c}{2\pi a} \tag{3.21}$$

where c is the speed of light (m/s), a is the internal radius of the circular waveguide (m). In our design, the inner radius is set to be 1.5 cm. Thus the cutoff frequency is 5.86 GHz, which is much higher than the operating frequency generated by the electromagnetic source during the entire rewarming process.

After the rewarming process, the surface temperature profile was recorded by an infra-red temperature sensor (FLIR ONE, FLIR systems, Wilsonville, Oregon, USA). The temperature

data in the central part of the cryopreserved sample recorded by the fiber optic meter and the thermometer surface temperature profile are combined to analyze the temperature gradient (Figure 4-7).

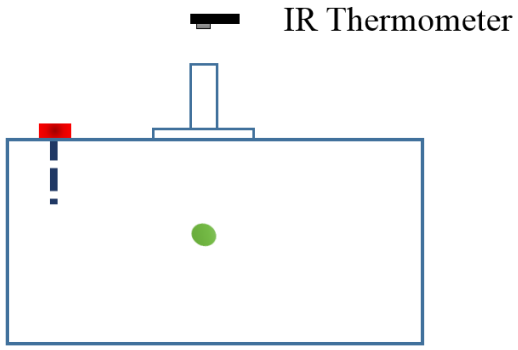

Figure 4-7. Post-thawing surface temperature measurement.

4.5 EXTENDED PROBE ANTENNA

The electromagnetic energy was conducted from the electromagnetic source part into the resonant cavity through coaxial transmission lines and a coaxial probe antenna (N Type Straight Jack, Amphenol, Wallingford, CT, USA) at the end. While it was examined that the quality factor of the resonant cavity did not approach the theoretical value. To establish a strong electromagnetic field, the length of the probe antenna was prolonged to adjust the coupling or impedance matching between the electromagnetic source and the resonant cavity. The extension stick is manufactured with copper and added to the probe with electrical conductive glue mixture with silver powder (Figure 4-8).

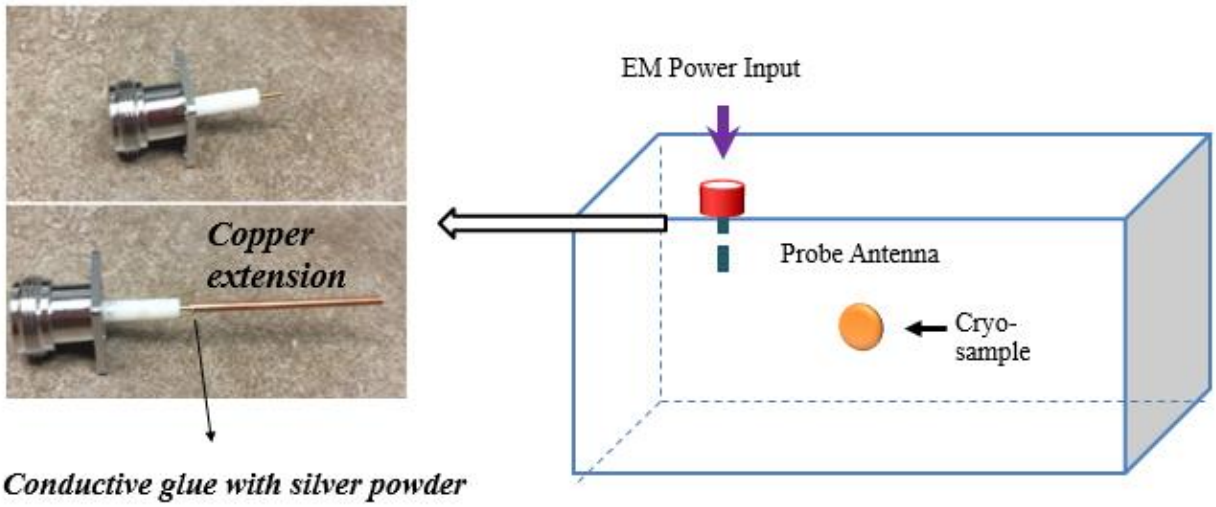

Figure 4-8. Original coaxial probe antenna and probe with copper extension.

4.6 ENHANCEMENT OF ELECTRIC FIELD MAGNITUDE OF THE RESONANT CAVITY

In the numerical simulation model, the probe length was adjusted to be the original probe length and the extended probe length. The electric field intensity excited in the sample inside the cavity was calculated. As shown in Figure 4-9, the electric field intensity in the cryopreserved material increases almost ten times larger than that using the original probe antenna, which suggests that the impedance matching between the loaded cavity and the electromagnetic source is greatly improved by adopting an extended probe antenna.

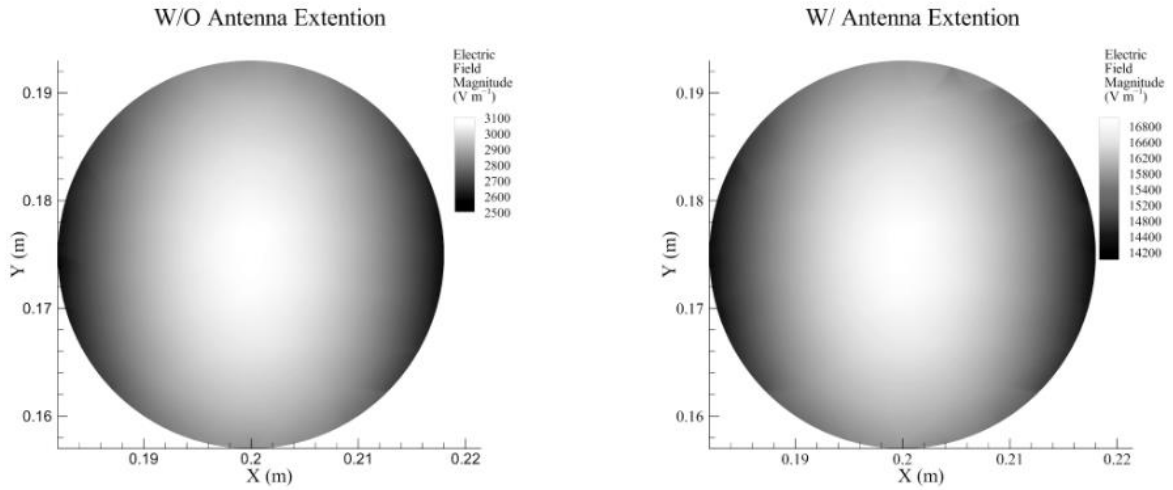

Figure 4-9． Electric field intensity comparison. Left: before optimization of the electromagnetic system. Right: after optimization of the system.

Since electric field power is proportional to the square of the electric field intensity. Which means we could have much more power to heat the material using the optimized extended probe antenna. Then the experimental measurement for the quality of the resonant cavity was conducted.

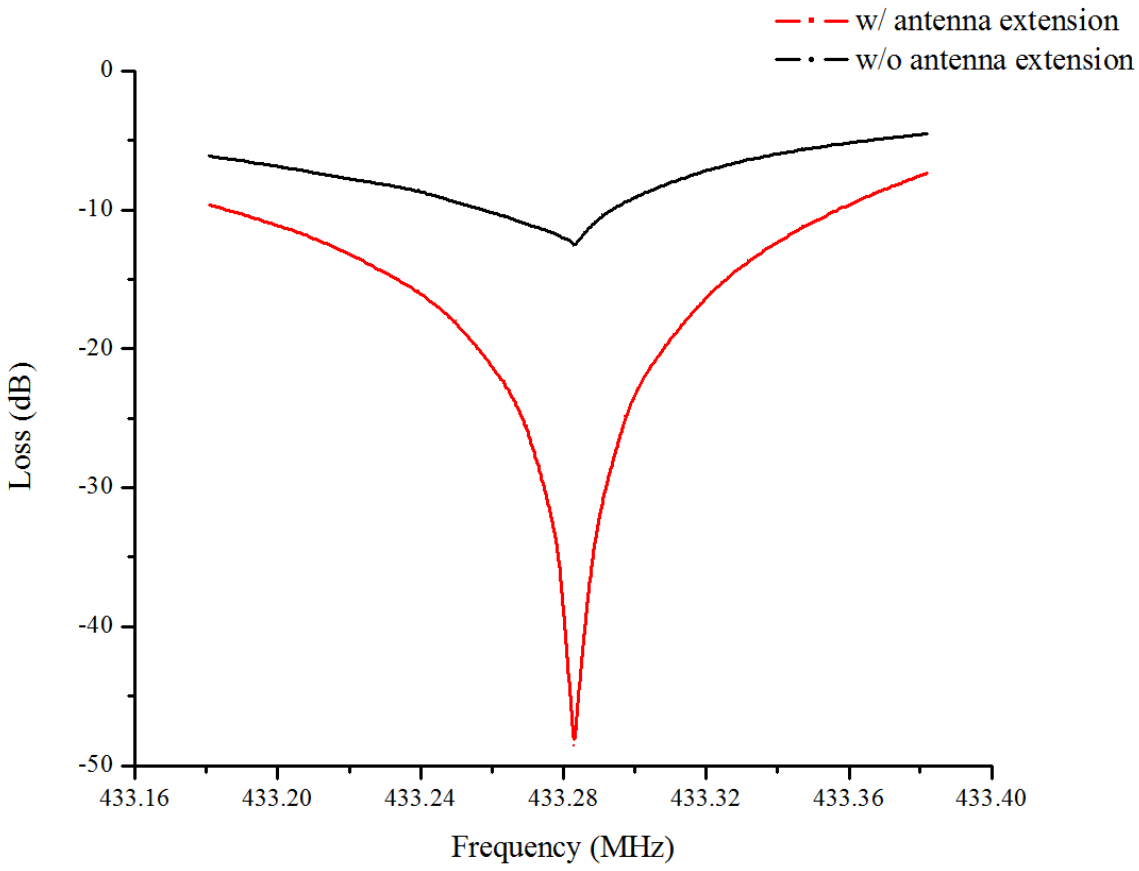

Figure 4-10. Experimental results of the resonant cavity.

Figure 4-10 is the reflected power signal received by the network analyzer with or without the copper antenna extension. The horizontal axis is frequency band, vertical axis is the reflected power corresponding to the frequency. At the frequency 433.28MHz we have a very small loss received by the network analyzer, which means most power was locked in the cavity; the frequency is also the resonant frequency. And with the extended probe antenna, it has a better resonance state, more power will stay in the cavity, which means we have more power to heat the cryopreserved samples.

This numerical estimation of the electric field gives guidance to the experiment. S_{11} was measured by a network analyzer and the quality factor of the loaded cavity was determined based

on the reflection coefficient. It is found the quality factor of the loaded cavity was improved from 1681 to 5577 after adding the probe extension, which can establish a much stronger electromagnetic field inside the cavity for the rapid rewarming of the cryopreserved biomaterials.

Chapter 5. Experimental Results and Iron Oxide Nanoparticle Enhancement

5.1 INTRODUCTION

Over the past decades, magnetic nanoparticles (MNPs) have played a significant role in various diagnosis and therapeutic practices including non-invasive magnetic resonance imaging (MRI), drug delivery, and hyperthermia therapy [94-99]. By harnessing the heating effects of MNPs under the external strong oscillating magnetic field, MNPs-based hyperthermia may achieve a selective and effective localized temperature rising intolerable to cancerous cells but less lethal to normal cells, while other cancer treatments may have difficulty solely targeting specific cancerous area. Recently, the combination of radiofrequency electromagnetic system generating alternating magnetic and MNPs as thermal meditators was applied from hyperthermia into another thriving biomedical field, cryopreservation [85, 86], attempting to address the unmet need for transplantation due to tissue and organ shortage [100].

Cryopreservation, using low temperature to preserve biomaterials, serves as an important role facilitating biomedical research and clinical treatment. The major progress in cryopreservation is confined to simple and/or small volume biomaterials such as red blood cells [101], stem cells [102], sperms [103] and oocytes [104]. Albeit the successful preservation may considerably alleviate the waiting for transplantation and allow for sufficient time in donor-recipient matching, complex and larger tissues/organs exhibit much more problems in establishing mature preservation methods. Vitrification, forming amorphous state by fast cooling and adding high concentration cryoprotective agents (CPA), showed its promising future for organ preservation [23]. Yet the perilous devitrification and/or thermal induced fracturing can

hardly be eliminated during the rewarming process from the low storage temperature (typically −80 °C or −196 °C) to physiologically normal temperature.

The lack of rapid and uniform rewarming techniques has limited the development of tissue and organ cryopreservation for a long time. By vibrating the electrical dipole molecules, high power electromagnetic cavity heating systems [51, 76] can generate a volumetric dielectric heating and overcome the problem of low thermal conductivity and high specific heat of biological materials, which rules out the possibility of using traditional water bath for thawing large cryopreserved samples. However, the associated "thermal runaway" problem [105], temperature difference growing due to temperature dependent electromagnetic power absorption ability, hindered these multimode or unstable resonant electromagnetic systems with inadequate control to obtain an effective rewarming protocol.

The recent "nanowarming" method [86], i.e., a MNPs-based heating technique, utilized the oscillating magnetic field generated by a commercial available radiofrequency (RF) electromagnetic coil system, provided an impressive solution for the large tissue (over 1 mL to tens of mL) cryopreservation. But a few concerns remain. The heat generation inside the cryopreserved material mainly rely on the ability of embedded MNPs to convert magnetic field energy into heat. Whereas cytotoxicity of MNPs reported in specific types of cells [106, 107] should be noted. For organs or more complex tissues where cellular uptake of nanoparticles could take place [108], high dosage of MNPs in organs may result in undesired side effects. On the other hand, the serious increasing technical difficulty to enlarge RF power [109], an inevitable obstacle due to the relatively low energy utilization efficiency, may inhibit the system scaling up to organ preservation.

In this chapter, to achieve high energy conversion efficiency as well as minimize the dosage of MNPs, we describe the setup and the optimization of a dynamically controlled electromagnetic resonance rewarming system. To utilize both electric field and magnetic field energy, 10nm or 15nm iron oxide nanoparticles at different low concentrations were incorporated in the CPA solutions rewarmed by the optimized rewarming system for the proof of concept purpose. The average highest warming rate (over 200 °C min^{-1}) for bulk cryopreserved material was achieved using smaller electromagnetic power compared to the RF coil magnetic rewarming or unoptimized electromagnetic systems. The post-rewarming temperature distribution were determined, and thermal analyses were conducted to investigate the enhanced effects brought by the nanoparticles. The optimum amount of nanoparticle required was largely reduced (0.1 mg Fe mL^{-1}) for the rapid and uniform rewarming by using this optimized electromagnetic resonance rewarming system, which will pose less side effects for the subsequent biological trials. With the great decrement of MNPs dosage and enhanced heating efficiency, this preliminary study points to a promising alternative strategy to deal with the rewarming problem towards tissue and organ preservation

5.2 MATERIALS AND METHODS

5.2.1 *CPA/vitrification solution*

DPVP contains 5.2 M dimethyl sulfoxide (DMSO; Sigma-Aldrich, St. Louis, MI, USA), 6% (g/dl) polyvinylpyrrolidone (PVP; Sigma-Aldrich) in PBS (Sigma-Aldrich) solution. The thermal and electric properties of DPVP were determined in Chapter 2 and partial numerical simulation demonstrated the feasibility to achieve a higher warming rate and smaller temperature difference. Hence, it was used in this investigation of nanoparticle enhancement effect. 5.2 M

DMSO solution was used as comparison in the freezing/vitrifying examination. Solutions were prepared the day before the cooling and rewarming experiment.

5.2.2 *Magnetic nanoparticles*

The MNPs used in this study were 10, 15nm iron oxide nanoparticles (Fe_3O_4) with amine group dissolved in 10 mM PBS (Ocean NanoTech LLC, San Diego, CA, USA). After diluting MNPs solution in the CPA solutions, the composite of CPA solution with MNPs achieved low concentrations of 0.05, 0.1, 0.2 mg mL^{-1} Fe respectively for DPVP solutions. The distribution of MNPs of two different sizes in the DPVP solutions were examined with transmission electron microscopy (TEM). DPVP with embedded MNPs droplets were casted onto either 200 mesh carbon coated grids or 300 mesh lacey carbon grids (Electron Microscopy Sciences, Hatfield, PA, USA). Imaged with a Gatan Ultrascan CCD using Digital Micrograph software (Gatan, Pleasanton, CA, USA).

5.2.3 *Cooling/vitrification process*

The bulk CPA solutions (20 mL in 30 mm × 100 mm holder) were held by an aluminum hook, placed in a liquid nitrogen container above the liquid level, and cooled by the vapor phase nitrogen as illustrated in Figure 5-1. The cooling rate could be roughly estimated by adjusting the distance between the CPA and the liquid level. The temperature change of the CPA solutions was recorded, and the cooling rate was estimated for the following thermal analysis. After reaching −140 °C, the CPA solutions were observed to check if the transparent amorphous state or opaque crystalline solid state was achieved.

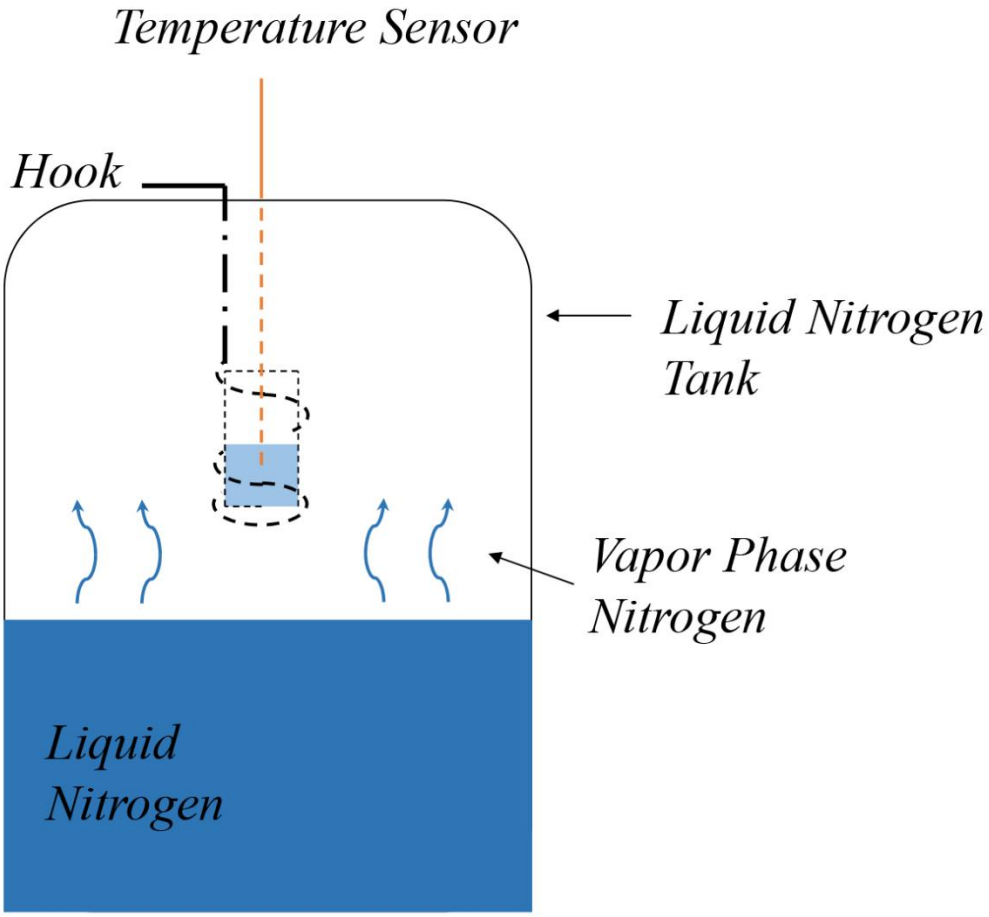

Figure 5-1. Schematic illustration of the controlled cooling setup.

5.2.4 *Temperature profile measurement*

In the previous numerical simulation and rewarming system description, the temperature measurement method was introduced. In order to avoid interfering the established electromagnetic field distribution, fiber optic sensor connected to a thermometer (Neoptix, Quebec city, QC, Canada) was inserted into the CPA solutions to record real-time temperature during the rewarming process. When the cryopreserved CPA solutions reached 0 °C (i.e., passed

the lethal temperature zone −60 °C to −5 °C [15], or devitrification/recrystallization zone), the infrared thermal camera (FLIR, Wilsonville, OR, USA) was used to take thermography of the surface of the CPA solutions.

5.2.5 *Freezing-thawing behavior characterization and visualization*

Differential scanning calorimetry measurements were conducted to determine the freezing-thawing behavior and specific heat of the sample solution with different concentrations of MNPs by a differential scanning calorimeter (DSC; Perkin Elmer, Waltham, MA, USA). An empty pan was used as reference. Calibrations of temperature, heat flow were conducted before the measurements using n-dodecance and n-octane. 6 μL of each sample solution was placed and sealed in aluminum pans and transferred into DSC for measurements. All measurements were repeated for three times. For the analysis of freezing-thawing behavior, the samples were cooled down to −150 °C at 5 °C min^{-1} followed by heating up to 20 °C at 100 °C min^{-1}.

5.2.6 *Thermal conductivity assessment of the vitrification solutions with nanoparticles*

As introduced in chapter 2, the thermal conductivity measurement system for CPA solutions developed by Liang, *et al.* [73] consists of a digital multimeter (Keithley, Cleveland, OH, USA), a microfabricated thermal sensor and a computer for data acquisition. The sensor works on the principle of transient hot wire (THW). This miniaturized device utilizes a SiO_2/Au/SiO_2 sandwiched structure to protect the microfabricated serpentine gold coil, which functions as both the heater and a passive thermometer. The sensor has already been tested and shown to measure thermal conductivity of biomaterials and solutions with high accuracy, repeatability and reliability. The thermal conductivities of vitrification solutions with different

concentration of nanoparticles were determined. All measurements were performed for three times from −30 to 20 °C.

5.2.7 *Statistical analysis*

The statistical analysis was carried out using R (version 3.2.4). The data were presented as mean value ± standard deviation. Differences of $p < 0.05$ were considered to be of statistical significance.

5.3 Results and Discussion

5.3.1 *MNP embedded CPA solutions*

Fe_3O_4 were incorporated into the DPVP solutions (41% dimethyl sulfoxide (DMSO), 6% polyvinylpyrrolidone) to make use of the magnetic field component in this electromagnetic resonance system aiming to improve the rewarming results. Figure 5-2A shows the CPA solutions with 10 nm or 15 nm iron oxide nanoparticles at 0, 0.05, 0.2 mg Fe mL^{-1} respectively. All these solutions went through freezing process down to −80 °C, storage at the −80 °C freezer for at least one day and the following thawing processes. There were no visible nanoparticle clusters or solution stratification which occurred elsewhere in other CPA solutions after adding iron oxide nanoparticles [86]. For the MNP-based RF heating biomedical applications, it was reported that the aggregation of nanoparticles hindered the ability to convert electromagnetic energies[110], which should be avoided to obtain an efficient magnetic heat induction. The TEM images (Figure 5-2B) demonstrate that the nanoparticles were dispersed without significant aggregations at the low concentrations used in this work, which may be desired to interact with

the electromagnetic field. The potential unexpected inhomogeneity due to large nanoparticle aggregation could also be mitigated in the electromagnetic rewarming.

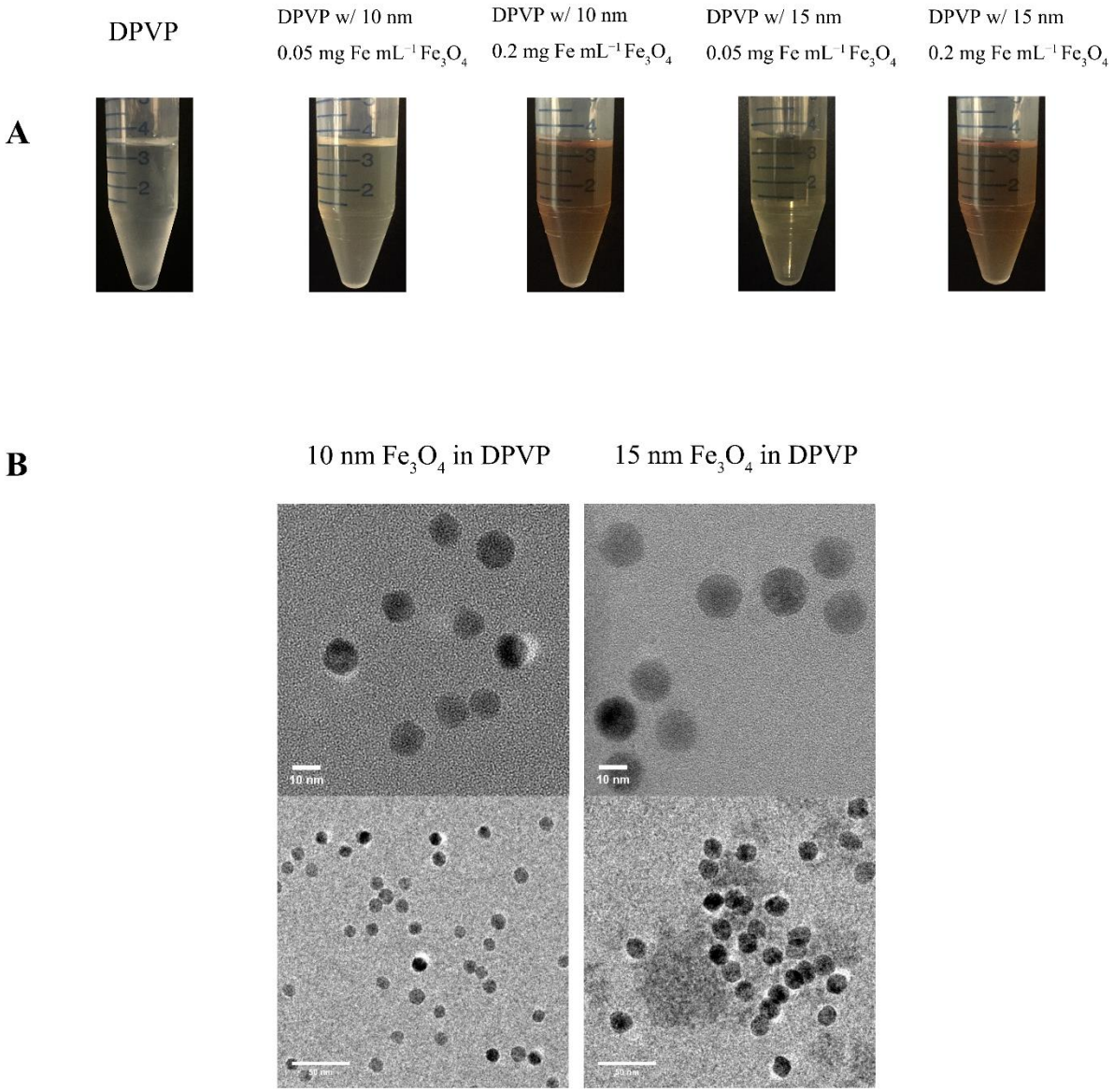

Figure 5-2. DPVP solutions with 10, 15nm Fe3O4 nanoparticles: (A) visual examination of solutions w/ or w/o different concentration nanoparticles after slow cooling and rapid rewarming; (B) transmission electron microscopy images. Stratified solution after rewarming or nanoparticle aggregations were not observed.

To achieve vitrification of the CPA solutions, controlled slow cooling procedures were performed using the designed cooling device (Figure 5-1). The critical cooling rate (CCR; the necessary cooling rate above which to avoid noticeable ice formation) [24] of DPVP [74] was below 10 °C min^{-1}. Figure 5-3 shows a typical temperature change for DPVP during the cooling process. The cooling was slow but at a higher rate than the CCR. An annealing process was carried out right after the temperature reached *Tg* to release the residual thermal stress that may result in devitrification.

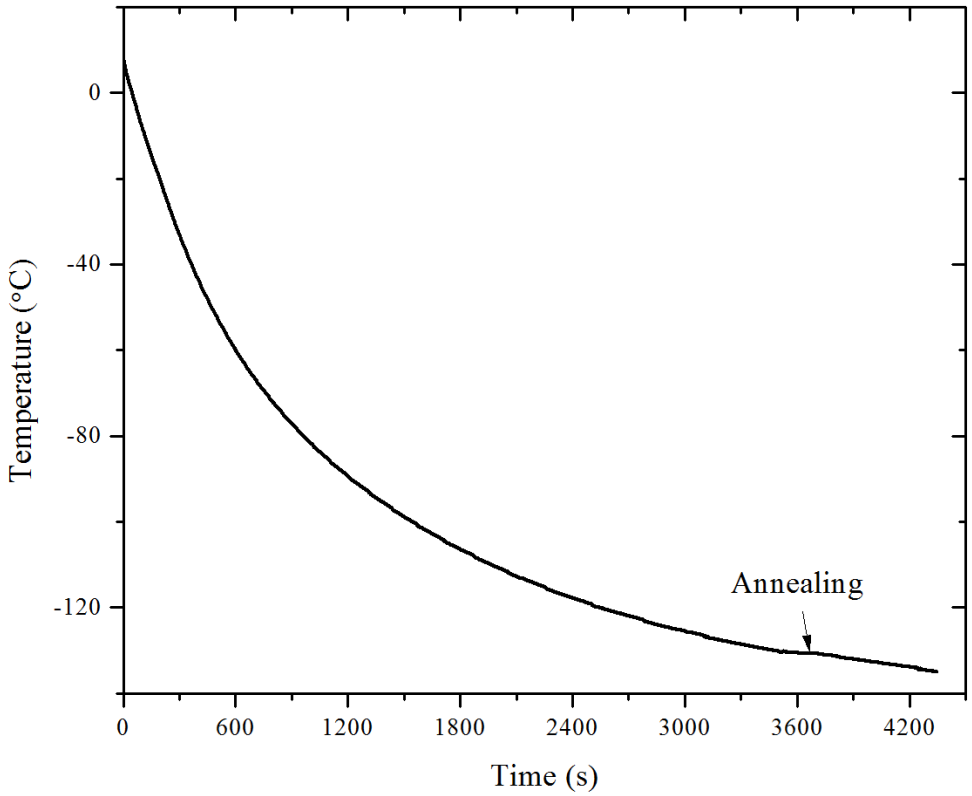

Figure 5-3. A representative temperature change is illustrated using the vapor phase cooling method recorded by thermal sensors.

As Figure 5-4 shows, transparent solids were formed at −140 °C by this vapor phase nitrogen cooling for every DPVP solutions with nanoparticles at different concentrations in the current study. Instead, opaque crystalline solids were observed, if the relatively lower concentration CPAs (5.2 M DMSO was used here) were slowly cooled down to −140 °C. Often, the vitrification of small volume cryopreserved biomaterial requires ultra-rapid cooling achieved by direct immersion into liquid nitrogen[111, 112]. However, it is extremely difficult to cool a bulk cryopreserved material both rapidly and uniformly. Non-uniform temperature profile associated with rapid cooling can induce mechanical stresses and cracks for bulk cryopreserved materials.

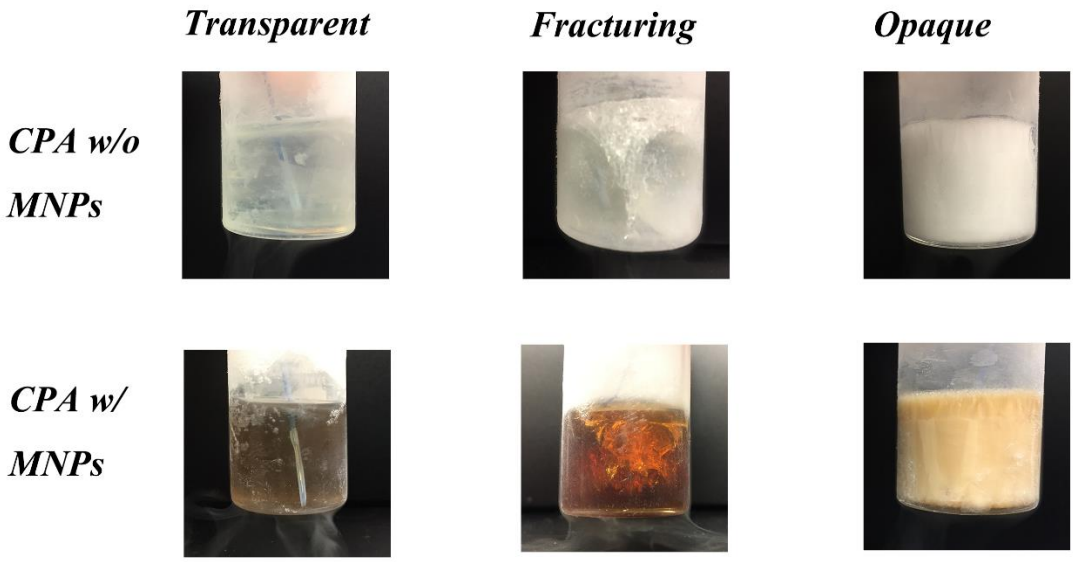

Figure 5-4. Typical visual images of CPA solutions cooled down to −140 °C. DPVP (41% DMSO, 6% PVP) w/ or w/o Fe_3O_4 nanoparticles formed transparent solid (left) using the vapor phase cooling method. Cracks (middle) were seen after plunging the bulk DPVP w/ or w/o nanoparticles into liquid nitrogen. Opaque crystalline solid (right) were observed for slowly cooled 5.2 M DMSO, the concentration of CPA is insufficient to achieve vitrification at this low cooling rate.

As can be seen in Figure 5-4, substantial ice crystals were observed around the fracture planes in the CPA solutions plunged into liquid nitrogen rather than cooled by vapor phase nitrogen avoiding the cracks otherwise.

5.3.2 *The EM resonance rewarming of CPA solutions; enhanced rates by Fe_3O_4 nanoparticles*

After cooled by vapor phase nitrogen as described, the samples were covered by Styrofoam to reduce natural convection effects, transferred into the center of the resonance chamber, and rewarmed by the optimized electromagnetic resonance rewarming system. The temperature changes from −130 °C to 0 °C for DPVP with different concentrations of 10nm, 15nm Fe_3O_4 (Figure 5-5) were recorded by the fiber optic thermometer.

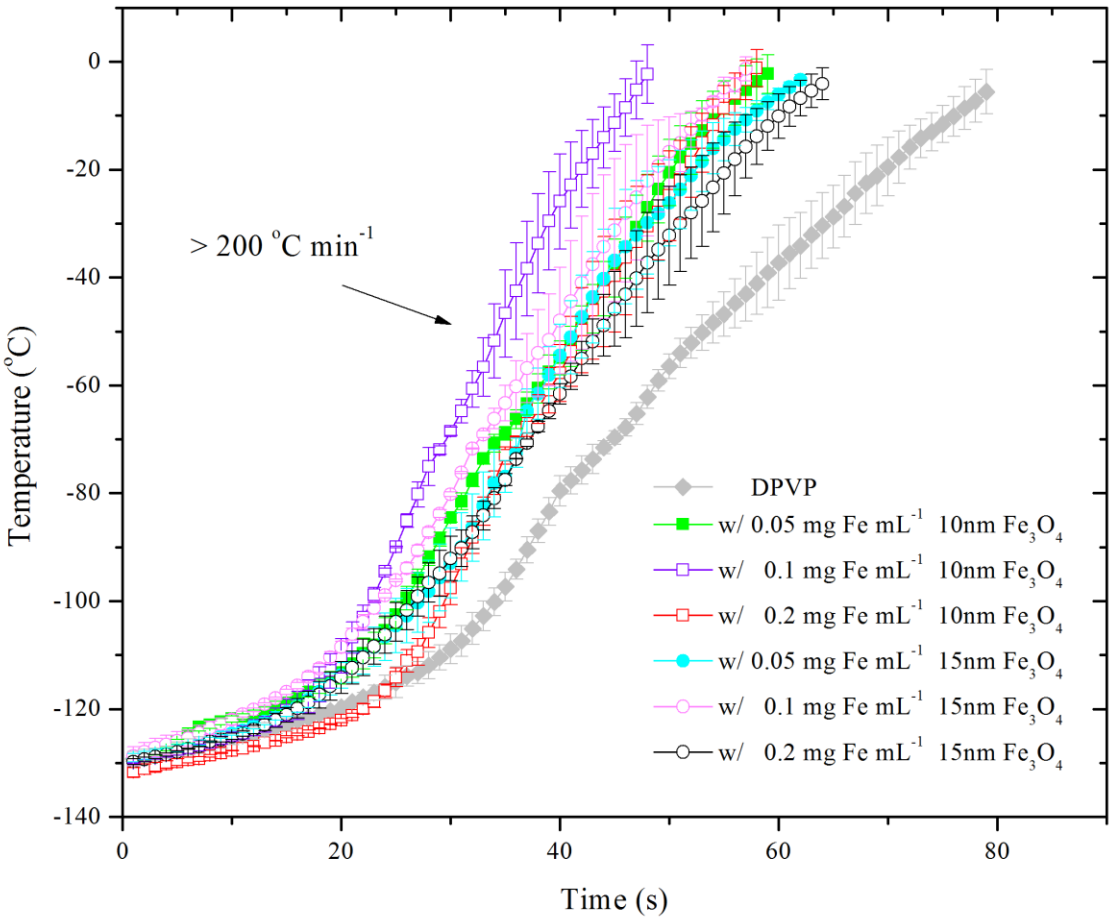

Figure 5-5. Temperature change of the CPA solutions during the rewarming process. Average value of temperature versus time was given based on four times measurements.

Because the onset of devitrification (formation of small ice crystals) may be less lethal to tissues compared to recrystallization (the growth of ice crystals). For large tissue cryopreservation, it is assumed that relatively slow warming rate should be used initially to avoid fractures or cracks induced by uneven warming. Then the warming should be as rapid as possible to pass through the recrystallization zone. Moreover, an ice free cryopreservation protocol was proposed for tissue preservation in the last decade [113, 114]. In brief, CPA solution at a concentration high enough to achieve vitrification was used in the preservation but cryopreserved tissues were stored above the glass transition temperature (around −80 °C). Hence, the entire

rewarming temperature range was separated into two sections: −130 °C to −70 °C and −70 °C to 0 °C, and corresponding average rewarming rates were reported (Figure 5-6 and Figure 5-7).

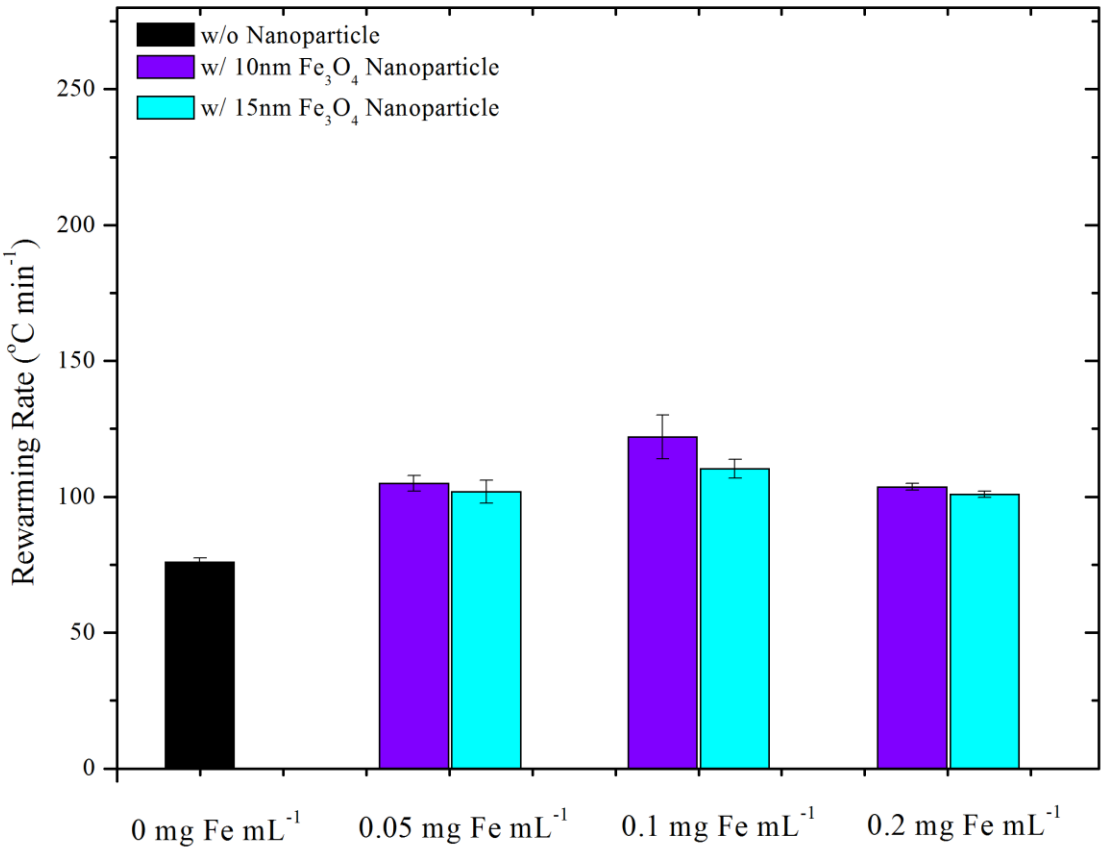

Figure 5-6. Average warming rates were determined for the rewarming temperature range −130 °C to −70 °C.

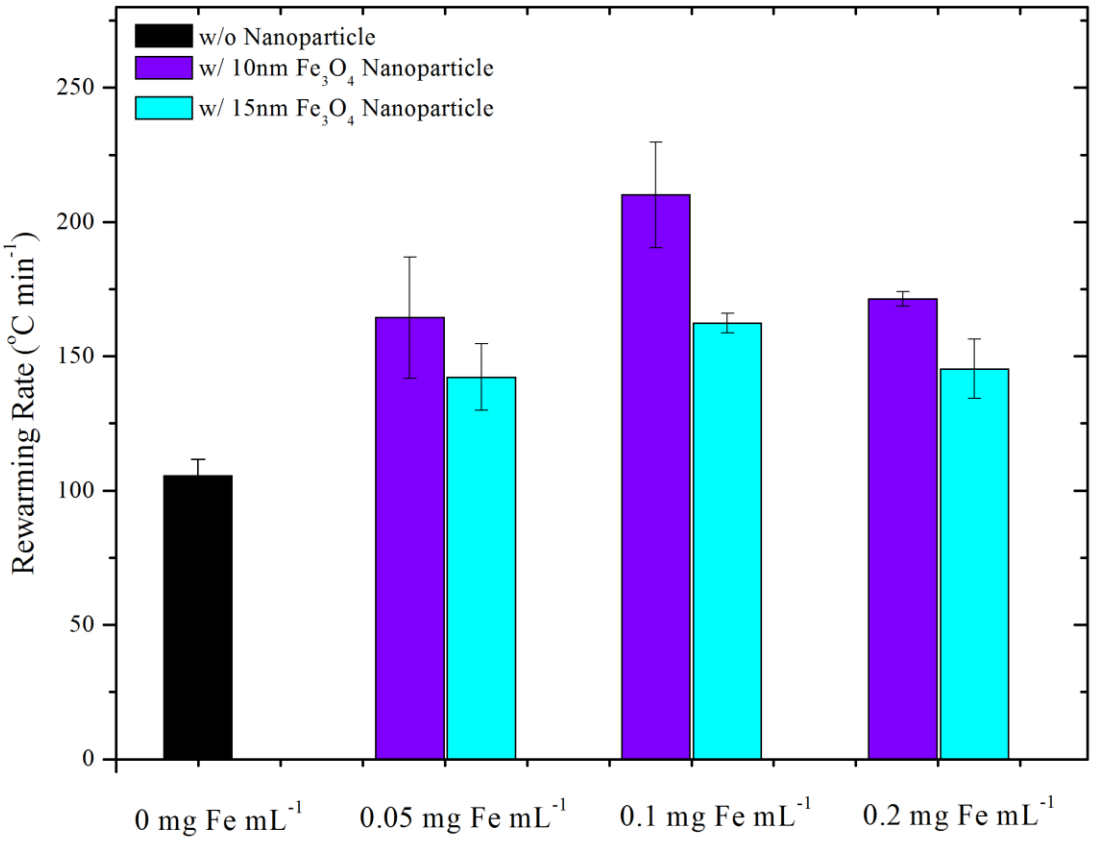

Figure 5-7. Average warming rates were determined for the rewarming temperature range −70 °C to 0 °C.

We emphasized the rapidity of rewarming during the temperature range −70 °C to 0 °C which is more perilous to cryopreserved materials. Without adding Fe_3O_4 nanoparticles, the average warming rate for DPVP reached 76.0 ± 1.5 °C min^{-1} from −130 °C to −70 °C, and 105.6 ± 6.0 °C min^{-1} from −70 °C to 0 °C using this optimized EM resonance system. To investigate the impact of nanoparticles of different sizes, 10nm and 15nm Fe_3O_4 nanoparticles were added since the MNPs exhibit superparamagnetic properties with size reduced to about 15 nm [115]. Superparamagnetic MNPs possess remarkable heating capabilities at lower magnetic fields [116]. After adding Fe_3O_4 nanoparticles at the concentration of 0.05 mg Fe mL^{-1} (lowest concentration used in this study), the rewarming rates in the temperature range −130 °C to −70

°C were increased to 104.9 ± 2.9 °C min^{-1} and 101.9 ± 4.3 °C min^{-1} for 10 nm and 15 nm Fe_3O_4 nanoparticles. In the temperature range from −70 °C to 0 °C, the warming rates were enhanced to 164.4 ± 22.6 °C min^{-1} and 142.3 ± 12.3 °C min^{-1} for 10 nm and 15 nm Fe_3O_4 nanoparticles respectively, corresponding to a 61.2% and 39.6% rewarming rate enhancement. Figure 5-8 and Figure 5-9 show that the freeze-warming behavior of CPA solutions determined by differential scanning calorimetry (DSC). The cooling rates and heating rates for the minuscule sample in DSC were set in agreement with the bulk cryopreserved materials rewarmed by the resonance system. The addition of Fe_3O_4 nanoparticles in DPVP did not change the heat flow during the rewarming. Also, the devitrification phenomena for DPVP w/ or w/o Fe_3O_4 nanoparticles were not observed using the rapid warming rates, illustrating that the ultrafast rewarming achieved by the electromagnetic resonance rewarming system can prevent severe devitrification or recrystallization.

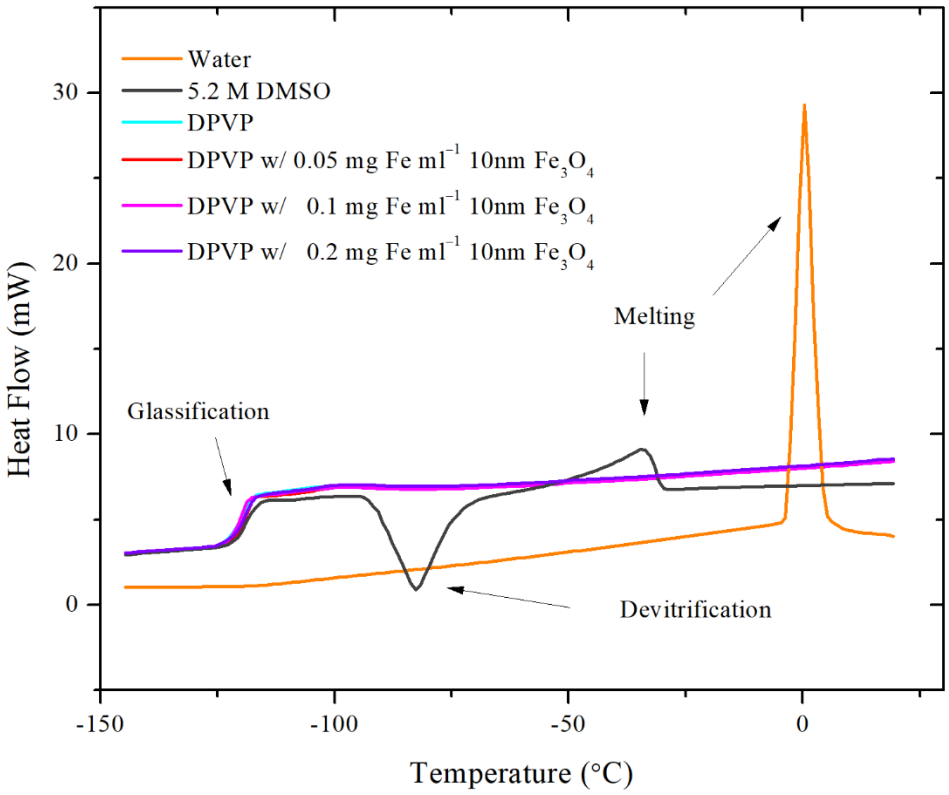

Figure 5-8. Freeze-rewarming behavior of CPA solutions with 10nm Fe_3O_4 nanoparticles.

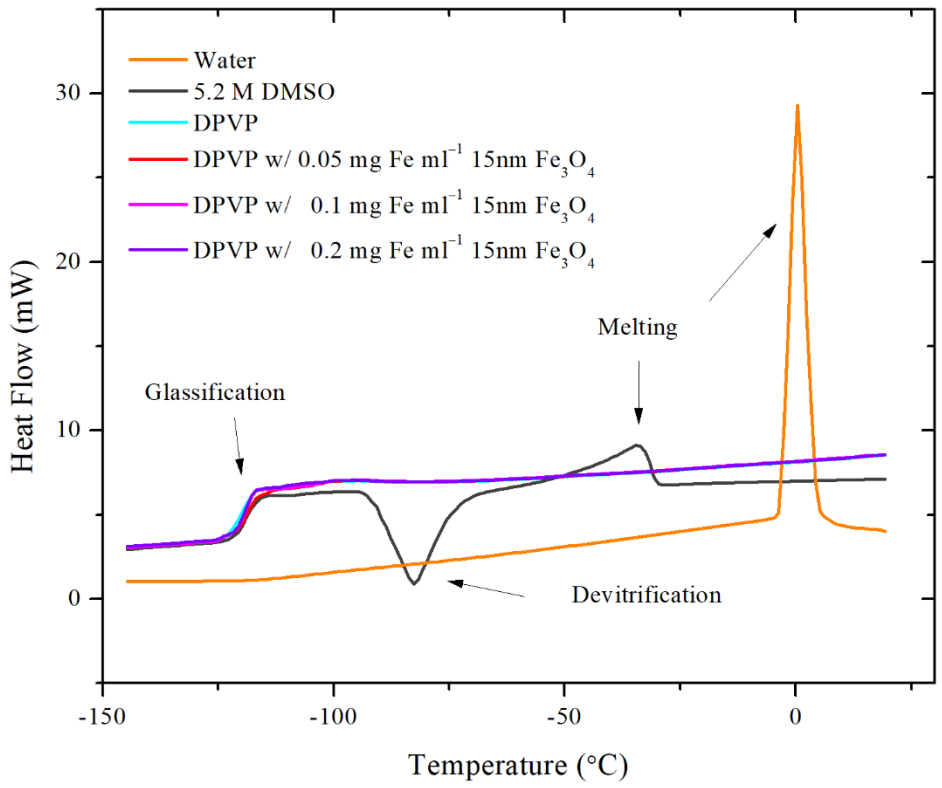

Figure 5-9. Freeze-rewarming behavior of CPA solutions with 15nm Fe_3O_4 nanoparticles.

Fundamentally, the MNPs heat release under oscillating magnetic fields (RF coil heating) are due to several mechanisms of magnetic energy conversion: hysteresis, relaxation rotation of the particles in the fluid (referred to Brownian relaxation) and rotation within the particle (known as Nèel relation) [102]. Magnetic hysteresis can be neglected in the context using superparamagnetic MNPs [117]. Therefore, magnetic heat generation is owning to the latter effects which provide energy after displacing the moment of nanoparticles and relaxing back to the equilibrium. The characteristic time for Brownian and Nèel relaxation mechanisms were described by the following equations [118, 119]:

$$\tau_B = \frac{3\eta V_H}{kT} \tag{5.1}$$

$$\tau_N = \frac{\tau_0}{2}\sqrt{\pi \frac{kT}{KV}} e^{KV/kT} \tag{5.2}$$

where η is the viscosity of the fluid and V_H is the hydrodynamic volume of the particle. K represents the anisotropy constant and V denotes the volume of the particle. The effective relaxation time accounting for the combination of the two mechanisms and heat generation related to the relaxation are given by [119]:

$$\frac{1}{\tau} = \frac{1}{\tau_B} + \frac{1}{\tau_N} \tag{5.3}$$

$$P = \frac{1}{2}\omega \mu_0 \chi_0 H^2 \frac{\omega\tau}{1+\omega^2\tau^2} \tag{5.4}$$

where ω is the angular frequency of the applied magnetic field and H represents the field magnitude. The effective relaxation time is dominated by the shorter response. For larger particles, the Brownian relaxation tends to play a significant role while Neel relaxation for smaller particles [102].

When taking account of the complex interactions between the oscillating magnetic field and MNPs, the optimal nanoparticle size for different biomedical applications should be different. For the MNPs heating under the oscillating magnetic field created by RF coil (used in hyperthermia study), it is commonly noted that the MNPs electromagnetic heating generation is dependent on the MNP size [120-122]. The difference can result from the electromagnetic field frequency, intensity as well as the pattern of electromagnetic field distribution. Also, the magnetization of MNPs affected by the temperature as can be seen in eq.(5.1), (5.2), and was experimentally tested [122, 123]. Thus, the difference in temperature range make the MNPs enhanced heating in cryopreservation (could be as low as −196 °C) identical to other applications

such as magnetic hyperthermia which focus the heating around 40 °C. Here in our work focusing on the cryogenic temperature range, the resonance system operating at different frequency range (hundreds of MHz versus hundreds of kHz), and dissimilar electromagnetic field distribution compared to RF coil heating devices which used in hyperthermia or "nanowarming" technique. Thus, the optimum nanoparticle size from the perspective of electromagnetic energy absorption can't be defined by those RF heating investigations yet.

As shown in Fig. 5C, rewarmed by this optimized electromagnetic resonance system, DPVP with 10 nm Fe_3O_4 yielded higher rewarming rates than 15 nm Fe_3O_4 nanoparticle: 164.4 ± 22.6 °C min^{-1} versus 142.3 ± 12.3 °C min^{-1} at 0.05 mg Fe mL^{-1} (not significant, $p = 0.15$); 210.1 ± 19.7 °C min^{-1} versus 162.4 ± 3.7 °C min^{-1} at 0.1 mg Fe mL^{-1} ($p < 0.05$); 171.4 ± 2.7 °C min^{-1} versus 145.3 ± 11.0 °C min^{-1} at 0.2 mg Fe mL^{-1} ($p < 0.05$) in the temperature range from −70 °C to 0 °C. The results implied that 10 nm iron oxides may be favored from the perspective of electromagnetic energy absorption in our system.

The effect of nanoparticles concentration on the rewarming rate was also demonstrated in Figure 5-7 for either 10 nm or 15 nm Fe_3O_4. The rewarming rate of DPVP solution embedded with 10 nm Fe_3O_4 nanoparticles at the concentration of 0.1 mg Fe mL was 210.1 ± 19.7 °C min^{-1}. significantly more rapid than the lower concentration of 0.05 mg Fe mL^{-1} or higher concentration of 0.2 mg Fe mL^{-1} ($p < 0.05$). The rewarming study of 15nm Fe_3O_4 nanoparticles indicated the similar result. The highest rewarming rate was observed at 0.1 mg Fe mL^{-1} rather than the other two concentrations. The rewarming rates did not progressively increase along with the concentration of Fe_3O_4. We hypothesize that collective behavior between MNPs occurs as the concentration increases but the increasing collective behavior did not contribute to a higher ability to absorb electromagnetic energy into heat in the rewarming temperature range in

cryopreservation using our electromagnetic resonance rewarming method. Invisible ice recrystallization might interact with more concentrated nanoparticles and hinder the heating. In addition, the underlying mechanisms of the increasing inter-particle interactions on the influence of heating efficiency are not well established yet. There are several studies reporting that the heating efficiencies tend to decrease as the concentration of MNPs increases [124-126] while some experimental studies showed the opposite trend [127, 128]. For the purpose of ultrafast rewarming in cryopreservation. More experimental findings are needed to get a profound understanding on the EM energy conversion ability in this low temperature range at specific applied electromagnetic frequency. Nevertheless, the small amount but effective Fe_3O_4 nanoparticles in the current work is beneficial to avoid the potential hazards due to excessive dosage of MNPs.

5.3.3 *The efficiency of the electromagnetic rewarming*

Often, the electromagnetic-thermal energy transfer efficiency of the MNPs under the external magnetic field is described as specific absorbance rate (SAR) or referred to as specific loss powers (SLP) in some cases.

$$SAR = \frac{Cm_{total}}{m_{Fe}} \frac{\Delta T}{\Delta t} \tag{5.5}$$

In most RF coil heating applicators, electric field component is circular along the RF coil used to generate the EM field, while the magnetic field component is perpendicular to the electric field plane. Under the low frequency and small magnetic MNPs, the possible associated electric filed induced heating effects (i.e. eddy currents) are neglected [121]. Hence, SAR represents the efficiency of magnetic field energy conversion. Commonly, SAR [99, 110, 129, 130] were

located in the range of 50–500 W g^{-1}. By improving the design and synthesis of MNPs, SAR [122, 131-133] can be increased to 1000–4000 W g^{-1}. This level of SAR for RF coil magnetic heating can result in a heating rate of less than 10 °C min^{-1} in the temperature range between 30–50 °C, which is sufficient for biomedical applications in need of only a few temperature increase to release drug[94] or eradicate tumor cells[99].

However, that level of SAR may not be high enough in the context of cryopreservation of large volume samples, where hundreds of °C min^{-1} or even higher to thousands of °C min^{-1} are preferred for tissue preservation. The insufficient energy transfer efficiency leads to the adoption of higher electromagnetic source power for RF coil system [86] or other unoptimized electromagnetic system [84]. In this optimized electromagnetic resonance rewarming system, both magnetic field and electric filed contribute to the rewarming. An average warming rate of over 200 °C min^{-1} during the dangerous recrystallization temperature range was achieved for large volume cryopreserved samples.

Here the contribution of electrical heating and magnetic heating could hardly be differentiated, exact SAR with respect to the MNPs was not determined yet (if incorporating the electrical heating in the calculation of SAR, SAR would unrealistically turn to over 5000 W g^{-1}). Nevertheless, the power utilization efficiency can be compared with the other studies. To heat the sample in the same order of volume size, RF coil magnetic system [86] adopted over 10 kW achieving an average warming rate of around 120 °C min^{-1}. Another MNPs based electromagnetic heating from numerical simulation [82] pointed out 8000 W source power can yield approximately 120 °C min^{-1}. The ultrahigh source power issue should be addressed in various electromagnetic heating applications where a significant part of energy was not used to heat the target cells/materials but turned into heat within the electromagnetic generation system

or connective circuits. Thus water cooling [129, 130] for these systems must be assembled to prevent high power system malfunction. Whereas this optimized electromagnetic resonance system only used 500 W with the dynamic resonance tracking to increase the electromagnetic energy transfer efficiency and prevent the overheating caused by reflected power. The experimental results and analysis show that the system with MNPs not only can obtain higher warming rate, but also convert energy very efficiently.

5.3.4 *Post-thawing temperature distribution*

Temperature distributions recorded by IR thermometer (Figure 5-10) were analyzed to characterize the temperature gradients after the rewarming. The large temperature difference of DPVP without Fe_3O_4 (Over 30 °C) imply that threatening thermal stresses may occur. The addition of Fe_3O_4, either 10nm or 15nm, notably reduced the inhomogeneity in the final temperature distribution. Here the temperature gradient was calculated as the maximum temperature difference divided by the distance.

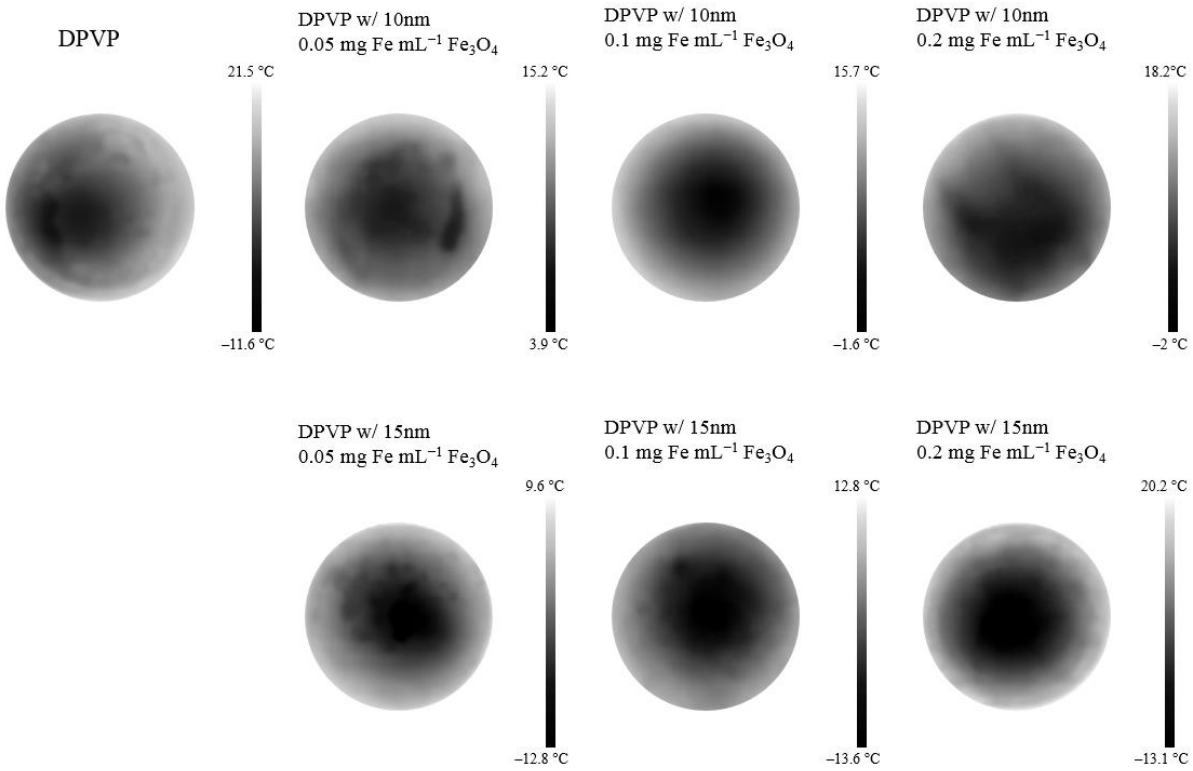

Figure 5-10. The surface temperature distribution of the post-rewarming of CPA solutions with embedded Fe3O4 nanoparticles using the electromagnetic resonance system.

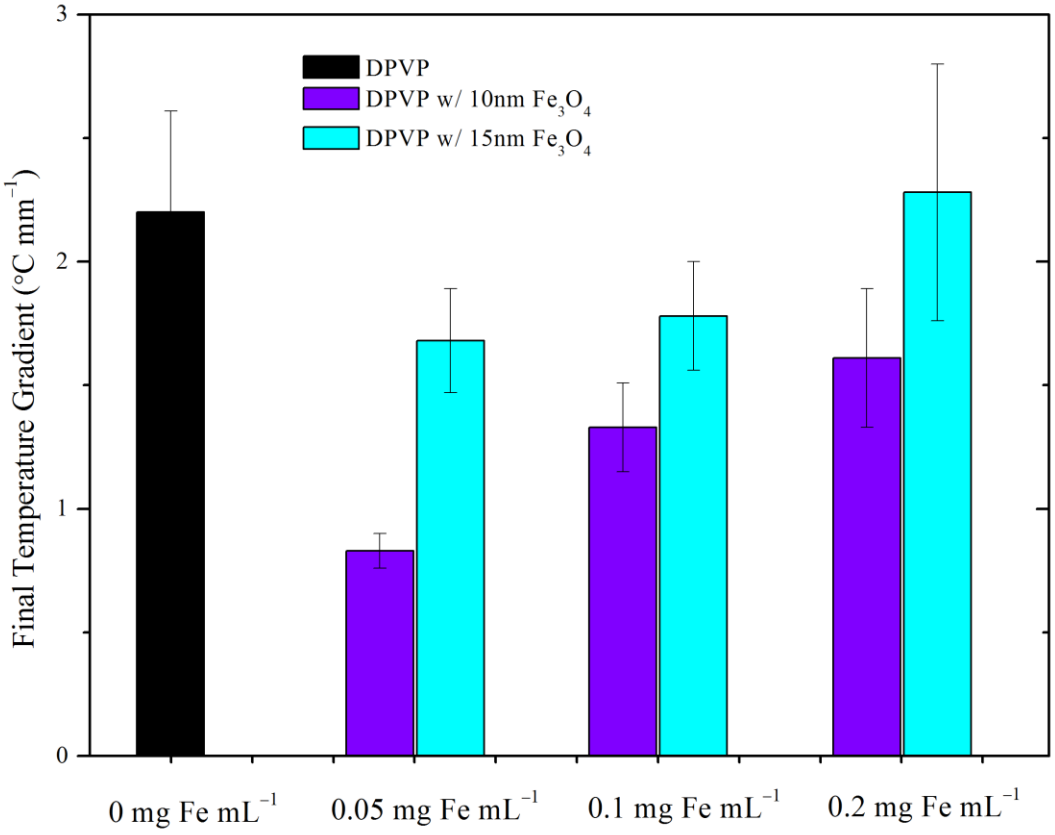

Figure 5-11. The temperature gradients were calculated as the maximum temperature difference divided by the distance. Mean values ± standard deviations were determined based on four measurements.

As Figure 5-11 shows, the temperature gradients for DPVP with 10nm Fe_3O_4 are lower than those with 15nm Fe_3O_4: 0.83 ± 0.07 °C mm^{-1} versus 1.68± 0.21 °C mm^{-1} at 0.05 mg Fe mL^{-1}; 1.33 ± 0.18 °C mm^{-1} versus 1.78 ± 0.22 °C mm^{-1} at 1 mg Fe mL^{-1}; 1.61 ± 0.28 °C mm^{-1} versus 2.28 ± 0.52 °C mm^{-1} at 0.2 mg Fe mL^{-1}. It was noted that the temperature gradient slightly increased as the concentration of Fe_3O_4, irrespective of the nanoparticle size. The thermal conductivities of the CPAs were determined in the temperature range from −30 °C to 20 °C as shown in Figure 5-12 and Figure 5-13.

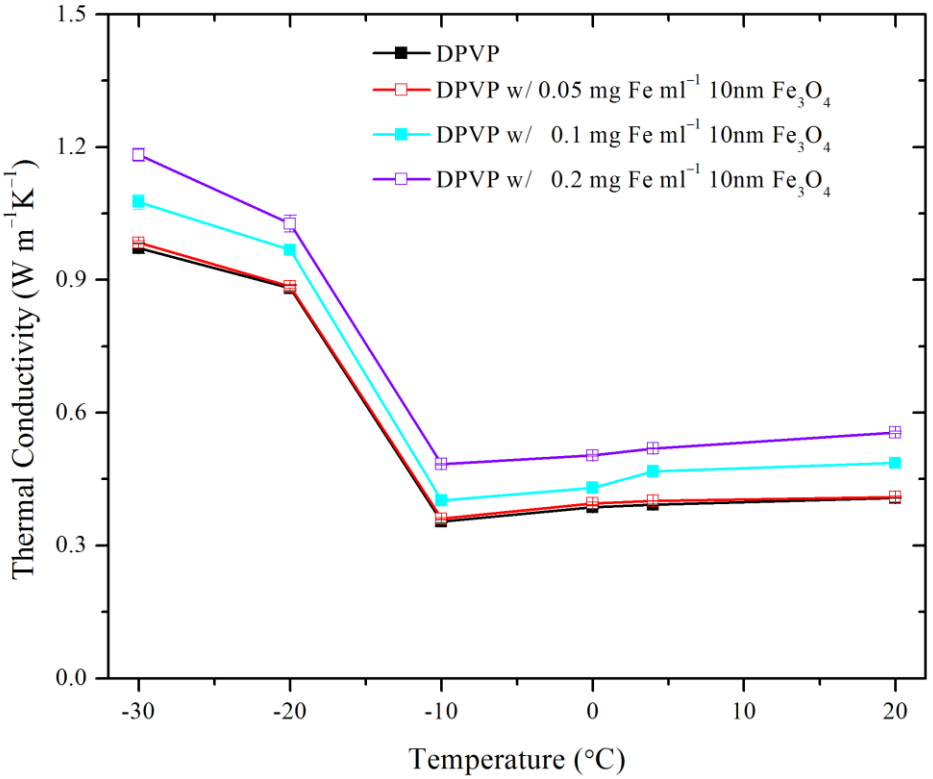

Figure 5-12. Thermal conductivities of CPA solution with 10nm Fe_3O_4 nanoparticles.

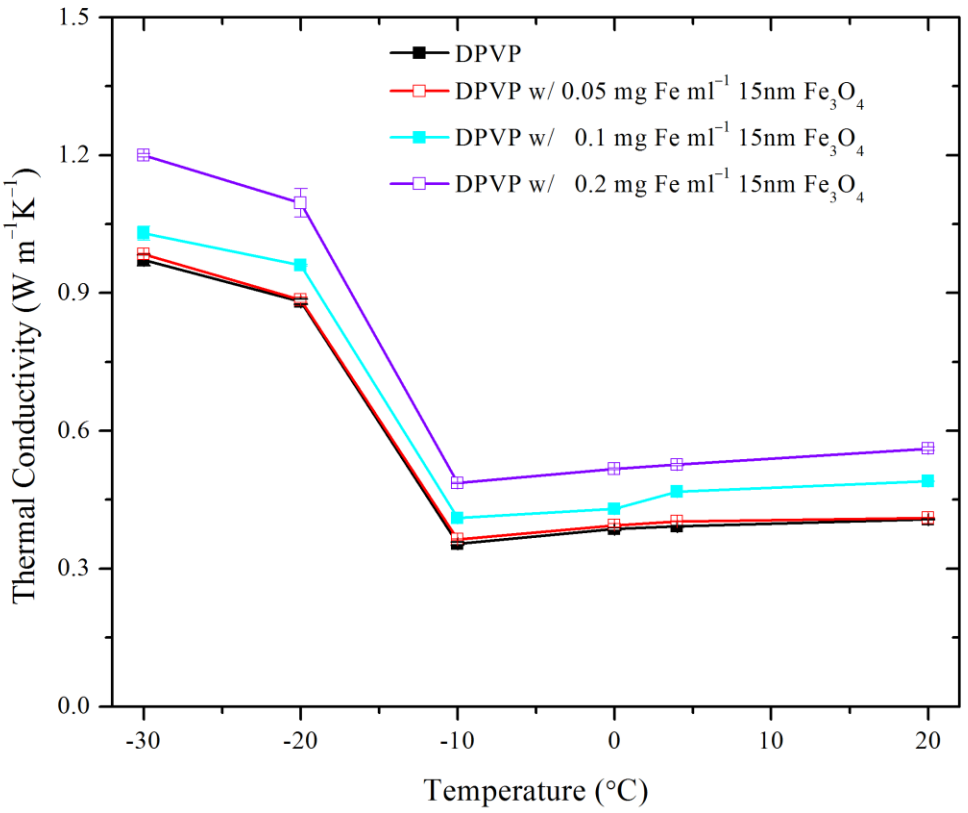

Figure 5-13. Thermal conductivities of CPA solution with 15nm Fe_3O_4 nanoparticles.

The higher concentration of Fe_3O_4 enhanced the thermal conductivities. Since conduction is the only heat transfer approach within the cryopreserved material for the boundary rewarming technique, a higher thermal conductivity generally increases the uniformity of temperature distribution. Whereas in this study, the enhancement of thermal conductivities was observed as the increase of the concentration of Fe_3O_4, but the improvement in the uniformity was not found. Hence, we assume that the electric and magnetic properties change due to the addition of MNPs altered the interaction between the CPAs and applied electromagnetic fields. In the short period time by this optimized rewarming system compared to the traditional boundary heating approach, the heating is dominant by the electromagnetic energy conversion instead of

conductive heat transfer. The electromagnetic field distribution inside the CPAs and the electric properties is more important than the enhancement of thermal conductivity in determining the uniformity of temperature distribution.

5.4 CONCLUSION

In summary, we developed an optimized electromagnetic resonance rewarming system augmented with a dynamical control component. With the introduction of Fe_3O_4 nanoparticles, the electromagnetic field provided a higher efficiency rapid and uniform rewarming of large cryopreserved objects. The rewarming of the CPA with 10nm Fe_3O_4 at 0.1 mg mL showed a significant enhancement in the rate (210.1 °C min^{-1}) and final temperature uniformity (1.33 °C mm^{-1}), which opens another gate to solve the rewarming bottleneck problem in tissue or organ preservation.

This study merely practiced 500 W source power due to the efficient electromagnetic energy utilization. Avoiding the difficulty in escalating commercial available RF source power[109], the electromagnetic resonance approach is more feasible to scale up for larger biomaterials preservation by controlling the system during the dynamic heating process, maintaining the high energy conversion efficiency. Moreover, RF radiation, the frequency range 30 kHz-300 GHz electromagnetic waves including the microwave, was defined a ‘possible’ human carcinogen (Group 2B) by World Health Organization[134] in 2011, and the classification was not changed [135] at a meeting in 2017. Minimizing radiation power in our closed electromagnetic system (the resonance rewarming chamber acts as electromagnetic shielding) can be beneficial to avoid the potential risk brought by electromagnetic exposure in the open system, such as the high-power RF coil heating device.

Finally, the thermal analysis partly elucidated the contribution of Fe_3O_4 nanoparticles in the cooling and rewarming. To fully understand the quantitative enhancement of embedded MNPs in the electromagnetic rewarming and cryopreservation, particularly in separating the improvement in electric field absorption and magnetic field energy utilization, more extensive studies are needed to explore the electromagnetic -thermal conversion effects of MNPs in different CPAs in subzero temperature ranges; quantitatively analyze the influences on the magnetic properties and the electric properties, which can facilitate the optimization of the MNPs assisted electromagnetic rewarming for tissue or organ preservation.

Chapter 6. Summary and Future work

6.1 SUMMARY

The traditional cryopreservation technique is mostly effective to specific single type of cells, which involves the compromise between solution effects and intracellular ice formation. However, it is not appropriate for tissues or organs which are composed of various types of cells and vascular tissue in which case even extracellular ice formation can lead to significant damages. Vitrification is an alternative possible approach to achieve the goal of the long-term preservation of large biomaterials, facilitating the tissue and organ preservation. Hindered by a lack of effective rewarming technique, the benefits of cryopreservation of tissue or organ by vitrification has not been fully exploited. Thus, in this dissertation, an effective rewarming technique is developed to deal with this difficult problem.

The effective rewarming technique for cryopreservation of large biomaterials should be both rapid and uniform. The size of target biomaterials such as tissues and organs rules out the possibility using the conventional water bath, which inevitably results in temperature difference induced thermal stresses. In comparison, electromagnetic waves are considered as a feasible approach with the ability to generate volumetric heating within the large cryopreserved samples. The design of electromagnetic resonance rewarming in this work is based on several previous investigations. To further realize the advantages of electromagnetic waves warming method over convective warming methods, essential physical properties including complex permittivity, thermal conductivity and specific heat were determined for several vitrification solutions. Analysis were performed based on the properties to estimate the possibility of rapid warming rate and the likelihood of thermal runaway phenomenon. One of the vitrification solutions DPVP

(41% DMSO and 6% PVP) was assumed to be a suitable candidate for electromagnetic rewarming due to its higher ability to convert electromagnetic energy into heat and relatively small specific heat that requires less energy to be rewarmed. According to the comparisons and analysis among the tested vitrification solutions, it was proposed that the imaginary part of complex permittivity of vitrification solution should be high to absorb more electric field energy. Also, a negative gradient of the imaginary part can suppress the increasing temperature difference. The experimentally determined properties laid a foundation for the development of a more profound and clear theoretical analysis for the electromagnetic resonance rewarming.

In order to assist in the design and optimization of electromagnetic rewarming system, a numerical simulation model based on finite element method was established on the basis of the measured properties of vitrification solutions. A number of factors that may affect the final rewarming outcomes were tested including the type, sample shape of CPA solutions, and the coupling between the electromagnetic system components. The temperature change over the entire region and whole rewarming process could be determined by the numerical model which is more difficult to access by experimental approaches. Therefore, this model can determine the rapidity of the electromagnetic rewarming and occurrence of thermal runaway. These preliminary results gave insights for the following experimental platform setup. We also proposed a novel rewarming concept which combines the electromagnetic rewarming and the conductive rewarming. The concept was tested by designing a cylindrical sample holder which was embedded with a rod in the center. The rod can absorb the electromagnetic energy and conduct heat to the surrounding cryopreserved materials and facilitate the temperature nonuniformity based on experimental trials. The material properties of the rod and specific field

distribution with the rod should be further validated. On-going work is being carried out on the optimization of this combined electromagnetic-conduction heat transfer method.

The preliminary results from numerical simulation provided guidance for the following optimization of the electromagnetic resonance rewarming system. Although it is of significance in the determination of the system parameters, a key part in the electromagnetic resonance rewarming system, the frequency tracking component, cannot be realized in the simulation for now. Moreover, practical electromagnetic sealing problems cannot be tested by the simulations by far: the electromagnetic power leakage from the manufacturing; and the necessary opening for the loading and accessing the samples in the cavity. Hence, there are still a lot of work to be considered in the experimental system design. The frequency source is preset before the theoretical simulation of the electromagnetic rewarming. As the temperature of the inserted cryopreserved materials increases, the electric property change associated with the temperature of the cryopreserved materials lead to a resonant frequency shift. The frequency tracking system is of great importance to ensure most of the electromagnetic energy are confined in the resonant state and converted into heat, which demonstrated the efficacy and of great potential to ensure electromagnetic resonance rewarming.

Finally, this study tested the enhanced effects of magnetic nanoparticles. It was found that the addition of small amounts of nanoparticles would not affect the vitrification by slow cooling provided with sufficient high concentration of CPAs. In the following rewarming process, the vitrification solutions with magnetic nanoparticles demonstrated a significant higher warming rates heated by the electromagnetic resonance rewarming system. The final temperature uniformity was also improved by the nanoparticles. However, the warming rate did not monotonically increase as the increase of nanoparticle concentrations, which indicated an

optimal nanoparticle concentration. In comparison to the radiofrequency electromagnetic rewarming that only utilize the magnetic field component energy, the energy conversion efficiency is significantly increased; the required amounts of nanoparticles are greatly reduced. The optimization in the electromagnetic resonance rewarming can be both beneficial to reduce potential hazards to the operators who are exposed to the applied electromagnetic field as well as to minimize the complexity of the washing of nanoparticles out of the cryopreserved materials after the rewarming process.

6.2 FUTURE WORK

There remains many challenges to further understand the mechanisms of the vitrification and electromagnetic rewarming. At the same time, many opportunities will come out after more solid and systematic investigations. A very interesting phenomenon that intrigues us is the electromagnetic rewarming of vitrification solutions with embedded nanoparticles. Intuitively, the rewarming rate should increase when adding more nanoparticles. However, the highest concentration of nanoparticles did not yield a highest warming rate. We currently hypothesize the vitrification by slow cooling immobilized the nanoparticles and may lead to some clusters at the low temperature range. The collective effects may inhibit the rewarming rates as more aggregation of nanoparticles generated. This hypothesis should be validated with advanced measurement methods to determine the electric and/or magnetic properties. A cryo-EM microscopy may possibly be helpful to inspect whether clusters of nanoparticles are formed at the vitrification state in the slow cooling process. We are currently in short of lab facilities to clearly separate the enhanced electric effects and magnetic heating effects. The magnetic properties, electric properties should both be determined at the subzero temperature range. In

addition, a numerical simulation that involves dipole electric heating, magnetic heating (hysteresis, Neel relaxation, Brownian relaxation) should be helpful to determine the contribution of nanoparticles precisely. The optimal amount of nanoparticles could also be derived.

Other than developing theoretical models to elucidate the interaction mechanism between nanoparticles, cooling and electromagnetic rewarming, this dissertation particularly focuses on the optimization of the resonance rewarming system to avoid the devitrification or recrystallization. One part of work is devoted to the electromagnetic system development. The other part is to improve the vitrification solution to enhance the ability to convert electromagnetic energy into heat. In the future work to develop the electromagnetic resonance rewarming systems, temperature monitoring should be upgraded by using advanced infrared cameras during the entire rewarming period rather than merely determine the post-rewarming thermal graph. More fiber optic sensors during the rewarming process should be adopted to get a detailed internal temperature distribution. On the other hand, this work only tested phantom tissue materials for now. Hence, the vitrification solutions may be improved to ensure efficacy in terms of vitrifying biological materials. The tissues must be able to tolerate the vitrification as well as maintain function after the removal of the vitrification solutions. A lot of other issues should be taken into consideration such as the tendency to vitrify, the toxicity of the vitrification solutions to the tissues. Besides, the cooling process can be modified such as using spray of nitrogen gas. The current commercially available freezer is limited to the small volume of cryopreserved cell suspensions. A more delicate design of the cooling system specifically for tissue should be able to monitor the temperatures at various positions, control the cooling rate by changing the nitrogen supply and maintain the temperature for annealing to release thermal

stresses. As for organ preservation, it is even more complicated to achieve vitrification both in the cooling and rewarming process. A delicate perfusion protocol to deliver vitrification solutions in the organ must be designed to avoid partial devitrification during the cooling process. The electromagnetic resonance rewarming system, currently achieving over 200 °C min^{-1} for 20 mL samples, should also be optimized to meet more challenging demands called from organ preservation. The dimension of the cavity and the position of power feeding port where the electromagnetic field is applied into the cavity are essential to determine the field distribution inside the cavity. If the size of target organ to be cryopreserved is increased from 20 mL to over 100 mL, the dimension of the cavity should be revised accordingly, and different frequency band may be used to adjust the electromagnetic penetration. In addition, the determination of usage of assisted materials such as the gel and nanoparticles is closely related to the design of electromagnetic resonance rewarming system. The electromagnetic power absorption abilities of gels and nanoparticles are dependent on the electromagnetic frequency. The electromagnetic resonant frequency of the electromagnetic resonance cavity is determined by its dimension. Thus, when optimizing the electromagnetic resonance system, the supplementary materials should also be tested with the new design (frequency, electromagnetic field pattern) simultaneously. Through the approach as this dissertation presented: material properties measurement, numerical simulation and then experimental tests. In all, the fundamental mechanisms of vitrification, nanoparticle interaction with electromagnetic fields should be elucidated; additional property measurement should be conducted, and preliminary simulation models and tests are required to achieve the ultimate goal of tissue and organ preservation.

Finally, the current electromagnetic resonance rewarming system frequency is between hundreds of MHz. There are some other frequency ranges that could be utilized such as low radiofrequency rage (hundreds of kHz) and laser (up to hundreds of GHz) which demonstrated significantly different heating mechanisms. The electromagnetic waves in different frequency range demonstrate different penetration depth into the biomaterials. Also, the embedded nanoparticles have different absorption ability to these electromagnetic waves. Therefore, by designing the combination of heating devices (the power of different devices, target heating area by electromagnetic waves in different frequency range), the concentration of nanoparticles at specific area, we may develop more unconventional and highly efficient rewarming techniques.

Reference

[1] C. Polge, A.U. Smith, A.S. Parkes, Revival of Spermatozoa after Vitrification and Dehydration at Low Temperatures, Nature, 164(4172) (1949) 666-666.

[2] A. Sputtek, Cryopreservation of red blood cells and platelets, Methods in molecular biology, 368 (2007) 283-301.

[3] S.J. Behrman, D.R. Ackerman, Freeze Preservation of Human Sperm, Am J Obstet Gynecol, 103(5) (1969) 654-&.

[4] R.G. Bunge, W.C. Keettel, J.K. Sherman, Clinical Use of Frozen Semen - Report of 4 Cases, Fertil Steril, 5(6) (1954) 520-529.

[5] S. al-Hasani, J. Kirsch, K. Diedrich, S. Blanke, H. van der Ven, D. Krebs, Successful embryo transfer of cryopreserved and in-vitro fertilized rabbit oocytes, Hum Reprod, 4(1) (1989) 77-79.

[6] C. Chen, Pregnancy after Human Oocyte Cryopreservation, Lancet, 1(8486) (1986) 884-886.

[7] M. Richards, C.Y. Fong, S. Tan, W.K. Chan, A. Bongso, An efficient and safe Xeno-Free Cryopreservation method for the storage of human embryonic stem cells, Stem Cells, 22(5) (2004) 779-789.

[8] B. Diener, D. Utesch, N. Beer, H. Durk, F. Oesch, A Method for the Cryopreservation of Liver Parenchymal-Cells for Studies of Xenobiotics, Cryobiology, 30(2) (1993) 116-127.

[9] C. Baxter, S. Aggarwal, K.R. Diller, Cryopreservation of Skin - a Review, Transpl P, 17(6) (1985) 112-120.

[10] F.O. Mueller, P.D. Trevorroper, T.A. Casey, Use of Deep-Frozen Human Cornea in Full-Thickness Grafts, Brit Med J, 2(540) (1964) 473-&.

[11] R.S. Weiner, Cryopreservation of Lymphocytes for Use in Invitro Assays of Cellular Immunity, J Immunol Methods, 10(1) (1976) 49-60.

[12] J.E. Lovelock, The Haemolysis of Human Red Blood-Cells by Freezing and Thawing, Biochim Biophys Acta, 10(3) (1953) 414-426.

[13] H.T. Meryman, Freezing injury and its prevention in living cells, Annual review of biophysics and bioengineering, 3(0) (1974) 341-363.

[14] P. Mazur, S.P. Leibo, E.H. Chu, A two-factor hypothesis of freezing injury. Evidence from Chinese hamster tissue-culture cells, Experimental cell research, 71(2) (1972) 345-355.

[15] D. Gao, J.K. Critser, Mechanisms of cryoinjury in living cells, ILAR journal, 41(4) (2000) 187-196.

[16] P. Mazur, Kinetics of Water Loss from Cells at Subzero Temperatures and Likelihood of Intracellular Freezing, J Gen Physiol, 47(2) (1963) 347-&.

[17] P. Mazur, Freezing of Living Cells - Mechanisms and Implications, Am J Physiol, 247(3) (1984) C125-C142.

[18] P. Mazur, Cryobiology: the freezing of biological systems, Science, 168(3934) (1970) 939-949.

[19] P. Mazur, Cryobiology - Freezing of Biological Systems, Science, 168(3934) (1970) 939-&.

[20] K.G. Brockbank, F.G. Lightfoot, Y.C. Song, M.J. Taylor, Interstitial ice formation in cryopreserved homografts: a possible cause of tissue deterioration and calcification in vivo, The Journal of heart valve disease, 9(2) (2000) 200-206.

[21] B. Wowk, Thermodynamic aspects of vitrification, Cryobiology, 60(1) (2010) 11-22.

[22] G.M. Fahy, B. Wowk, J. Wu, Cryopreservation of complex systems: the missing link in the regenerative medicine supply chain, Rejuvenation Res, 9(2) (2006) 279-291.

[23] G.M. Fahy, D.R. MacFarlane, C.A. Angell, H.T. Meryman, Vitrification as an approach to cryopreservation, Cryobiology, 21(4) (1984) 407-426.

[24] P. Boutron, A. Kaufmann, Stability of the amorphous state in the system water--glycerol--dimethylsulfoxide, Cryobiology, 15(1) (1978) 93-108.

[25] H.S. Ren, Y. Wei, T.C. Hua, J. Zhang, Theoretical Prediction of Vitrification and Devitrification Tendencies for Cryoprotective Solutions, Cryobiology, 31(1) (1994) 47-56.

[26] C.A. Amorim, M. Curaba, A. Van Langendonckt, M.M. Dolmans, J. Donnez, Vitrification as an alternative means of cryopreserving ovarian tissue, Reprod Biomed Online, 23(2) (2011) 160-186.

[27] A.A. Carvalho, L.R. Faustino, C.M.G. Silva, S.V. Castro, C.A.P. Lopes, R.R. Santos, S.N. Bao, J.R. Figueiredo, A.P.R. Rodrigues, Novel wide-capacity method for vitrification of caprine ovaries: Ovarian Tissue Cryosystem (OTC), Anim Reprod Sci, 138(3-4) (2013) 220-227.

[28] Y.K. Chong, T.B. Toh, N. Zaiden, A. Poonepalli, S.H. Leong, C.E.L. Ong, Y. Yu, P.B. Tan, S.J. See, W.H. Ng, I. Ng, M.P. Hande, O.L. Kon, B.T. Ang, C. Tang, Cryopreservation of neurospheres derived from human glioblastoma multiforme, Stem Cells, 27(1) (2009) 29-39.

[29] H.U. Kasper, E. Konze, N.K. Canova, H.P. Dienes, V. Dries, Cryopreservation of precision cut tissue slices (PCTS): Investigation of morphology and reactivity, Exp Toxicol Pathol, 63(6) (2011) 575-580.

[30] M. Kuwayama, G. Vajta, O. Kato, S.P. Leibo, Highly efficient vitrification method for cryopreservation of human oocytes, Reprod Biomed Online, 11(3) (2005) 300-308.

[31] O. Merino, J. Risopatron, R. Sanchez, E. Isachenko, E. Figueroa, I. Valdebenito, V. Isachenko, Fish (Oncorhynchus mykiss) spermatozoa cryoprotectant-free vitrification: Stability of mitochondrion as criterion of effectiveness, Anim Reprod Sci, 124(1-2) (2011) 125-131.

[32] M.A. Silvestre, A.M. Saeed, M.J. Escriba, F. Garcia-Ximenez, Vitrification and rapid freezing of rabbit fetal tissues and skin samples from rabbits and pigs, Theriogenology, 58(1) (2002) 69-76.

[33] M.A. Silvestre, J.P. Sanchez, E.A. Gomez, Vitrification of goat, sheep, and cattle skin samples from whole ear extirpated after death and maintained at different storage times and temperatures, Cryobiology, 49(3) (2004) 221-229.

[34] Y.C. Song, Z.Z. Chen, N. Mukherjee, F.G. Lightfoot, M.J. Taylor, K.G. Brockbank, A. Sambanis, Vitrification of tissue engineered pancreatic substitute, Transpl P, 37(1) (2005) 253-255.

[35] Y.C. Song, B.S. Khirabadi, F. Lightfoot, K.G.M. Brockbank, M.J. Taylor, Vitreous cryopreservation maintains the function of vascular grafts, Nat Biotechnol, 18(3) (2000) 296-299.

[36] A.Y. Ting, R.R. Yeoman, M.S. Lawson, M.B. Zelinski, In vitro development of secondary follicles from cryopreserved rhesus macaque ovarian tissue after slow-rate freeze or vitrification, Hum Reprod, 26(9) (2011) 2461-2472.

[37] M. Milenkovic, C. Diaz-Garcia, A. Wallin, M. Brannstrom, Viability and function of the cryopreserved whole rat ovary: comparison between slow-freezing and vitrification, Fertil Steril, 97(5) (2012) 1176-1182.

[38] P. Mazur, K.W. Cole, J.W. Hall, P.D. Schreuders, A.P. Mahowald, Cryobiological preservation of Drosophila embryos, Science, 258(5090) (1992) 1932-1935.

[39] S. Seki, B. Jin, P. Mazur, Extreme rapid warming yields high functional survivals of vitrified 8-cell mouse embryos even when suspended in a half-strength vitrification solution and cooled at moderate rates to -196 degrees C, Cryobiology, 68(1) (2014) 71-78.

[40] M. Kuwayama, Highly efficient vitrification for cryopreservation of human oocytes and embryos: the Cryotop method, Theriogenology, 67(1) (2007) 73-80.

[41] P.L. Spencer, Electronic cooking US2582174, in: U.S.P. Office (Ed.), 1949.

[42] P.L. Spencer, Prepared food article and method of preparing US2480679, in: U.S.P. Office (Ed.), 1947.

[43] P.L. Spencer, Food cooking US2540036, in: U.S.P. Office (Ed.), 1948.

[44] P.L. Spencer, Method of treating foodstuffs US2495429, in: U.S.P. Office (Ed.), 1945.

[45] F.D. Ketterer, H.I. Holst, H.B. Lehr, Improved Viability of Kidneys with Microwave Thawing, Cryobiology, 8(4) (1971) 395-&.

[46] F.M. Guttman, J. Lizin, P. Robitaille, H. Blanchard, C. Turgeonknaack, Survival of Canine Kidneys after Treatment with Dimethyl-Sulfoxide, Freezing at -80-Degrees-C, and Thawing by Microwave Illumination, Cryobiology, 14(5) (1977) 559-567.

[47] D.E. Pegg, C.J. Green, C.A. Walter, Attempted Canine Renal Cryopreservation Using Dimethyl-Sulfoxide Helium Perfusion and Microwave Thawing, Cryobiology, 15(6) (1978) 618-626.

[48] E.C. Burdette, A.M. Karow, A.H. Jeske, Design, Development, and Performance of an Electromagnetic Illumination System for Thawing Cryopreserved Kidneys of Rabbits and Dogs, Cryobiology, 15(2) (1978) 152-167.

[49] P.S. Ruggera, G.M. Fahy, Rapid and Uniform Electromagnetic Heating of Aqueous Cryoprotectant Solutions from Cryogenic Temperatures, Cryobiology, 27(5) (1990) 465-478.

[50] M.J. Rachman, S. Evans, D.E. Pegg, Experimental Results on the Rewarming of a Cryopreserved Organ Phantom in a Uhf Field, J Biomed Eng, 14(5) (1992) 397-403.

[51] M.P. Robinson, D.E. Pegg, Rapid electromagnetic warming of cells and tissues, IEEE transactions on bio-medical engineering, 46(12) (1999) 1413-1425.

[52] M.P. Robinson, M.C. Wusteman, L.H. Wang, D.E. Pegg, Electromagnetic re-warming of cryopreserved tissues: effect of choice of cryoprotectant and sample shape on uniformity of heating, Phys Med Biol, 47(13) (2002) 2311-2325.

[53] M.C. Wusteman, D.E. Pegg, M.P. Robinson, L.H. Wang, P. Fitch, Vitrification media: toxicity, permeability, and dielectric properties, Cryobiology, 44(1) (2002) 24-37.

[54] D.P. Eisenberg, M.J. Taylor, Y. Rabin, Thermal expansion of the cryoprotectant cocktail DP6 combined with synthetic ice modulators in presence and absence of biological tissues, Cryobiology, 65(2) (2012) 117-125.

[55] D.E. Pegg, M.C. Wusteman, S. Boylan, Fractures in cryopreserved elastic arteries, Cryobiology, 34(2) (1997) 183-192.

[56] U.C. Hasar, E.A. Oral, A Metric Function for Fast and Accurate Permittivity Determination of Low-to-High-Loss Materials from Reflection Measurements, Prog Electromagn Res, 107 (2010) 397-412.

[57] S. Ansorge, G. Esteban, G. Schmid, Multifrequency Permittivity Measurements Enable On-Line Monitoring of Changes in Intracellular Conductivity Due to Nutrient Limitations During Batch Cultivations of CHO Cells, Biotechnol Progr, 26(1) (2010) 272-283.

[58] P. Juan-Garcia, J.M. Torrents, Measurement of mortar permittivity during setting using a coplanar waveguide, Meas Sci Technol, 21(4) (2010).

[59] K.Y. Lee, Z. Abbas, Y.K. Yeow, M.D.N. Sharizan, C.E. Meng, In situ measurements of complex permittivity and moisture content in oil palm fruits, Eur Phys J-Appl Phys, 49(3) (2010).

[60] J.H. Bradford, J.T. Harper, J. Brown, Complex dielectric permittivity measurements from ground-penetrating radar data to estimate snow liquid water content in the pendular regime (vol 46, pW02901, 2010), Water Resour Res, 46 (2010).

[61] D.D. Ba, P. Sabouroux, EpsiMu, A TOOLKIT FOR PERMITTIVITY AND PERMEABILITY MEASUREMENT IN MICROWAVE DOMAIN AT REAL TIME OF ALL MATERIALS: APPLICATIONS TO SOLID AND SEMISOLID MATERIALS, Microw Opt Techn Let, 52(12) (2010) 2643-2648.

[62] T.I. Zohdi, F.A. Kuypers, W.C. Lee, Estimation of red blood cell volume fraction from overall permittivity measurements, Int J Eng Sci, 48(11) (2010) 1681-1691.

[63] R.J. Sengwa, V. Khatri, S. Choudhary, Molecular interactions in binary mixtures of 2-aminoethanol with 1,4-dioxane and dimethyl sulphoxide investigated by static permittivity measurements, Indian J Chem A, 49(12) (2010) 1612-1616.

[64] U.C. Hasar, M.T. Yurtcan, A microwave method based on amplitude-only reflection measurements for permittivity determination of low-loss materials, Measurement, 43(9) (2010) 1255-1265.

[65] K. Shibata, Measurement of Complex Permittivity for Liquid Materials Using the Open-Ended Cut-Off Waveguide Reflection Method, Ieice T Electron, E93c(11) (2010) 1621-1629.

[66] V. Komarov, Wang, S., Tang, J., Permittivity and measurements, in: K. Chang (Ed.) Encyclopedia of RF and microwave engineering(3693-3711), John Wiley and Sons, Inc, New York, 2005.

[67] M. Lin, M.H. Duane, M.N. Afsar, Cavity-perturbation measurement of complex permittivity and permeability of common ferrimagnetics in microwave-frequency range, Ieee T Magn, 42(10) (2006) 2885-2887.

[68] R.A. Waldron, Perturbation theory of resonant cavities, Proc. Inst. Electr. Eng., 107C (1960) 272-274.

[69] A.W. Kraszewski, S.O. Nelson, Oberservations on resonant cavity perturbation by dielectric objects, Ieee T Microw Theory, 40(1) (1992) 151-155.

[70] H. Altschuler, in: M. Sucher, J. Fox (Eds.) Handbook of Microwave Measurements, Polytechnic Press, Brooklyn, NY, 1963, pp. 530-536.

[71] A. Hasan, A.F. Peterson, Measurement of Complex Permittivity using Artificial Neural Networks, Ieee Antenn Propag M, 53(1) (2011) 200-203.

[72] M.P. Robinson, D.E. Pegg, Rapid electromagnetic warming of cells and tissues, Ieee T Bio-Med Eng, 46(12) (1999) 1413-1425.

[73] X.M. Liang, P.K. Sekar, G. Zhao, X.M. Zhou, Z.Q. Shu, Z. Huang, W. Ding, Q. Zhang, D.Y. Gao, High accuracy thermal conductivity measurement of aqueous cryoprotective agents and semi-rigid biological tissues using a microfabricated thermal sensor, Sci Rep-Uk, 5 (2015).

[74] G.M. Fahy, B. Wowk, J. Wu, S. Paynter, Improved vitrification solutions based on the predictability of vitrification solution toxicity, Cryobiology, 48(3) (2004) 365-365.

[75] A.V. Hippel, Dielectrics and Waves, Wiley, New York, 1954.

[76] S. Evans, M.J. Rachman, D.E. Pegg, Design of a UHF applicator for rewarming of cryopreserved biomaterials, Ieee T Bio-Med Eng, 39(3) (1992) 217-225.

[77] D.W. Luo, C. Yu, L.Q. He, C.C. Lu, D.Y. Gao, Development of a single mode electromagnetic resonant cavity for rewarming of cryopreserved biomaterials, Cryobiology, 53(2) (2006) 288-293.

[78] X. Bai, D.E. Pegg, S. Evans, J.D.J. Penfold, Analysis of electromagnetic heating patterns inside a cryopreserved organ, J Biomed Eng, 14(6) (1992) 459-466.

[79] C.C. Lu, H.Z. Li, D.Y. Gao, Combined electromagnetic and heat-conduction analysis of rapid rewarminging of cryopreserved tissues, Ieee T Microw Theory, 48(11) (2000) 2185-2190.

[80] J.D.J. Penfold, S. Evans, Control of thermal runaway and uniformity of heating in the electromagnetic rewarming of a cryopreserved kidney phantom, Cryobiology, 30(5) (1993) 493-508.

[81] X. Han, D. Gao, D. Luo, C. Yu, C. Lu, Numerical simulation of the microwave rewarming process of cryopreserved organs, Microw Opt Techn Let, 46(3) (2005) 201-205.

[82] T. Wang, G. Zhao, X.M. Liang, Y.P. Xu, Y. Li, H.Y. Tang, R. Jiang, D.Y. Gao, Numerical simulation of the effect of superparamagnetic nanoparticles on microwave rewarming of cryopreserved tissues, Cryobiology, 68(2) (2014) 234-243.

[83] R.H. Vaz, J.M.C. Pereira, A.R. Ervilha, J.C.F. Pereira, Simulation and uncertainty quantification in high temperature microwave heating, Appl Therm Eng, 70(1) (2014) 1025-1039.

[84] T. Wang, G. Zhao, Z.S. Deng, C. Gao, Y.X. Cao, D.Y. Gao, Theoretical investigation of a novel microwave antenna aided cryovial for rapid and uniform rewarming of frozen cryoprotective agent solutions, Appl Therm Eng, 89 (2015) 968-977.

[85] M.L. Etheridge, Y. Xu, L. Rott, J. Choi, B. Glasmacher, J.C. Bischof, RF heating of magnetic nanoparticles improves the thawing of cryopreserved biomaterials, Tehnology, 2(3) (2014) 229-242.

[86] N. Manuchehrabadi, Z. Gao, J.J. Zhang, H.L. Ring, Q. Shao, F. Liu, M. McDermott, A. Fok, Y. Rabin, K.G.M. Brockbank, M. Garwood, C.L. Haynes, J.C. Bischof, Improved tissue cryopreservation using inductive heating of magnetic nanoparticles, Sci Transl Med, 9(379) (2017).

[87] T. Basak, K. Aparna, A. Meenakshl, A.R. Balakrishnan, Effect of ceramic supports on microwave processing of porous food samples, Int J Heat Mass Tran, 49(23-24) (2006) 4325-4339.

[88] C. Mirabito, A. Narayanan, D. Perez, B. Stone, FEMLAB model of a coupled electromagnetic-thermal boundary value problem, Research Experience: Worcester Polytechnic Institute, Worcester, Mass, USA, 2005.

[89] H. Zhang, A.K. Datta, I.A. Taub, C. Doona, Electromagnetics, heat transfer, and thermokinetics in microwave sterilization, Aiche J, 47(9) (2001) 1957-1968.

[90] S. Farag, A. Sobhy, C. Akyel, J. Doucet, J. Chaouki, Temperature profile prediction within selected materials heated by microwaves at 2.45GHz, Appl Therm Eng, 36 (2012) 360-369.

[91] D. Luo, Electromagnetic rewarming of cryopreserved biomaterials, University of Kentucky, 2005.

[92] Y.G. Lv, Z.S. Deng, J. Liu, 3-D numerical study on the induced heating effects of embedded micro/nanoparticles on human body subject to external medical electromagnetic field, Ieee T Nanobiosci, 4(4) (2005) 284-294.

[93] J.Y. Wang, G. Zhao, Z.L. Zhang, X.L. Xu, X.M. He, Magnetic induction heating of superparamagnetic nanoparticles during rewarming augments the recovery of hUCM-MSCs cryopreserved by vitrification, Acta Biomater, 33 (2016) 264-274.

[94] K. Hayashi, K. Ono, H. Suzuki, M. Sawada, M. Moriya, W. Sakamoto, T. Yogo, High-Frequency, Magnetic-Field-Responsive Drug Release from Magnetic Nanoparticle/Organic Hybrid Based on Hyperthermic Effect, Acs Appl Mater Inter, 2(7) (2010) 1903-1911.

[95] C.S.S.R. Kumar, F. Mohammad, Magnetic nanomaterials for hyperthermia-based therapy and controlled drug delivery, Adv Drug Deliver Rev, 63(9) (2011) 789-808.

[96] M. Liong, J. Lu, M. Kovochich, T. Xia, S.G. Ruehm, A.E. Nel, F. Tamanoi, J.I. Zink, Multifunctional inorganic nanoparticles for imaging, targeting, and drug delivery, Acs Nano, 2(5) (2008) 889-896.

[97] C. Sun, J.S.H. Lee, M.Q. Zhang, Magnetic nanoparticles in MR imaging and drug delivery, Adv Drug Deliver Rev, 60(11) (2008) 1252-1265.

[98] J.H. Park, G. von Maltzahn, M.J. Xu, V. Fogal, V.R. Kotamraju, E. Ruoslahti, S.N. Bhatia, M.J. Sailor, Cooperative nanomaterial system to sensitize, target, and treat tumors, P Natl Acad Sci USA, 107(3) (2010) 981-986.

[99] M. Johannsen, U. Gneueckow, B. Thiesen, K. Taymoorian, C.H. Cho, N. Waldofner, R. Scholz, A. Jordan, S.A. Loening, P. Wust, Thermotherapy of prostate cancer using magnetic nanoparticles: Feasibility, imaging, and three-dimensional temperature distribution, Eur Urol, 52(6) (2007) 1653-1662.

[100] S. Giwa, J.K. Lewis, L. Alvarez, R. Langer, A.E. Roth, G.M. Church, J.F. Markmann, D.H. Sachs, A. Chandraker, J.A. Wertheim, M. Rothblatt, E.S. Boyden, E. Eidbo, W.P.A. Lee, B. Pomahac, G. Brandacher, D.M. Weinstock, G. Elliott, D. Nelson, J.P. Acker, K. Uygun, B. Schmalz, B.P. Weegman, A. Tocchio, G.M. Fahy, K.B. Storey, B. Rubinsky, J. Bischof, J.A.W. Elliott, T.K. Woodruff, G.J. Morris, U. Demirci, K.G.M. Brockbank, E.J. Woods, R.N. Ben, J.G. Baust, D.Y. Gao, B. Fuller, Y. Rabin, D.C. Kravitz, M.J. Taylor, M. Toner, The promise of organ and tissue preservation to transform medicine, Nat Biotechnol, 35(6) (2017) 530-542.

[101] K.L. Scott, J. Lecak, J.P. Acker, Biopreservation of red blood cells: Past, present, and future, Transfus Med Rev, 19(2) (2005) 127-142.

[102] H.E. Broxmeyer, E.F. Srour, G. Hangoc, S. Cooper, S.A. Anderson, D.M. Bodine, High-efficiency recovery of functional hematopoietic progenitor and stem cells from human cord blood cryopreserved for 15 years, P Natl Acad Sci USA, 100(2) (2003) 645-650.

[103] M.A. Henry, E.E. Noiles, D.Y. Gao, P. Mazur, J.K. Critser, Cryopreservation of Human Spermatozoa .4. The Effects of Cooling Rate and Warming Rate on the Maintenance of Motility, Plasma-Membrane Integrity, and Mitochondrial-Function, Fertil Steril, 60(5) (1993) 911-918.

[104] A. Bernard, B.J. Fuller, Cryopreservation of human oocytes: A review of current problems and perspectives, Hum Reprod Update, 2(3) (1996) 193-207.

[105] S. Evans, J. Penfold, Thermal runaway in electromagnetic heating, with application to the reheating of cryopreserved biomaterials, J Microwave Power Ee, 28(2) (1993) 84-92.

[106] H.L. Rodriguez-Luccioni, M. Latorre-Esteves, J. Mendez-Vega, O. Soto, A.R. Rodriguez, C. Rinaldi, M. Torres-Lugo, Enhanced reduction in cell viability by hyperthermia induced by magnetic nanoparticles, Int J Nanomed, 6 (2011) 373-380.

[107] A. Jordan, P. Wust, R. Scholz, B. Tesche, H. Fahling, T. Mitrovics, T. Vogl, J. CervosNavarro, R. Felix, Cellular uptake of magnetic fluid particles and their effects on human adenocarcinoma cells exposed to AC magnetic fields in vitro, Int J Hyperther, 12(6) (1996) 705-722.

[108] I. Brigger, C. Dubernet, P. Couvreur, Nanoparticles in cancer therapy and diagnosis, Adv Drug Deliv Rev, 54(5) (2002) 631-651.

[109] S. Dutz, R. Hergt, Magnetic particle hyperthermia-a promising tumour therapy?, Nanotechnology, 25(45) (2014).

[110] S. Jeon, K.R. Hurley, J.C. Bischof, C.L. Haynes, C.J. Hogan, Quantifying intra- and extracellular aggregation of iron oxide nanoparticles and its influence on specific absorption rate, Nanoscale, 8(35) (2016) 16053-16064.

[111] H.S. Huang, J.K. Choi, W. Rao, S.T. Zhao, P. Agarwal, G. Zhao, X.M. He, Alginate Hydrogel Microencapsulation Inhibits Devitrification and Enables Large-Volume Low-CPA Cell Vitrification, Adv Funct Mater, 25(44) (2015) 6839-6850.

[112] G. Zhao, J.P. Fu, Microfluidics for cryopreservation, Biotechnol Adv, 35(2) (2017) 323-336.

[113] K.G.M. Brockbank, G.J. Wright, E.D. Greene, Z.Z. Chen, K. Schenke-Layland, Allogeneic Heart Valve Storage Above the Glass Transition at-80 degrees C, Ann Thorac Surg, 91(6) (2011) 1829-1835.

[114] M. Lisy, J. Pennecke, K.G.M. Brockbank, O. Fritze, M. Schleicher, K. Schenke-Layland, R. Kaulitz, I. Riemann, C.N. Weber, J. Braun, K.E. Mueller, F. Fend, T. Scheunert, A.D. Gruber, J.M. Albes, A.J. Huber, U.A. Stock, The performance of ice-free cryopreserved heart valve allografts in an orthotopic pulmonary sheep model, Biomaterials, 31(20) (2010) 5306-5311.

[115] A.E. Deatsch, B.A. Evans, Heating efficiency in magnetic nanoparticle hyperthermia, J Magn Magn Mater, 354 (2014) 163-172.

[116] Q.A. Pankhurst, J. Connolly, S.K. Jones, J. Dobson, Applications of magnetic nanoparticles in biomedicine, J Phys D Appl Phys, 36(13) (2003) R167-R181.

[117] K. Tanaka, A. Ito, T. Kobayashi, T. Kawamura, S. Shimada, K. Matsumoto, T. Saida, H. Honda, Cancer immunotherapy using hyperthermia with magnetic nanoparticles and dendritic cells, J Biotechnol, 118 (2005) S73-S73.

[118] W.F. Brown, Thermal Fluctuations of a Single-Domain Particle, Phys Rev, 130(5) (1963) 1677-+.

[119] R.E. Rosensweig, Heating magnetic fluid with alternating magnetic field, J Magn Magn Mater, 252(1-3) (2002) 370-374.

[120] M. Gonzales-Weimuller, M. Zeisberger, K.M. Krishnan, Size-dependant heating rates of iron oxide nanoparticles for magnetic fluid hyperthermia, J Magn Magn Mater, 321(13) (2009) 1947-1950.

[121] V.S. Kalambur, B. Han, B.E. Hammer, T.W. Shield, J.C. Bischof, In vitro characterization of movement, heating and visualization of magnetic nanoparticles for biomedical applications, Nanotechnology, 16(8) (2005) 1221-1233.

[122] D. Ho, X.L. Sun, S.H. Sun, Monodisperse Magnetic Nanoparticles for Theranostic Applications, Accounts Chem Res, 44(10) (2011) 875-882.

[123] M. Blanco-Mantecon, K. O'Grady, Interaction and size effects in magnetic nanoparticles, J Magn Magn Mater, 296(2) (2006) 124-133.

[124] Y. Pineiro-Redondo, M. Banobre-Lopez, I. Pardinas-Blanco, G. Goya, M.A. Lopez-Quintela, J. Rivas, The influence of colloidal parameters on the specific power absorption of PAA-coated magnetite nanoparticles, Nanoscale Res Lett, 6 (2011).

[125] X.M. Wang, H.C. Gu, Z.Q. Yang, The heating effect of magnetic fluids in an alternating magnetic field, J Magn Magn Mater, 293(1) (2005) 334-340.

[126] A. Urtizberea, E. Natividad, A. Arizaga, M. Castro, A. Mediano, Specific Absorption Rates and Magnetic Properties of Ferrofluids with Interaction Effects at Low Concentrations, J Phys Chem C, 114(11) (2010) 4916-4922.

[127] C.L. Dennis, A.J. Jackson, J.A. Borchers, R. Ivkov, A.R. Foreman, J.W. Lau, E. Goernitz, C. Gruettner, The influence of collective behavior on the magnetic and heating properties of iron oxide nanoparticles, J Appl Phys, 103(7) (2008).

[128] M.A. Verges, R. Costo, A.G. Roca, J.F. Marco, G.F. Goya, C.J. Serna, M.P. Morales, Uniform and water stable magnetite nanoparticles with diameters around the monodomain-multidomain limit, J Phys D Appl Phys, 41(13) (2008).

[129] S.J. DeNardo, G.L. DeNardo, A. Natarajan, L.A. Miers, A.R. Foreman, C. Gruettner, G.N. Adamson, R. Ivkov, Thermal dosimetry predictive of efficacy of In-111-ChL6 nanoparticle AMF-induced thermoablative therapy for human breast cancer in mice, J Nucl Med, 48(3) (2007) 437-444.

[130] M. Creixell, A.C. Bohorquez, M. Torres-Lugo, C. Rinaldi, EGFR-Targeted Magnetic Nanoparticle Heaters Kill Cancer Cells without a Perceptible Temperature Rise, Acs Nano, 5(9) (2011) 7124-7129.

[131] L. Lartigue, P. Hugounenq, D. Alloyeau, S.P. Clarke, M. Levy, J.C. Bacri, R. Bazzi, D.F. Brougham, C. Wilhelm, F. Gazeau, Cooperative Organization in Iron Oxide Multi-Core Nanoparticles Potentiates Their Efficiency as Heating Mediators and MRI Contrast Agents, Acs Nano, 6(12) (2012) 10935-10949.

[132] P. Guardia, R. Di Corato, L. Lartigue, C. Wilhelm, A. Espinosa, M. Garcia-Hernandez, F. Gazeau, L. Manna, T. Pellegrino, Water-Soluble Iron Oxide Nanocubes with High Values of Specific Absorption Rate for Cancer Cell Hyperthermia Treatment, Acs Nano, 6(4) (2012) 3080-3091.

[133] J.H. Lee, J.T. Jang, J.S. Choi, S.H. Moon, S.H. Noh, J.W. Kim, J.G. Kim, I.S. Kim, K.I. Park, J. Cheon, Exchange-coupled magnetic nanoparticles for efficient heat induction, Nat Nanotechnol, 6(7) (2011) 418-422.

[134] R. Baan, Y. Grosse, B. Lauby-Secretan, F. El Ghissassi, V. Bouvard, L. Benbrahim-Tallaa, N. Guha, F. Islami, L. Galichet, K. Straif, W.I.A.R.C.M. Wo, Carcinogenicity of radiofrequency electromagnetic fields, Lancet Oncol, 12(7) (2011) 624-626.

[135] L. Hardell, World Health Organization, radiofrequency radiation and health - a hard nut to crack (Review), Int J Oncol, 51(2) (2017) 405-413.